FACIES MODELING USING 3D PRE-STACK SIMULTANEOUS SEISMIC INVERSION AND MULTI-ATTRIBUTE PROBABILITY NEURAL NETWORK TRANSFORM IN THE WATTENBERG FIELD, COLORADO

by

Sheila Harryandi

© Copyright by Sheila Harryandi, 2017

All Rights Reserved

A thesis submitted to the Faculty and the Board of Trustees of the Colorado School of Mines in partial fulfillment of the requirements for the degree of Master of Science (Geophysics).

Golden, Colorado

Date _____

Signed: _____
Sheila Harryandi

Signed: _____
Dr. Ali Tura
Thesis Advisor

Golden, Colorado

Date _____

Signed: _____
Dr. John Bradford
Professor and Head
Department of Geophysics

ABSTRACT

The Niobrara/Codell unconventional tight reservoir play at Wattenberg Field, Colorado has potentially two billion barrels of oil equivalent requiring hundreds of wells to access this resource. The Reservoir Characterization Project (RCP), in conjunction with Anadarko Petroleum Corporation (APC), began reservoir characterization research to determine how to increase reservoir recovery while maximizing operational efficiency. Past research results indicate that targeting the highest rock quality within the reservoir section for hydraulic fracturing is optimal for improving horizontal well stimulation through multi-stage hydraulic fracturing. The reservoir is highly heterogeneous, consisting of alternating chalks and marls. Modeling the facies within the reservoir is very important to be able to capture the heterogeneity at the well-bore scale; this heterogeneity is then upscaled from the borehole scale to the seismic scale to distribute the heterogeneity in the inter-well space.

I performed facies clustering analysis to create several facies defining the reservoir interval in the RCP Wattenberg Field study area. Each facies can be expressed in terms of a range of rock property values from wells obtained by cluster analysis. I used the facies classification from the wells to guide the pre-stack seismic inversion and multi-attribute transform. The seismic data extended the facies information and rock quality information from the wells. By obtaining this information from the 3D facies model, I generated a facies volume capturing the reservoir heterogeneity throughout a ten square mile study-area within the field area. Recommendations are made based on the facies modeling, which include the location for future hydraulic fracturing/re-fracturing treatments to improve recovery from the reservoir, and potential deeper intervals for future exploration drilling targets.

TABLE OF CONTENTS

ABSTRACT iii

LIST OF FIGURES vi

LIST OF TABLES xii

ACKNOWLEDGMENTS xiii

CHAPTER 1 INTRODUCTION 1

1.1 Research Value 2

1.2 Geology Background 4

1.2.1 Field Overview 4

1.2.2 Depositional History and Stratigraphy 5

1.2.3 Tectonic Settings 6

1.2.4 Petroleum System 8

1.3 Available Data 9

1.3.1 Seismic Data 10

1.3.2 Well Data 12

CHAPTER 2 FACIES PREDICTION FROM WELLS 15

2.1 Facies Description From Literature 16

2.2 Core Description and RQI Analysis from Previous Research 19

2.2.1 Facies Description from the Core 20

2.2.2 Rock Quality Index (RQI) Work 23

2.3 Facies Clustering from the Well Logs 24

2.4 Integration between Cores Description, Facies Clustering, RQI and Elastic Properties . . . 27

CHAPTER 3 SIMULTANEOUS SEISMIC INVERSION . . . 32

3.1 Seismic Data Processing . . . 33

3.2 Seismic Data Conditioning . . . 34

3.3 Simultaneous Seismic Inversion . . . 40

3.3.1 Basic Theory . . . 40

3.3.2 Wavelet Estimation and Well-to-Seismic Tie . . . 43

3.3.3 Low Frequency Model Building . . . 47

3.3.4 Inversion Parameters Testing and Results . . . 48

CHAPTER 4 MULTI-ATTRIBUTE TRANSFORM FOR PREDICTING LOG PROPERTIES FROM SEISMIC . . . 54

4.1 Utilizing Density Information in Facies Modeling . . . 54

4.2 Multi-attribute Transform . . . 57

CHAPTER 5 FACIES MODELING AND ANALYSIS . . . 63

5.1 Facies Modeling Results . . . 65

5.2 Application for Preliminary Evaluation of Greenhorn Exploration . . . 73

5.3 Uncertainties . . . 74

CHAPTER 6 CONCLUSIONS AND RECOMMENDATIONS . . . 77

6.1 Conclusions . . . 77

6.2 Recommendations . . . 78

REFERENCES CITED . . . 80

LIST OF FIGURES

Figure 1.1 Wattenberg field location shown on green colored shade. The main data being used for the research is located in the southern part of the Wattenberg field (RCP, 2017). 4

Figure 1.2 General stratigraphic column of the Wattenberg Field, showing the main development target, Niobrara intervals, and other multiple pays above and below it. SR stands for the Source Rocks. The A, B, C, and D intervals are parts of the Smoky Hill Member within the Niobrara formation. The other member of the Niobrara formation is the Fort Hays limestone underlying the Smoky Hill Member (modified from Sonnenberg).. 7

Figure 1.3 Section view of Denver basin, showing the westward-thickening shape of the basin. Red dashed line demarcates the depth of the oil window 8

Figure 1.4 Petroleum system event chart of the Wattenberg play, modified from Higley and Cox. 10

Figure 1.5 Basemap of the study area showing the main seismic data used for this research, with the Anatoli 3D/3C colored in green. Annotated Well 1, Core Well 3 and Core Well 5 are the main wells for this study (RCP, 2017). 11

Figure 1.6 Zoomed-in Anatoli survey area with the Top Niobrara time structure map and 13 vertical wells inside the seismic survey. Well 1 on the most southern part is the only well with measured sonic logs.. 13

Figure 1.7 Type log of main units in Wattenberg area from Core Well 5, showing the Niobrara (A-B-C Chalks and Marls, D Facies, Fort Hays) to Greenhorn intervals (Bridge Creek, Hartland, Lincoln). 14

Figure 2.1 P- vs S-impedance cross-plots from three main wells, color coded by well log properties. The input data is from the Smoky Hill Member of the Niobrara interval. The drawn polygons for each cross-plot emphasizes the trend of log values that support facies characterization. . . . 26

Figure 2.2 Core Well 3 section, comparing the main well logs being used for the facies clustering, the facies clusters, and the core interpretation. Core data were described by Brugioni. Details of each core facies are presented in Table 2.3.. 29

Figure 2.3 Cross-plot of P- vs S-impedance values from 13 vertical wells inside the 3D Anatoli seismic survey, color coded by the facies from clustering analysis. The ellipses represent fitted PDF for every facies, with the maximum (bigger ellipses) and minimum (smaller ellipses) PDF ranges. The input interval is highlighted (pink) in the stratigraphic section view. . 30

Figure 2.4 Cross-plot of P- and S-impedance vs RQI, color coded by the facies from clustering analysis. Linear relationship between higher RQI to higher impedance values is observed. 31

Figure 3.1 Wattenberg project timeline, highlighting the Anatoli 3D/3C seismic acquisition which took place at the same time as the acquisition of 4D Turkey Shoot baseline. 32

Figure 3.2 An example of the Radon noise attenuation result in one CIP gather within the seismic dataset. The image on the right is the residual between the CIP gather before and after the conditioning, showing that the attenuation was focusing on random noise while preserving the seismic signals. 36

Figure 3.3 Representative CIP gather before (left) and after (right), applying trim statics conditioning process. Note the slightly more flat reflectors on the right image, highlighted by the red arrows. 37

Figure 3.4 Fold Map of the 3D Anatoli P-Wave CIP gathers, overlain by all vertical wells within the survey. Some wells are located on the edge of the seismic survey, where the seismic acquisition fold is very low. 38

Figure 3.5 An example of one CIP gather, color coded by the reflection angle of the dataset. This image shows that the zone of interest has the critical angle of approximately 45°. 39

Figure 3.6 The alignment of each angle stack; near, mid-near, mid-far, far stacks, shown in one section view in different seismic trace colors. Frequency difference is observed due to wavelet stretch, but good time alignment is observed. 39

Figure 3.7 Illustration of the relationship between the geology model and the seismic trace showing forward modeling and inversion. For forward modeling, the reflectivity is convolved with a wavelet to create a seismic synthetic, while for seismic inversion, the wavelet is removed from the seismic trace to estimate the possible geological model in the subsurface . . 41

Figure 3.8 General workflow of the Seismic Inversion work 44

Figure 3.9 Average wavelets for each partial angle stack are highlighted in black. The background for each average wavelet is a set of estimated wavelets from all 13 wells. 45

Figure 3.10 Seismic-to-well tie example from Well 11 showing a good match between the seismic and synthetic traces. High correlation is indicated by hot colors. On the right column, the comparison between time-depth relationship before and after adjustment is shown, indicating very minimum modification. 46

Figure 3.11 Correlation coefficient of each well-to-seismic tie from 11 wells. Overall correlations are high (in a scale of 0 to 1), except the far stack that generally has the least acquisition folds and lowest seismic frequency. Time window of the well-to-seismic process (±500 ms) was set for a stable correlation, as it is approximately four times the wavelet length. . . . 47

Figure 3.12 Extracted P-impedance (RMS values) from the Low Frequency Model (LFM), with the extraction window from top of Niobrara to the top of Codell. The map shows general trend of the P-impedance is higher to the east. Red dots show the input wells for the LFM. Pink line and star symbol represent the section view line on Figure 3.13 and the well location plotted on it. 48

Figure 3.13 Low Frequency Model (LFM) in section view, showing four main input horizons and the higher impedance trend in the Niobrara interval. P-impedance log is plotted from Well 7 (shown as star symbol in the Figure 3.12). 49

Figure 3.14 The frequency ranges of well data and seismic data, showing the overlap (merge-cutoff frequency) at 11Hz between the seismic and the well. Merge-cutoff frequency was chosen after numerous inversion parameters tests which give the most optimal final result. 50

Figure 3.15 Inversion result (P- and S-impedance) on map view, extracted from the Root-Mean-Square (RMS) values at the interval of 10 ms-15 ms below the Top of the Niobrara horizon. Higher impedance areas are indicated in hotter colors. The yellow line crossing Well 7 and Well 4 as the blind wells also shows the impedances in section view (Figure 3.16). 51

Figure 3.16 Elastic Properties: P-impedance (upper) and S-impedance (lower) volumes from seismic inversion in section view. The line crosses the Well 7 and Well 4, which are the blind wells. Note the good matches between P-impedance and S-impedance from the well and seismic inversion at the blind-well locations.. 52

Figure 3.17 A closer look at Well 7 and Well 4 (blind wells), comparing the P-impedance (Z_p) and S-impedance (Z_s) from the well logs and seismic inversion. A good match is indicated from these curve plots (errors <5%). . 52

Figure 3.18 Cross-plot of estimated P-impedance and S-impedance from seismic inversion. The higher impedance values are shown in hotter color. Plotted on the top-right corner of the figure, is the Probability Distribution Function (PDF) of the Pure-Chalk from well log clustering. . . 53

Figure 4.1 Cross-plot of P-impedance and S-impedance values from the wells inside the 3D Anatoli survey, color coded by the facies within the Smoky Hill Member. The grey dots on the background shows the overlapping facies distribution of the zones below the Smoky Hill Member. 56

Figure 4.2 Cross-plot of P-impedance and S-impedance values from the wells inside the 3D Anatoli survey, color coded by the facies below the Smoky Hill Member. The grey dots on the background shows the overlapping facies distribution of the Smoky Hill Member zone. 56

Figure 4.3 Cross-plot of P-impedance and density values from wells inside the 3D Anatoli survey, color coded by the facies from the Top of Niobrara to the Base of Codell Sandstone. By using the relationship between P-impedance and density, all of the facies between this interval can be modeled, with the exception of the Codell Sandstone which still has overlapping values to the other facies (showed in grey dots). 57

Figure 4.4 Comparison plot between predicted density from Probability Neural Network (Multi-Attribute Transform) and measured density from the well logs. The target interval is shown by the highlighted markers; approximately 100 ms between Top Niobrara to Top Graneros. Note that the biggest mismatch is found at the Well 1, which is the well with measured V_p and V_s logs. 59

Figure 4.5 Cross-plot of actual density vs. predicted density at well locations, color coded by each of 13 input wells. This plot displays the 0.9 correlation coefficient between the two properties, with all wells used in the training set. For blind well cross-validation, the average of the correlation coefficients is 0.75. 60

Figure 4.6 Two inline sections crossing Well 8 show the comparison between density property from seismic inversion (top) and density property from multi-attribute probability neural network transform (bottom). The extraction of density from multi-attribute PNN for Niobrara interval is shown on the top right corner map, with the location of displayed inline (yellow). For this map, the hot colors indicate higher density values, ranging between 2.52-2.58 g/cc. 61

Figure 4.7 Cross-plot of P-impedance from the seismic inversion vs. density from multi-attribute transform, showing the alignment of each facies distribution to the PDF from well log cross-plot (see Figure 4.3). It is observed that there are parts of pure-chalk facies distribution identified as the mixed marl-chalk facies, and the limestone facies cannot be modeled from the seismic, which is due to the small thickness. 62

Figure 5.1 Arbitrary line crossing six wells across the Anatoli seismic survey, showing the Bayesian most probable facies from the PDFs generated by Z_p and Z_s (above) and Z_p and ρ (below) relationships. The top-right corner map is extracted from the chalk probability of the Smoky Hill Member interval, using the facies modeling from Z_p and ρ, with the black lines indicating the map view of the arbitrary section. 66

Figure 5.2 Arbitrary line crossing six wells across the Anatoli seismic survey, showing the pure chalk probability from the PDFs generated by Z_p and Z_s (above) and Z_p and ρ (below) relationships. The top-right corner map is extracted from the chalk probability of the Niobrara interval using the facies modeling from Z_p and ρ. 67

Figure 5.3 Base map of the Wishbone section within the Wattenberg field, with 11 horizontal wells. The horizontal wells are plotted with the hydraulic stimulation stages and lithology information for each stages determined by the geosteering paths . Note that the 5C and 1N wells are used in the next figures for the facies modeling evaluation. 68

Figure 5.4 Cross-section views of three different attributes: the P-impedance from seismic inversion, density from the multi-attribute transform, and the most probable facies model generated from the two attributes. The section crosses the 5C horizontal well targeting the Codell sandstone interval. The top-right corner map shows the relative locations of the horizontal wells and the vertical wells within the 3D Anatoli seismic survey area. 69

Figure 5.5 Cross-section views of three different attributes: the P-impedance from seismic inversion, density from the multi-attribute transform, and the most probable facies model generated from the two attributes. The section crosses the 1N horizontal well targeting the chalks of Smoky Hill Member. The top-right corner map shows the relative locations of the horizontal wells and the vertical wells within the 3D Anatoli seismic survey area 70

Figure 5.6 Extraction map of the pure chalk facies probability within the Smoky Hill Member interval and the plotted vertical wells inside the survey area (RMS amplitude of the pure chalk facies probability, at the window of the Top of Niobrara horizon to 20ms below it). 71

Figure 5.7 Extraction map of the sandstone facies (Codell) probability and the plotted vertical wells inside the survey area (RMS amplitude of the sandstone facies probability, at the window of the Top of Codell horizon to 15ms below it). 71

Figure 5.8 Cross-plot of pure chalk facies probability from the map in Figure 5.6 at well locations (13 wells inside the seismic survey) versus the sum of the pure chalk facies thickness at each well. 72

Figure 5.9 Cross-plot of sandstone facies (Codell) probability from the map in Figure 5.7 at well locations (12 wells inside the seismic survey) versus the sandstone facies thickness at each well. 72

Figure 5.10 Extraction map of the limestone facies (Greenhorn-Bridge Creek) probability and the plotted vertical wells inside the survey area (RMS value of the basal chalk facies probability, at the window of 10 to 25 ms below the Top of Codell horizon). The limestone is modeled similarly to the basal chalk facies (D-facies), in terms of the high density and P-impedance values. These high values of elastic properties may be caused by the high compaction of the limestone interval as it is deposited deeper than the other facies. The hotter color shows the higher facies probability. 75

Figure 5.11 Cross-plot of limestone facies (Greenhorn - Bridge Creek) probability from the map in Figure 5.10 at well locations (12 wells inside the seismic survey) vs. the sum of the limestone facies thickness at each well. . 75

LIST OF TABLES

Table 1.1 Wattenberg Seismic Surveys 11

Table 2.1 Mineralogy of Niobrara and Codell Sandstone 17

Table 2.2 Mineralogy of Greenhorn from Core Well 5 data 19

Table 2.3 Facies Classification and Description from Cores Analysis 21

Table 2.4 Data Availability on Main Wells 25

Table 2.5 Well log values of three clustered facies within Smoky Hill Member 27

Table 3.1 Acquisition Parameters for Anatoli Survey (modified from Motamedi) 33

Table 3.2 Processing Steps for Anatoli P-wave Seismic Gathers (modified from White and Butler) 35

Table 4.1 Well log values of six facies from clustering 54

ACKNOWLEDGMENTS

First of all, I would like to thank Dr. Thomas Davis who has given me such a great opportunity to be a part of the Reservoir Characterization Project (RCP) group. I can't thank you enough for your continuous supports throughout my research and master's program. I would also thank Dr. Ali Tura, my thesis advisor, who has given very valuable geophysical insights into my thesis. I can't really express how grateful I am to be working with and learning from the geophysical experts, particularly in advanced seismic data interpretation.

To Dr. Walter Lynn, thank you for your willingness to be my thesis committee member and shared your expertise in seismic data. You taught a great course (seismic data processing) and I'm very grateful to be able to experience it. Thank you, Dr. Stephen Sonnenberg, for being my thesis committee member and minor representative in Geology. I have referred to your papers more than any other references in my thesis. Thank you for your valuable geological insights, particularly your expertise of the Wattenberg Field. To Dr. Jeffrey Shragge, thank you for accepting the proposal to be in my thesis committee. Your thorough edits of my thesis have strengthen the technical writing and the geophysical basis of my thesis.

Special thanks to Sue Jackson, for your great support to myself and the RCP group. I really appreciate how you have gracefully managed all of us within the research group. Also thank you, Michelle Szobody, who has been a great support throughout my master's program. Thank you for making sure I have check-listed all the requirements for my master's program completion. Thank you, all RCP mentors, especially Janel Andersen and Katie Joe McDonough. I'm very grateful to have the opportunity to learn from you as the industrial experts. Thank you to all of my friends in RCP and CSM. I'm sure we will cross-path again in the future. It's my honor to be able to know you all and work with some of you.

Last but not least, I would like to thank my family, papa, mama, kak Sylvan, Sandy, emak, for your continuous supports during my master's program. May God bless you all.

CHAPTER 1
INTRODUCTION

The Wattenberg Project is an unconventional tight reservoir play that has been one of the primary investigation areas of the Reservoir Characterization Project (RCP) Group at the Colorado School of Mines, since the Fall of 2013. Horizontal drilling and hydraulic fracturing treatment has been performed at the main reservoir, the Niobrara and Codell formations. After two phases of the RCP project (Phase XV and XVI), we are able to focus on realizing several key objectives of the research: including to increase recovery and reserves, profitability, minimize the drilling risk, and maximize the operational efficiency. To achieve these objectives, it is important to model reservoir behavior, both the in-situ condition (before well production and hydraulic stimulation process were conducted) and the dynamic changes due to stimulation and production. This thesis focuses on modeling the facies within the 3D Anatoli seismic survey, especially at the reservoir levels, by performing seismic inversion and multi-attribute transform analyses.

The Wattenberg Project within RCP is an integrated project between Geophysics, Geology, Petroleum Engineering and Economic disciplines. The contribution from each of these fields of study is very important for delivering a comprehensive and integrated interpretation of the area. One main focus within the Wattenberg Field is to locate the best zones for well completion, by comparing the geomechanical and reservoir quality information to the changes observed from the dynamic reservoir characterization work.

Before discussing the details of the facies modeling work performed in this research, this introduction will give provide additional information on the research value, the geology background of the field, and the data being used to achieve the research goals. The research value, the geology background, and the data information are the key points of my research, to which I will be referring later in the main discussion of my work.

1.1 Research Value

The oil and gas industry technology has significantly advanced such that we can now produce hydrocarbons from tight reservoirs that were formerly considered very high risk. The conventional concept of the petroleum geology focuses on targeting the main reservoir having high porosity and permeability. The main technology that has changed this conventional concept is the combination between horizontal drilling and multi-stage hydraulic fracturing. Even though the horizontal drilling and multi-stage hydraulic fracturing technologies demonstrably improve hydrocarbon production, the technology remains very expensive and needs to be optimized. By examining previous studies, we observe a trend toward progressively improving the methodology to define the sweet spots for the unconventional tight reservoirs. The sweet spots are mainly affected by mechanical stratigraphic factors and rock quality. These factors were used to build the Rock Quality Index (RQI) that has been analyzed previously within RCP for the Wattenberg reservoir characterization (Mabrey, 2016). Based on the study by Mabrey (2016), we expect to achieve a higher field recovery and more efficient operational cost by targeting the rocks with the highest RQI. This kind of study was also conducted in 2012 for Eagle Ford Fm, another successful unconventional tight reservoir play in the United States. Cipolla et al. (2012) reports that the initial production at the Eagle Ford Fm was increased by 20%, by designing the well perforation clusters based on the rock quality. It is very important, too, to have a good understanding of the characteristics of the unconventional tight reservoir play. While we try to target the high quality reservoir in terms of brittleness and organic content, the existence of an adjacent mature source rock with high total organic content is very crucial.

Given the previously elaborated background motivation, the main questions of this research are:

1. Can we interpret facies within the Wattenberg reservoir interval more quantitatively from the wells and estimate their lateral distribution?

2. What are the recommendations for future development of the Wattenberg project?

3. Is there any potential exploration target around the area that can be modeled from this work?

The Niobrara Fm of the Wattenberg is a deposition of alternating marls and chalks, which has been widely studied in the last several years. The marly part of the formation is interpreted as the main source rock with high organic matter (± 2-4% of Total Organic Content (TOC)), whereas the chalky part is interpreted as the reservoir with high brittleness and presence of fractures, adjacent to the mature source rock. Due to these factors, the chalk-rich part of the Niobrara - Smoky Hill Member has always been the horizontal drilling target. By using rock properties from well logs such as neutron porosity, gamma-ray, density, resistivity and compressional/shear velocity for clustering analysis, the facies prediction along the Niobrara Fm can be quantitatively interpreted. This facies prediction was also correlated to the previously completed RQI analysis and core description to ensure that the interpretation is geologically reasonable.

Completing the facies interpretation based on the well information, we need to extend the information laterally between wells. To achieve this, I performed a simultaneous P-wave seismic inversion of Anatoli seismic data set within the Wattenberg area of study. The reason for using this seismic data set specifically will be discussed in Section 1.3. The distribution of each facies from the wells can be distinguished using P- and S-impedance values from the well logs. Therefore, I expect to be able to estimate the facies distribution using the P- and S-impedance results through simultaneous seismic inversion. In addition, I performed multi-attribute transform using a non-linear algorithm (Probability Neural Network) to estimate density property. The combination between P-impedance and density was evaluated and compared to the P- and S-impedance in facies modeling.

1.2 Geology Background

Understanding the geological history of the Wattenberg Field is a critical part of the research goals and workflows. Geophysical theory, data, and methods are important in obtaining subsurface information, but we need to clearly understand and be consistent with the geological basis behind our interpretation. There were several studies on the Wattenberg and Niobrara Fm that are of particular importance to this thesis.

1.2.1 Field Overview

The Wattenberg field located in northeastern Colorado, was discovered in 1970 by the Amoco Production Company. Figure 1.1 shows the location of the field relative to the state of Colorado, Denver, and other surrounding cities. The project area is shown on the southern part of the Wattenberg field.

Figure 1.1: Wattenberg field location shown on green colored shade. The main data being used for the research is located in the southern part of the Wattenberg field (RCP, 2017).

Early stages of Wattenberg exploration and activity mainly focused on the Lower Cretaceous D and J sandstones (shown in Figure 1.2 at depth 7600-7800ft). Later discoveries showed that the Wattenberg Field had multiple pay intervals with each adding significant reserves to the field. The high temperature anomaly related to the Colorado Mineral Belts beneath the Denver Basin is arguably the principal reason for all the stacked pay zones in the Wattenberg (Higley et al., 2003). In the early 1980s, the Niobrara Fm and the Codell Sandstone of the Carlile Fm started to become important development targets. These units are considered unconventional reservoirs due to their low matrix porosity (<10%) and matrix permeability (<0.1md) that requires hydraulic stimulation to significantly improve well production. Current production of the Wattenberg Field from the Niobrara is approximately 20,000 BOPD and 180 MMCFGD, while the overall oil resource-in-place is estimated to be two to four billion BBE (Sonnenberg, 2013). In addition to these formations, there is another potential target at a deeper interval, namely the Greenhorn Fm. Numerous wells have penetrated this interval and the current status indicates that the operators are testing the new horizontal wells in the play. These intervals are analogous to the Niobrara play, hence a preliminary evaluation and recommendation of the Greenhorn play will be addressed as part of this research.

1.2.2 Depositional History and Stratigraphy

The Upper Cretaceous Niobrara Fm was deposited in a foreland basin setting in the Cretaceous Western Interior Seaway of North America during the time of major marine transgression. During sea-level highstands, coccolith-rich and planktonic foraminifer-rich carbonate sediments accumulated as chalks in the eastern half of the seaway. This chalk-rich facies grades westward into more siliciclastic-rich beds. The deposition of Niobrara Fm is highly correlated with regional paleo-climatic factors or sea level fluctuations. Sonnenberg (2013) classified the main Niobrara lithologies into chalk and marl, which are distinguishable based on carbonate and clay content. The chalk has relatively more than 70% of carbonate content, whereas the marl has between 30% and 70% carbonate or clay content. The chalk

deposition is related to high-stand sequences, while the interbedded marls are related to the combination of low stands and the influx of fresh-water runoff from the increased rainfall. The Niobrara Fm consists of two underlying main members, the Smoky Hill member and the Fort Hays Limestone member (see Figure 1.2).

The Smoky Hill member is an alternating marls and chalks deposition, named A, B, C, based on the order of depositional sequence. The Niobrara Fm overlies the Carlile Fm and its member, the equally productive tight reservoir called the Codell Sandstone. The Codell deposition is rather consistent across the Wattenberg field; hence, the present work on modeling the reservoir heterogeneity is focused more on the Niobrara section. Located deeper in the stratigraphic column are the Greenhorn and Graneros Fm. The Greenhorn Fm is divided into three main submembers: the Bridge Creek Limestone, Hartland Shale, and Lincoln Limestone. This cyclic deposition between chalky and marly units of the Greenhorn Fm is analogous to the existing development target, the Niobrara - Smoky Hill Member interval.

1.2.3 Tectonic Settings

The tectonic evolution of Denver Basin originated with the Cretaceous Western Interior Seaway subsidence occuring in Late Pennsylvanian, which was followed by the deposition of the Fountain Fm. Significant deformation during the Laramide Orogeny, largely formed the present-day asymmetric basin (Figure 1.3).

This asymmetrical basin dips steeply to the west and gently to the eastern side. The structural history of the basin plays as important of a role in the depositional of the modern basin as it largely controls present day fractures, pore pressure, and the reservoir compartmentalization. Basement listric faulting and/or solution of evaporites may have caused the folding that created the natural fractures. Fracturing of the Niobrara Fm is often associated with Laramide structures; however, these fractures are commonly filled with calcite, which has negative implications for petroleum production. It is interpreted that the Neogene extensional fracturing and/or microfracturing enhanced the production.

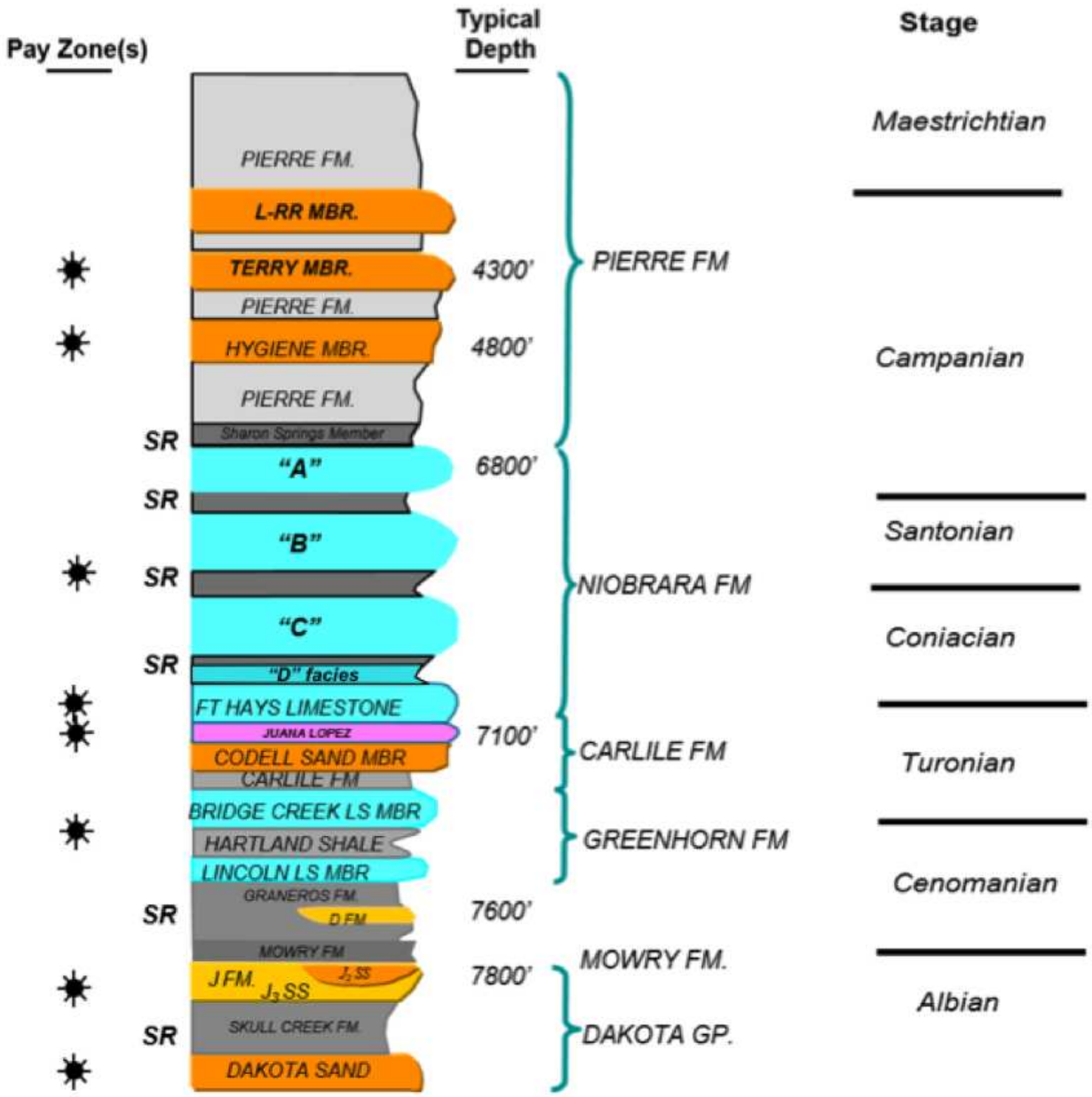

Figure 1.2: General stratigraphic column of the Wattenberg Field, showing the main development target, Niobrara intervals, and other multiple pays above and below it. SR stands for the Source Rocks. The A, B, C, and D intervals are parts of the Smoky Hill Member within the Niobrara formation. The other member of the Niobrara formation is the Fort Hays limestone underlying the Smoky Hill Member (modified from Sonnenberg (2015)).

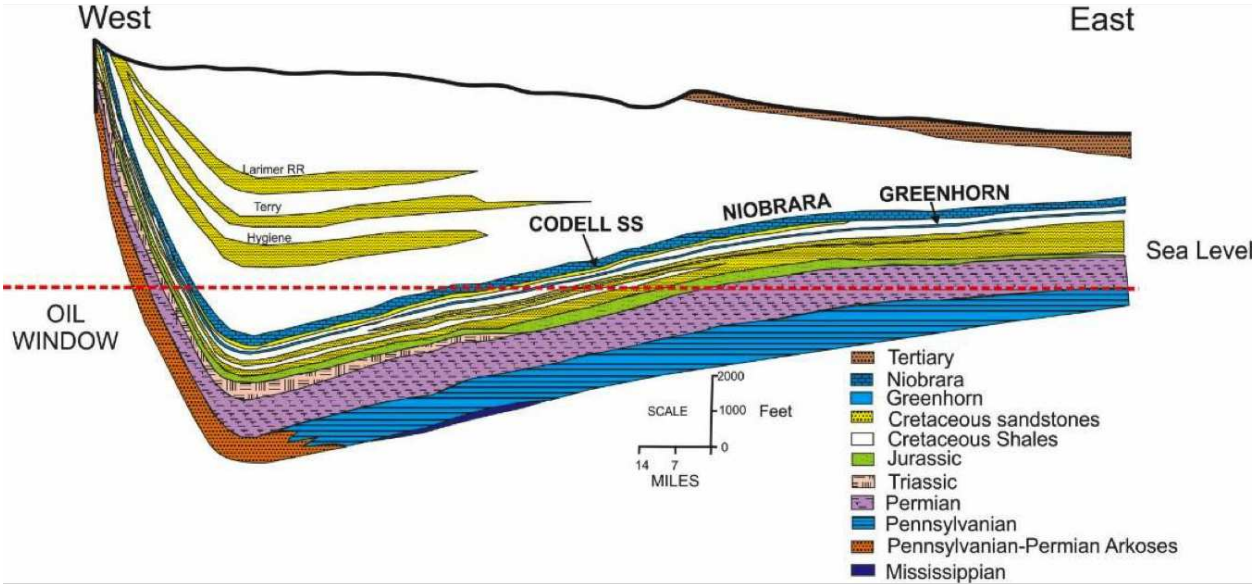

Figure 1.3: Section view of Denver basin, showing the westward-thickening shape of the basin. Red dashed line demarcates the depth of the oil window (Sonnenberg, 2013)

1.2.4 Petroleum System

The petroleum system elements of the Wattenberg Field are highly influenced by the depositional and tectonic history of the basin. Wattenberg is an unconventional petroleum system, specifically categorized as pervasive tight reservoir plays. Several factors supporting this interpretation are the tight nature of the reservoirs with significantly low porosity (<10%) and matrix permeability (<0.1 md), and the existence of adjacent mature source rock intervals encompassing the main reservoir. In addition, in order to mature, the source rock intervals needed to reach the oil window and create the force of expulsion. This produced the current overpressure condition for the Niobrara and Codell Fm. The existence of open natural fractures as the main permeability is also one of the characteristics that define Wattenberg as a tight reservoir play. The marl-rich part of the Niobrara is a better source rock with high TOC, ranging between 1-6 wt%. The kerogen is observed to be Type-II or oil prone. The organic-rich marls are also easily recognized from the gamma-ray logs,

as they are generally more radioactive relative to the chalks. The Sharon Spring Member of the Pierre Shale deposited above the Niobrara Fm is also an excellent source rock with TOC values ranging between 2-8 wt%. The Niobrara and Codell Fm are tight reservoir plays, buried sufficiently deep to have undergone mechanical and chemical compaction, creating the observed low porosity and permeability. The chalks were initially quite porous (>50%) but the mechanical compaction, dewatering, and grain breakage have reduced the overall matrix porosity. Thus, fracturing is important for enhancing the reservoir performance. The chalk beds tend to be more brittle and susceptible to fracturing than the marls, which makes the chalk-rich part of the Niobrara a better reservoir target unit for horizontal drilling. Seals for the Niobrara play include the marly part of the Niobrara and the overlying Pierre Shale. Durkee (2016) and Sonnenberg et al. (2016) have studied the petroleum system of the Greenhorn in more detail. Its reservoirs, the Bridge Creek Limestone and Lincoln Limestone members, encompass the adjacent mature source rock: the Hartland Shale. The Graneros Fm underlying the Lincoln Limestone member of the Greenhorn Fm is also a very prospective mature source rock for the play. The overlying Carlile Fm provides a seal for the system. Although the Greenhorn is buried deeper than the Niobrara, which made the porosity and permeability significantly lower, the main components of the unconventional play are analogous to the Niobrara, suggesting a potential future target. Figure 1.4 illustrates the petroleum events (Higley and Cox, 2007) that have been modified to include the petroleum system elements of the potential Greenhorn play.

1.3 Available Data

The Wattenberg Project is a part of RCP Phase XV and XVI with Anadarko Petroleum Corporation (APC) as the main sponsor. By acquiring and processing 3D multicomponent seismic surveys, the main objectives of understanding the in-situ reservoir condition and observing the rock changes due to hydraulic stimulation and well production are pursued. Figure 1.5 provides additional details about the project area and the data availability.

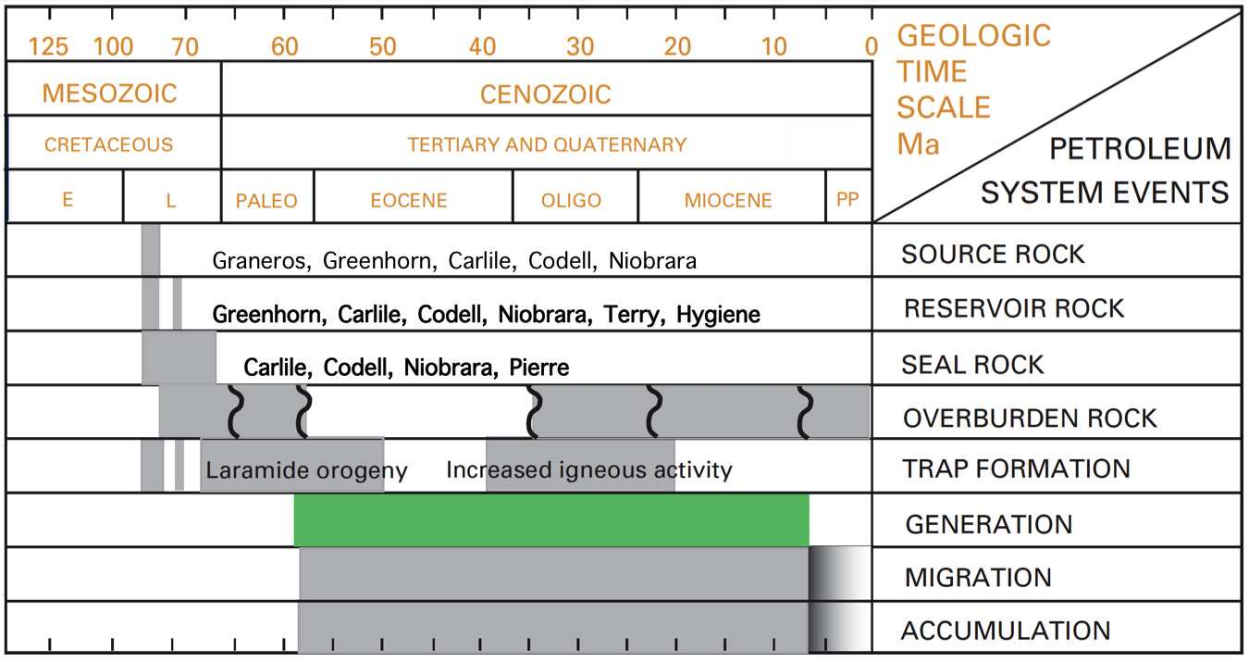

Figure 1.4: Petroleum system event chart of the Wattenberg play, modified from Higley and Cox (2007)

The smaller area (yellow square) is called the Wishbone section, where 11 horizontal wells were drilled and hydraulic stimulation was performed within the Niobrara and Codell Sandstone. The drilling of vertical wells targeting the Niobrara and Codell Sandstone units commenced in the early 1980, with the horizontal wells being drilled in June 2013. It is important to emphasize that this thesis is focused on the modeling and interpretation of the in-situ condition of the reservoir; hence, the priority is to use the vertical wells and a seismic survey that covers a broader area than the Wishbone section.

1.3.1 Seismic Data

There are several seismic surveys provided by the APC for the Wattenberg study, which vary in date of acquisition, area of coverage, and type of survey (Table 1.1). Figure 1.5 shows the extent of each seismic survey. The area of Aristocrat and Anatoli seismic surveys are the same, with different acquisition dates and type of surveys.

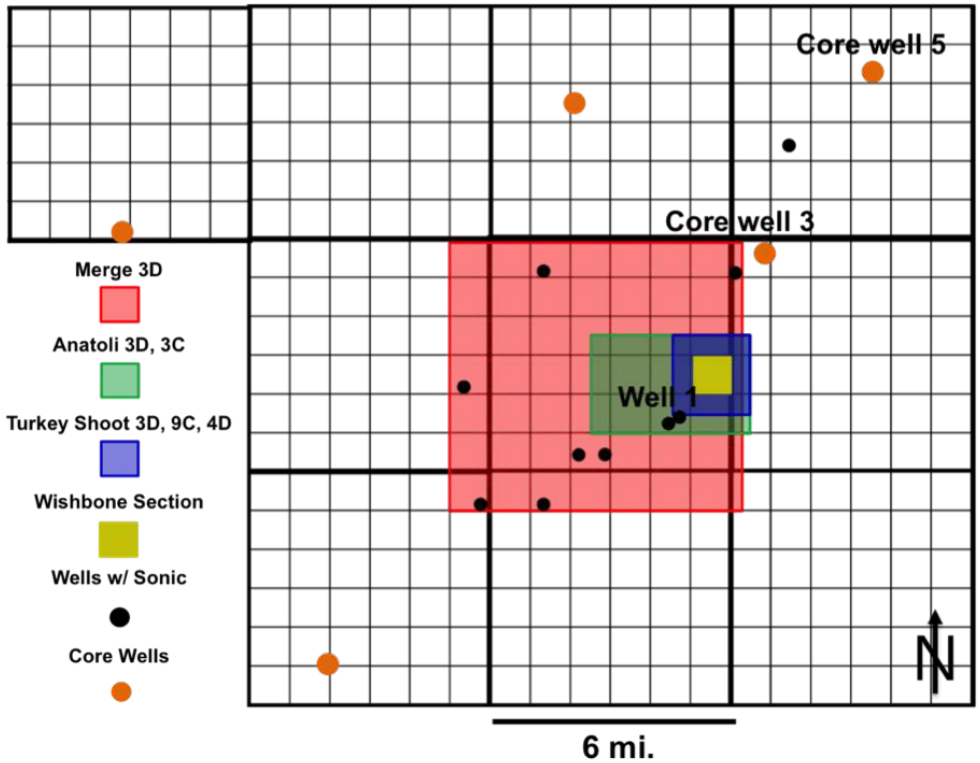

Figure 1.5: Basemap of the study area showing the main seismic data used for this research, with the Anatoli 3D/3C colored in green. Annotated Well 1, Core Well 3 and Core Well 5 are the main wells for this study (RCP, 2017).

Table 1.1: Wattenberg Seismic Surveys

Survey Name	**Acquisition Date**	**Area (sq.mi.)**	**Type of Survey**
Regional (Merge)	2010	50	WAZ 3D/1C
Aristocrat	2010	10	3D/1C
Anatoli	June/July 2013	10	3D/3C
Turkey Shoot Baseline	July 2013	4	4D/9C
Turkey Shoot Monitor 1	October 2013	4	4D/9C
Turkey Shoot Monitor 2	January 2016	4	4D/9C

The time-lapse nine-component seismic dataset is called the Turkey Shoot and covers a four square mile area focusing on the Wishbone section. It was acquired to monitor the changes of the reservoir due to the hydraulic stimulation and production. The seismic data being used for this particular research is a 3D P-wave seismic survey called the Anatoli survey, which covers a ten square mile area of the Wattenberg Field. This seismic survey was acquired at the same time as the Baseline survey of the Turkeyshoot seismic data, representing the in-situ conditions of the reservoir.

The decision to use the 3D Anatoli survey instead of the smaller Turkey Shoot time-lapse data is based on the following reasons:

1. The seismic data coverage is larger than the smaller Turkey Shoot survey with more wells, making it more suitable for understanding the regional reservoir deposition of the study area.

2. The modeling from the 3D Anatoli survey affords a comparison with the more detailed evaluation completed on the smaller area of Turkey Shoot / Wishbone section, and enables us to predict the potential target outside of the four square mile area.

1.3.2 Well Data

There are 11 horizontal wells being drilled along the Niobrara and Codell Sandstone inside the Turkey Shoot seismic survey coverage. In general, these horizontal wells have well logs such as gamma-ray and resistivity logs, but no sonic logs were acquired. For my research, I require dipole sonic logs and density logs that are essential for the seismic inversion process. For that objective, I used 13 vertical wells inside the 3D Anatoli seismic survey coverage (see Figure 1.6).

These wells have a moderately complete set of essential logs, including compressional sonic and shear sonic, resistivity, density, neutron porosity, and gamma-ray logs. However, most of the compressional and shear sonic logs were estimated using Neural Network calculation. Pitcher (2015) explained about the synthetic sonic log calculation for the area and stated

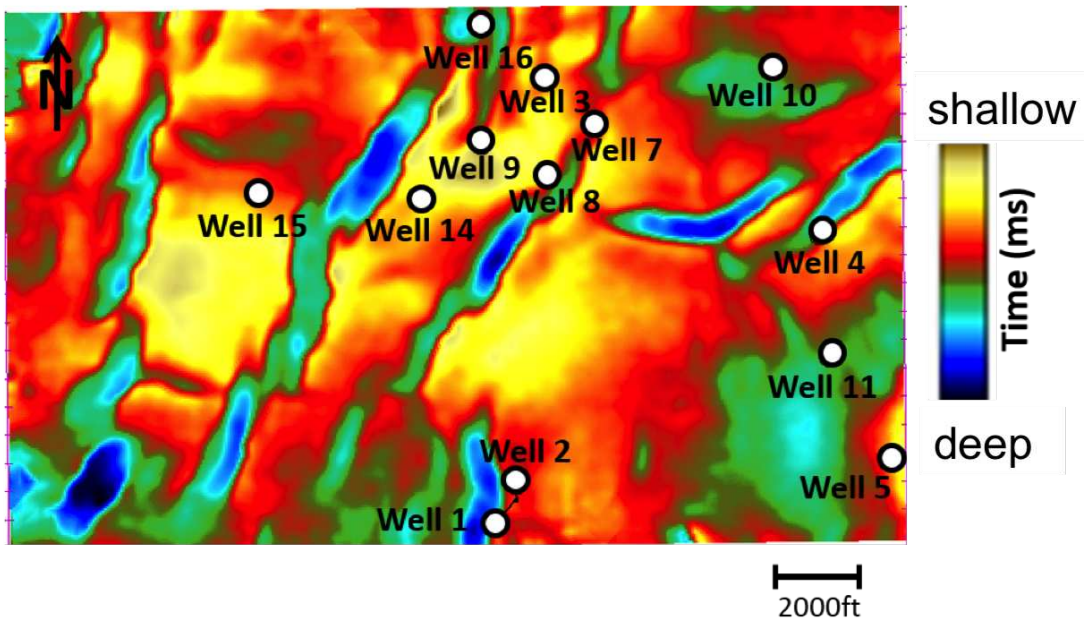

Figure 1.6: Zoomed-in Anatoli survey area with the Top Niobrara time structure map and 13 vertical wells inside the seismic survey. Well 1 on the most southern part is the only well with measured sonic logs.

that the synthetic sonic logs were calculated to a 94% accuracy.

Well 1 is the only borehole in the seismic survey that has compressional and shear sonic logs (Figure 1.6). However, this well is located at the fault zone, which makes it a challenge to correlate it with the other wells in the area. Additionally, I used two wells with cores outside the seismic survey (Core Well 3 and Core Wells 5) to validate my well log interpretations (see Figure 1.5). Figure 1.7 shows the type log from Core Well 5. These two core wells have the X-Ray Diffraction (XRD) data that supports the Rock Quality Index (RQI) calculation. The RQI estimates the optimal location for drilling and hydraulic fracturing. Facies interpretation from the well logs and cores is compared to RQI values and elastic properties to interpret the recommended intervals for drilling location.

The next chapters of this thesis detail the research work, including the facies modeling from the geology literatures and well data, facies modeling in the inter-well spaces by utilizing the seismic dataset (i.e., simultaneous seismic inversion, multi-attribute transform), the

combination of both dataset (well and seismic data) for facies modeling, and the conclusions and recommendations drawn from the research.

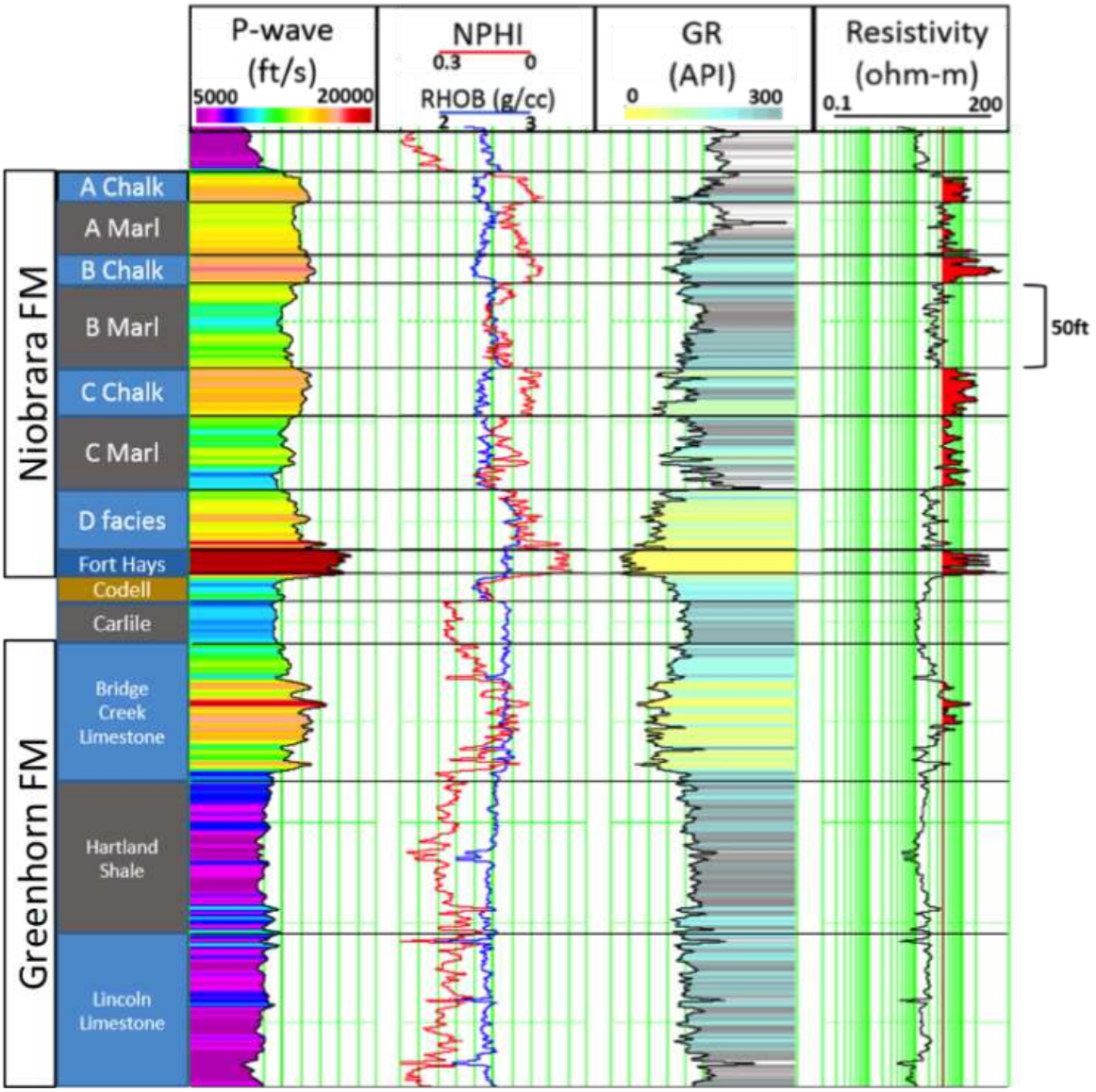

Figure 1.7: Type log of main units in Wattenberg area from Core Well 5, showing the Niobrara (A-B-C Chalks and Marls, D Facies, Fort Hays) to Greenhorn intervals (Bridge Creek, Hartland, Lincoln).

CHAPTER 2

FACIES PREDICTION FROM WELLS

Well data contain the rock properties acquired directly in the subsurface and have relatively high vertical resolution compared to seismic data. Well logging tools in general can reach approximately two feet of vertical resolution. Additionally, core analysis from wells provides the highest vertical resolution. The goal of this chapter is to predict the facies distribution of the main reservoirs in Wattenberg Field at the seismic scale. This evaluation can be useful for examining and evaluating other potential zones in addition to the Niobrara Fm. Numerous studies have been conducted prior to this research on the geology of Wattenberg and the Niobrara Fm (Sonnenberg (2013), Matthies (2014), etc). From these studies, engineers have been targeting the chalks and sandstone units in the Wattenberg as the main reservoir; however, there is ample evidence to support the marls as part of the overall reservoir. Facies prediction from the wells quantitatively defines each litho-facies based on several well log properties and compares it to the core analysis within the area.

The workflow of facies prediction from the wells in this study consists of five key steps:

1. Studying the literature of previous work on the Niobrara and Codell Sandstone reservoir, including the interpreted characteristics of each facies or lithology. Moreover, a general study of the Greenhorn interval is also examined as a prospective future target within the field.

2. Analyzing the core description of the target intervals in the area. The core description was completed by Brugioni (2017). Furthermore, the Rock Quality Index (RQI) calculation specifically on Niobrara interval is also included in this section (Mabrey, 2016).

3. Cross-plotting rock properties that are sensitive to facies characterization from the well logs.

4. Performing facies clustering by using the rock properties from the well logs. The approach used for clustering analysis is the Self-Organizing Feature Map (SOFM) algorithm.

5. Defining the optimal number of facies clusters to correlate to the facies from the core description. It is important to consider upscaling the facies definition from the well data to seismic data scale.

Each section of the workflow and the underlying theory will be elaborated in this chapter.

2.1 Facies Description From Literature

The previous chapter has provided an overview of the Wattenberg stratigraphy (see Figure 1.2). In general, several main lithologies are observed in the area:

- Niobrara - Smoky Hill Members (A Chalk, A Marl, B Chalk, B Marl, C Chalk, C Marl, D Facies)
- Niobrara - Fort Hays Limestone
- Carlile - Codell Sandstone

Additionally, a prospective future target is the lithology deposited deeper within the stratigraphy interval, the Greenhorn Fm:

- Greenhorn - Bridge Creek Limestone
- Greenhorn - Hartland Shale
- Greenhorn - Lincoln Limestone

Matthies (2014) detailed the Wattenberg main intervals (Niobrara Fm and Codell Sandstone of the Carlile Fm). Table 2.1 describes the mineralogy for each lithology. The mineralogy was analyzed using the XRD data.

Table 2.1: Mineralogy of Niobrara and Codell Sandstone (Matthies, 2014)

Lithology	**Average Mineralogy Composition**	**Additional Information**
A Chalk	(no data for the studied core with XRD samples)	mostly absent due to erosion
A Marl	50.9% carbonates, 21.8% clays, 13.0% quartz, 2.6% TOC, 11.7% other minerals	mostly absent due to erosion
B Chalk	71.8% carbonates, 10.7% clays, 7.2% quartz, 2.2% TOC, 8.1% other minerals	known important reservoir unit
B Marl	58.4% carbonates, 20.9% clays, 11.1% quartz, 2.7% TOC, 6.9% other minerals	similar to C Marl but lower TOC
C Chalk	79.2% carbonates, 7.8% clays, 4.9% quartz, 2.3% TOC, 5.8% other minerals	common drilling target
C Marl	55.4% carbonates, 16.1% clays, 12.3% quartz, 3.9% TOC, 12.3% other minerals	one of the most important source rock intervals
D Facies	48.1% carbonates, 25.1% clays, 19.8% quartz, 0.5% TOC, 6.5% other minerals	informally named unit of the Niobrara. Similar lithology to the chalk benches with very poor organic content.
Fort Hays	72.1% carbonates, 13.5% quartz, 8.8% clays, 0.2% TOC, 5.4% other minerals	-
Codell Sandstone	60.0% quartz, 20.9% clays, 2.3% carbonates, 0.6% TOC, 16.2% other minerals	known important reservoir unit

Horizontal wells commonly have targeted the chalk benches (B Chalk and C Chalk) and the Codell Sandstone. Each chalk bench within the Niobrara Fm contains a small proportion of marl deposition. Similarly, the marl benches consist of a small proportion of the chalk deposition. The A Chalk is another prospective zone, but operators have reported challenges in drilling the curved part of a horizontal well through the Sharon Springs interval (Sonnenberg, 2013). The A Chalk interval is considered not to be in the study area due to erosion. The D Facies underlying the C Marl is another specific lithology within the Niobrara interval. The categorization of the D Facies lithology was confused in previous theses as to whether it is more similar to the chalk benches or the marl benches within the Niobrara

Fm. The D Facies is identified as a basal chalk with similar lithology appearance to the other Niobrara chalk intervals. However, from the XRD data, the D Facies was found to have similar mineralogy of marls (Kamruzzaman, 2015). It has a relatively higher clay and quartz content than the chalks. The TOC for the D Facies interval is low compared to the other marls. From the combination of several rock properties, this D Facies is considered a different facies from the A, B, and C chalks and marls. Additionally, the D Facies is interpreted to be a hydraulic fracturing barrier to the Fort Hays Limestone and the Codell Sandstone. The Fort Hays limestone exhibits distinctive characteristics in the well logs, as compared to over- and underlying intervals, and is easily recognized from the significantly low gamma-ray and porosity values. Lastly, another important facies of this study is the Codell Sandstone Member of the Carlile Fm. The Codell Sandstone is a lithology with significantly different mineralogy compared to the carbonate depositions above it; hence, distinguishing the sandstone from the other facies within Niobrara is more feasible. The Codell deposition is very consistent across the Wattenberg (Matthies, 2014) and the boundary between this interval and the overlying Fort Hays is easily recognized.

Other than mineralogy descriptions from the XRD data, there are several other well logs that are typically used to define the general lithology of the Wattenberg (i.e., gamma-ray, neutron porosity, and resistivity). Since the marls of the Niobrara are the typical source rocks of the system, they contain the most organic matter, which is reflected in higher gamma-ray values. Additionally, the chalk intervals are the most brittle due to their mineralogical composition. Due to these characteristics, the chalks have undergone the most mechanical compaction causing them to have the lowest porosity, as observed from the neutron porosity log values. Resistivity logs can also be used to identify the chalk beds within the Niobrara interval, which typically have the highest resistivity values relative to the marls. However, these high resistivity values are interpreted to have more correlation to the hydrocarbon-filled fractures of the chalk beds (Sonnenberg, 2012).

In addition to the Niobrara and Codell intervals, there is a high potential future target, namely the Greenhorn Fm. This potential target is comparable to the Niobrara and a general analysis on this interval was performed. For this study, the mineralogy of the Greenhorn Fm was researched and compared for its similarity to the highly productive Niobrara intervals. The mineralogy information of the Greenhorn obtained from the Core Well 5 is summarized in Table 2.2.

Table 2.2: Mineralogy of Greenhorn from Core Well 5 data (Durkee, 2016)

Lithology	**Average Mineralogy Composition**	**Additional Information**
Bridge Creek Limestone	54% carbonates, 24.5% clays, 20% quartz, 0.5-3.4% TOC	High carbonate content, low organic content. Similar to Niobrara chalk beds.
Hartland Shale	37.5% carbonates, 36.75% clays, 20% quartz, 0.7-4.1% TOC	Potential source rock
Lincoln Limestone	31.33% carbonates, 36.33% clays, 23.75% quartz, 2.2-4.7% TOC	Known as most productive zone from vertical wells. Similar to Niobrara marl beds.

In terms of the mineralogy, the Greenhorn chalks are not as rich in carbonate content as the chalks in the Niobrara interval. The clay content is generally higher in the Greenhorn interval. However, this zone still has potential for further examination as the Greenhorn has a high organic content to be a highly productive source rock. In addition, Sonnenberg et al. (2016) stated that the Greenhorn is thermally mature in the Wattenberg Field and in deeper areas along the basin axis in the Northern Denver Basin, supporting future exploration of this interval.

2.2 Core Description and RQI Analysis from Previous Research

This section summarizes the research on the facies description from Core Well 3 data and Rock Quality Index (RQI) in Core Well 3 and 5 (location is shown in Figure 1.5). Both wells are located outside the Anatoli seismic survey area, respectively two and seven miles from the Anatoli survey to Core Well 3 and 5.

2.2.1 Facies Description from the Core

Brugioni (2017) described six main facies from cores, focused on the Niobrara interval. Table 2.3 presents the description for each facies, along with the images for each core sample for better visualization. The Niobrara formation experiences a highly heterogeneous deposition between alternating chalks and marls; hence, modeling these facies will be useful for identification of future drilling/hydraulic fracturing sweet spots.

Brugioni (2017) describes four cored wells, although Core Well 3 is the only well used for this research. Core Well 3 contains the complete core section for the Niobrara Fm and has an adequate set of logs relevant for this study. The main characteristics of the core description include the lithology, sedimentary structures, biogenic structures, and fossil content, described at a half an inch scale. The main observable characteristic used to differentiate between chalk and marl is the color change. Typically, the marls have a darker color and chalks have a lighter color. Some of the mixed zone between marl and chalk are more difficult to differentiate without a Grey Scale Chart and XRD data.

Even though this core description is an essential part of the facies modeling, the core vertical resolution (millimeter to a feet) are not resolved from the seismic inversion results. Furthermore, small scale heterogeneity is often not captured by the well logging tools, although it has a relatively lower vertical resolution than the core description. Some uncertainty related to the interpretation of the logging tools, and/or the measured depth can be found; hence, gamma-ray log is used to match the depth between the cores and other well log data. Section 2.4 presents the comparison between facies description from the core and facies from the well logs.

Table 2.3: Facies Classification and Description from Cores Analysis (Brugioni, 2017)

Facies Name	**Description**	**Core Samples**
Facies 1	***Fossiliferous Marly-Chalk to Chalk*** • Massive to slightly bioturbated • Has a high shell fragment concentration • Abundant pellets or foraminifera • occasionally has discontinuous, wavy and darker lamination	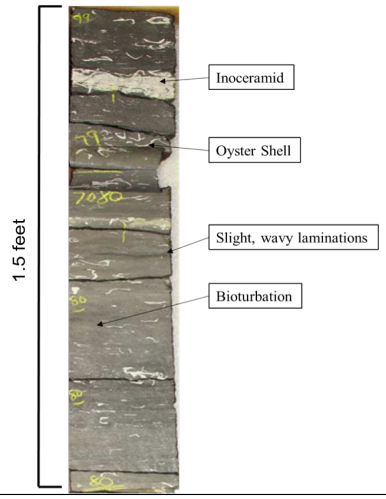
Facies 2	***Interbedded Bioturbated Marly-Chalk to Chalk*** • Dominated by bioturbated beds • Occasionally interbedded with continuous, planar, and parallel laminations • Contains pellets and foraminifera • Contains some thin bentonite ash beds	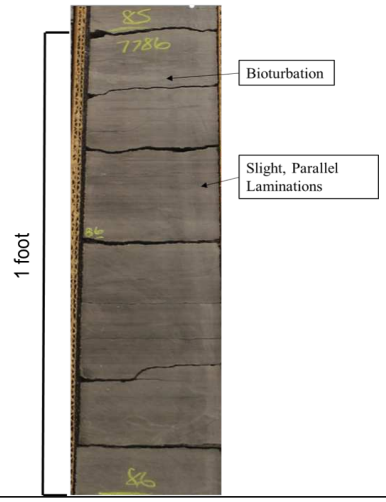
Facies 3	***Laminated Chalk*** • Interbedded series of continuous, planar, parallel laminated chalk and marl beds • Contains pellets and foraminifera • Stylolites are present • Occasional inoceramid fragments	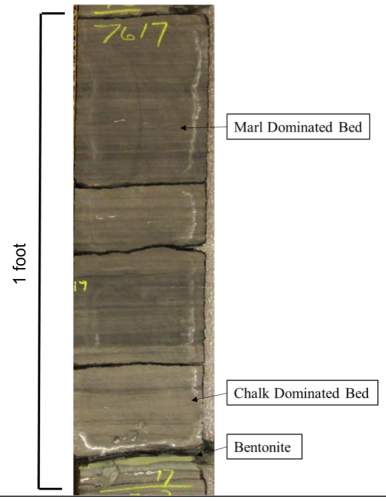

Facies 4	***Dark Gray Chalky-Marl*** • Marly-chalk to chalky-marl • Dark gray color • Dominated by marly-chalk beds that have marl-rich, continuous, planar, parallel laminations • Has the greatest abundance of pellet and foraminifera • Thin bentonite beds, inoceramid fragments, pyrite nodules	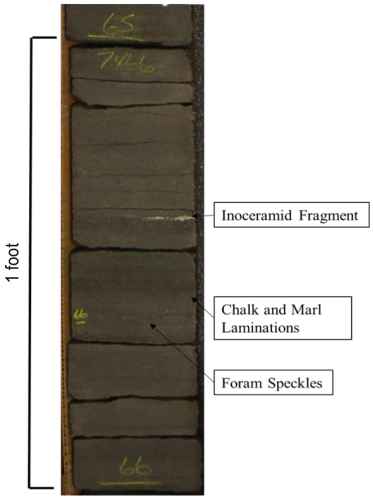
Facies 5	***Marl*** • Structureless marl • Darkest color • Rare inoceramid fragments and pyrite nodules	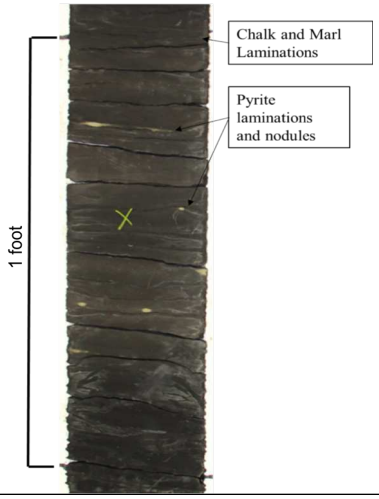
Facies 6	***Chalk*** • Purest chalk • Lightest color • Found in Fort Hays member • Massive chalk sections with heavy bioturbation • Stylolites are present • Inoceramid and oyster shell fragments • Abundant foraminifera and peloids	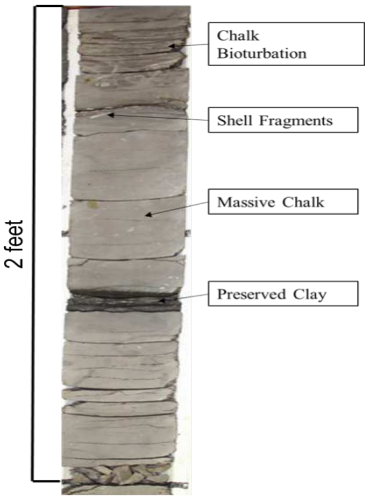

2.2.2 Rock Quality Index (RQI) Work

The RQI is a combination of rock composition brittleness, rock fabric brittleness, and stress differential to measure the optimal location for fracturing the reservoir. Mabrey (2016) developed the RQI of the Niobrara interval, using two vertical wells (Core Well 3 and Core Well 5) that have the X-Ray Diffraction (XRD) data. The data used by Mabrey (2016) for the RQI calculation include the compressional and shear sonic logs (V_p and V_s), XRD and bulk density (RHOB). Mabrey (2016) also referred to the thesis of Davey (2012), working on the Montney Shale geomechanical evaluation.

The first component of the RQI is the Brittleness Index based on the rock composition (RC_{BI}), presented in the Equation 2.1. This component is a function of mineralogy that has been adjusted to accommodate the Niobrara mineralogy. The numerator is determined by the stiffest minerals: quartz, calcite, pyrite, and plagioclase. In addition, the denominator of the fraction is determined by the clay content and TOC. With the relationship shown in Equation 2.1, higher content of stiff mineral within the rock will increase the RC_{BI} and higher clay content and TOC will decrease the RC_{BI}.

$$RC_{BI} = \frac{V_{quartz} + V_{calcite} + V_{pyrite} + V_{plagioclase}}{(V_{clay} + V_{others})(1 - TOC) + TOC} \tag{2.1}$$

The second component of the RQI is the Brittleness Index based on the rock fabric (RF_{BI}), shown in Equation 2.5. This index was derived from the unconfined rock strength (C_0), maximum past effective vertical stress ($\sigma_{v(max)}$), present day effective vertical stress (σ_v) and Over-Consolidation Ratio (OCR). Equation 2.2 defines C_0, which is a function of P-velocity (V_p).

$$C_0[MPa] = 0.77V_p[km/s]^{2.93} \tag{2.2}$$

This empirical relationship between C_0 and V_p is based on the laboratory rock strength tests with core data. V_p was determined to have an empirical relationship with σ_{vmax}, demonstrating that V_p increases with σ_{vmax}. The available V_p logs are then converted to C_0 (Equation 2.2) in order to convert sonic velocity values in terms of stress and pressure units

(Equation 2.3). The value of C_0 was derived from the V_p well logs. The RF_{BI} empirical relationships (Equation 2.5) have been determined from laboratory tests for seal leakage in shales and mudrocks.

$$\sigma_{v(max)}[MPa] = 8.6C_0[MPa]^{0.55} \tag{2.3}$$

$$OCR = \frac{\sigma_{v(max)}}{\sigma_v} \tag{2.4}$$

$$RF_{BI} = OCR^{0.89} \tag{2.5}$$

The last component of the RQI is the normalized stress differential ($\Delta\sigma$), shown in Equation (2.7). The normalized stress differential is calculated from the overburden maximum vertical stress (σ_v) and minimum horizontal stress (σ_h).

$$\sigma_h = \frac{PR}{1 - PR}(\sigma_v - Pp) + Pp \tag{2.6}$$

$$\Delta\sigma = ln[Norm(\sigma_v - \sigma_h)] \tag{2.7}$$

The σ_h is a function of Poisson Ratio (PR), σ_v and pore pressure (Pp), shown in Equation (2.6). With an increase of Pp in the reservoir, due to the initiation of hydraulic stimulation, σ_h will increase at about a rate of two-thirds of the Pp increase (Davey, 2012).

The value of RQI is calculated by

$$RQI = RC_{BI} + RF_{BI} - \Delta\sigma \tag{2.8}$$

With this relationship, a high value of RQI would indicate an ideal reservoir for hydraulic fracturing: high brittleness, low clay content, relatively high TOC, and low stress differential.

The RQI value indicates rock quality and geomechanical factors of the reservoir intervals; hence, correlating RQI to the facies characterization supports the recommendation for potential future targets for field development.

2.3 Facies Clustering from the Well Logs

In this study, there are 17 vertical wells inside and outside the Anatoli seismic survey that have been used for the input of clustering analysis. Prior to performing the clustering, the

sensitivity of each well log property was tested by creating cross-plots of elastic properties (P- vs. S-impedance) from three wells (Well 1, Core Well 3, and Core Well 5). These three wells are considered the key wells for this research due to the relevant data availability and geographic location (Table 2.4).

Table 2.4: Data Availability on Main Wells

Wells	**Cores**	**XRD**	**Measured** V_p	**Measured** V_s	**Location**
Well 1	-	-	✓	✓	inside Anatoli
Core Well 3	✓	✓	-	-	2 miles from Anatoli
Core Well 5	✓	✓	✓	✓	7 miles from Anatoli

The cross-plots were then color-coded by each well log property, to determine which can be used to characterize the reservoir interval facies. Figure 2.1 shows examples of the initial cross-plots generated for this study. From the cross-plots and observation of each well section, it was determined that the gamma-ray, resistivity, density, and neutron porosity are the well log properties that can be used to discriminate each facies within the whole formation. Clear trends (non-scattered) of each log properties are observed as the value of P- and S-impedance change. For example, P- and S-impedance cross-plot shows that higher impedance correlates to lower density, lower clay and organic content (reflected on gamma-ray values), very resistive and less porous lithology.

Clustering analysis was done in order to create facies logs from the top of Niobrara to the base of Codell Sandstone, although the main focus is to model the heterogeneous deposition of alternating chalks and marls within the Smoky Hill Member. The facies log defines vertical distribution of each particular lithology that has a similar value range to the input logs, along the target zone. The input for the clustering analysis includes compressional and shear sonic, density, resistivity, gamma-ray, and neutron porosity logs; the calculation uses the algorithm of Self-Organizing Feature Map (SOFM) within MATLAB programming software.

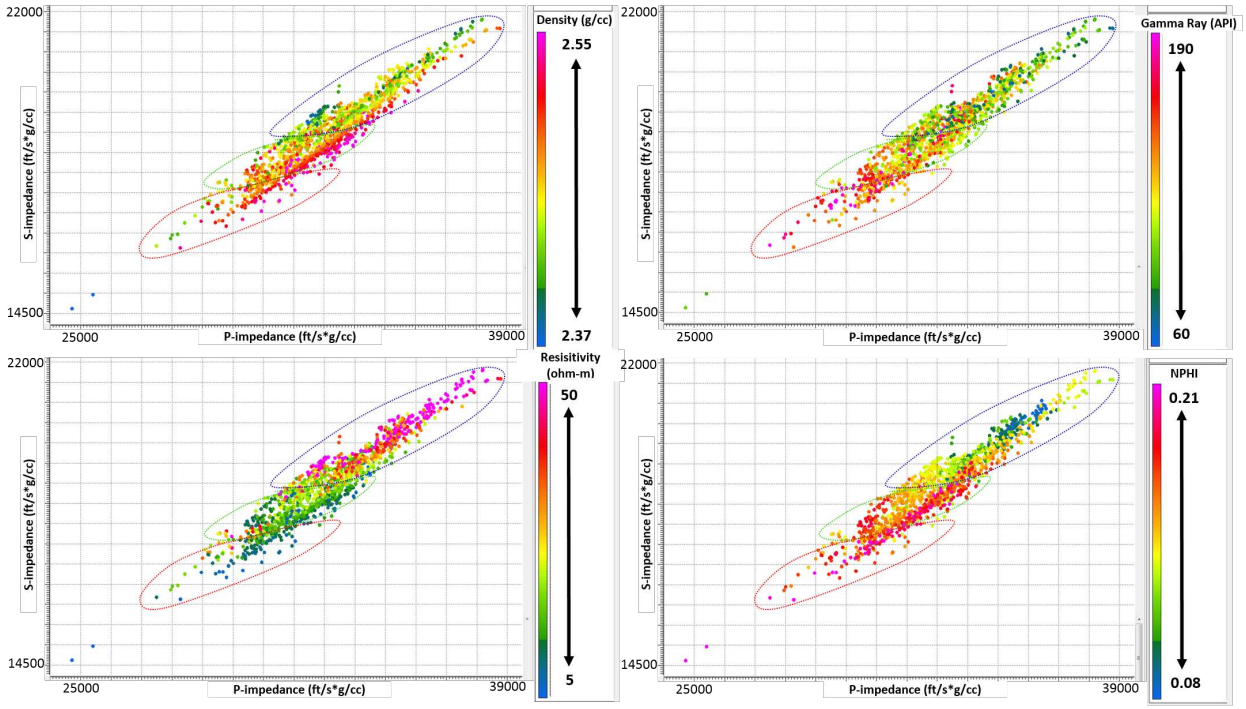

Figure 2.1: P- vs S-impedance cross-plots from three main wells, color coded by well log properties. The input data is from the Smoky Hill Member of the Niobrara interval. The drawn polygons for each cross-plot emphasizes the trend of log values that support facies characterization.

SOFM is a type of machine learning tool used to identify and analyze local clusters in a data set in an unsupervised fashion. Machine learning is a field of computer science where computers have the ability to learn without being explicitly programmed. Moreover, the term unsupervised itself means that the algorithm trains data samples that are not labeled by their category, which is commonly chosen to minimize computational cost (Duda, 2001). SOFM essentially converts complex, non-linear statistical relationships between high-dimensional data items into simple geometric relationships on a low-dimensional display. Another known type of unsupervised learning method is K-means clustering. However, the K-means clustering is sensitive to initialization, hence specifying the number of clusters in advance is needed. In contrast, the SOFM algorithm organizes the local clusters and gives an output of several clusters (Kohonen, 1990).

By comparing different numbers of clusters and previous facies interpretations from core description, I determined that six clusters are the optimal number of facies to define the Niobrara to Codell zone. The Smoky Hill Member of Niobrara in particular is divided into three main facies which are the pure chalk, pure marl, and mixed marl and chalk. The value ranges of the well log properties for these three facies are listed in Table 2.5.

Table 2.5: Well log values of three clustered facies within Smoky Hill Member

Facies	Vp(ft/s)	Vs(ft/s)	RES(ohm-m)	NPHI(%)	RHOB(g/cc)	GR(API)
Pure Marl	11100 -12500	6100 - 7400	0 - 40	15 - 28	2.46 - 2.62	100 - 250
Mixed Marl-Chalk	12200 - 14300	6900 - 8300	0 - 40	10 - 23	2.44 - 2.60	80 - 200
Pure Chalk	13300 - 15400	7700 - 8700	20 - 110	8 - 20	2.38 - 2.58	50 - 170

Moreover, the relationship between the calculated RQI and velocity shows that the rock with high quality has a relatively higher P- and S-wave velocity, which is reflected in high P- and S-impedance values (see Figure 2.4). This observation confirms that we are able to model the most chalky part of the Smoky Hill Member as the targeted interval for future hydraulic fracturing locations by its elastic properties. Three remaining facies below the Smoky Hill Member are clustered as the D Facies, Fort Hays Limestone and Codell Sandstone. Another consideration in choosing the number of clusters or facies is that we will need to eventually upscale the well information to the seismic scale. Therefore, it is important to define the number of facies that optimally characterize the rocks, but will still be resolved by seismic inversion.

2.4 Integration between Cores Description, Facies Clustering, RQI and Elastic Properties

Facies logs from all input wells were created by performing the cross-plot analyses and facies clustering discussed in the previous section. Calculated facies were then correlated back to the facies from core description to understand what actual rock composition is included into each defined facies log. Figure 2.2 shows the Core Well 3 with the input well logs for the clustering analysis, the facies clusters, and facies core description from the B

Chalk to the C Marl. From this well section view, we observe the correlation between the facies log and the other well logs used for the clustering analysis. It is also observed that most of the identified marls from the wells are clustered as the mixed marl and chalk facies (green color code). This observation indicates that every marl unit penetrated by the wells contains a fair amount of chalk. The interpretation is also supported by the core, that the marliest part of the Smoky Hill Member from the Core Well 3 exhibits more heterogeneity and bioturbation. The C Marl interval in particular shows strong correlation between the high intensity of alternating chalk-marl deposition from the clusters and the core facies. On the other hand, the zones with dominant chalk facies are slightly more homogeneous. This comparison between the well log interpretation and the core interpretation provides an understanding of heterogeneity observed in rocks compares with the well log dataset. It is recommended to perform a similar type of description to the Core Well 5 in the future, to get more samples for the interpretation.

There are 13 vertical wells inside the seismic survey that were used for seismic inversion. However, only 1 well has the measured compressional and shear sonic logs. The rest of the wells have synthetic compressional and shear sonic logs from a neural network prediction. The compressional sonic, shear sonic and density logs are the essential components to generate the elastic properties from the wells. From the seismic data, elastic properties such as P-impedance, S-impedance, and density can be estimated from pre-stack seismic inversion. However, the estimation of density from seismic data is challenging due to offset or angle limitation from the limited seismic acquisition aperture. Figure 2.3 shows the correlation between the P- and S-impedance values to the facies from clustering. From this cross-plot, a Probability Distribution Function (PDF) can be successfully created for each facies (marl, mixed marl-chalk, chalk) that will eventually be applied to the seismic inversion result in this thesis. A clear separation for each facies cluster by its P- and S-impedance supports the motivation for performing simultaneous seismic inversion work.

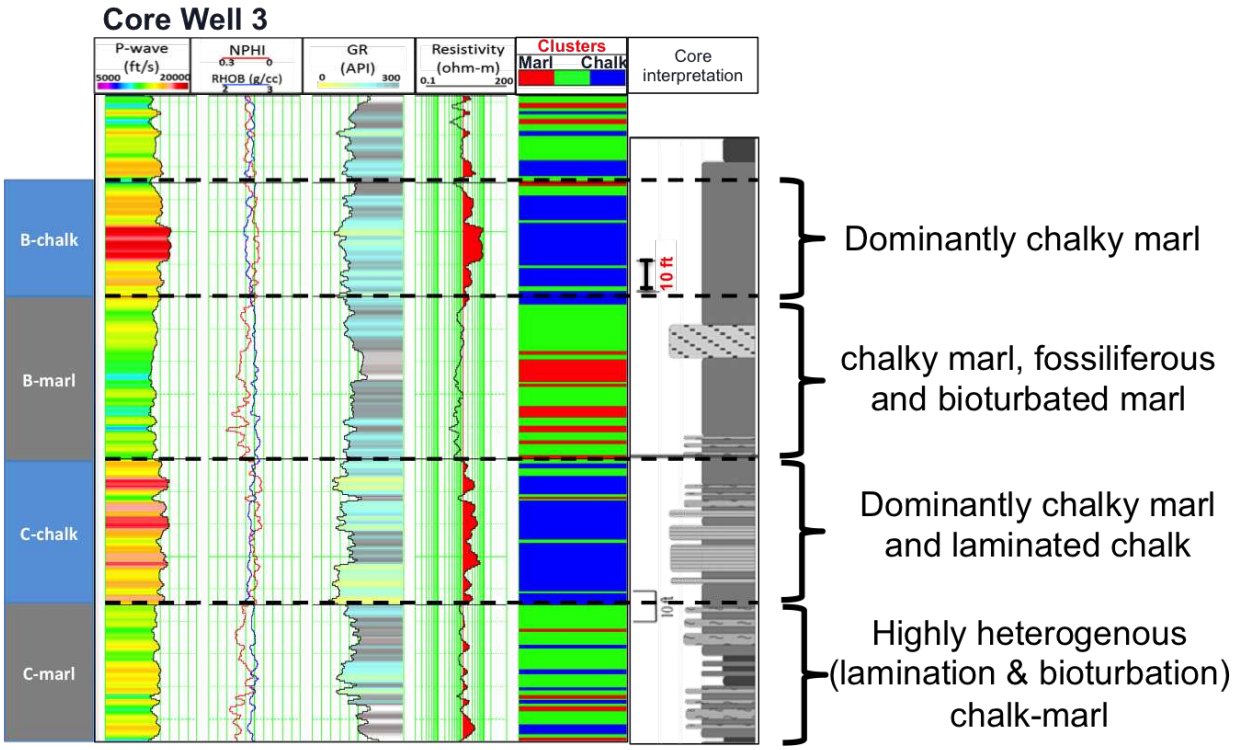

Figure 2.2: Core Well 3 section, comparing the main well logs being used for the facies clustering, the facies clusters, and the core interpretation. Core data were described by Brugioni (2017). Details of each core facies are presented in Table 2.3.

The final section of this chapter correlates the Rock Quality Index (RQI) information with the facies clusters and elastic properties. Figure 2.4 shows the cross-plots of P-impedance vs. RQI and S-impedance vs. RQI, color coded by facies. Core Well 3 and Core Well 5 were used to create this cross-plot, as those are the only vertical wells that have XRD data for RQI calculation. From this cross-plot, we observed that the chalk facies from the clustering have the highest RQI compared to the other facies, and it is also related to the highest P- and S-impedance values from well data. The P- and S-impedance values will be estimated from seismic inversion process, allowing us to model the lateral distribution of the chalk as the most targeted facies for hydraulic stimulation. These elastic properties (P- and S-impedance) will be obtained by elastic seismic inversion, as discussed in the next chapter.

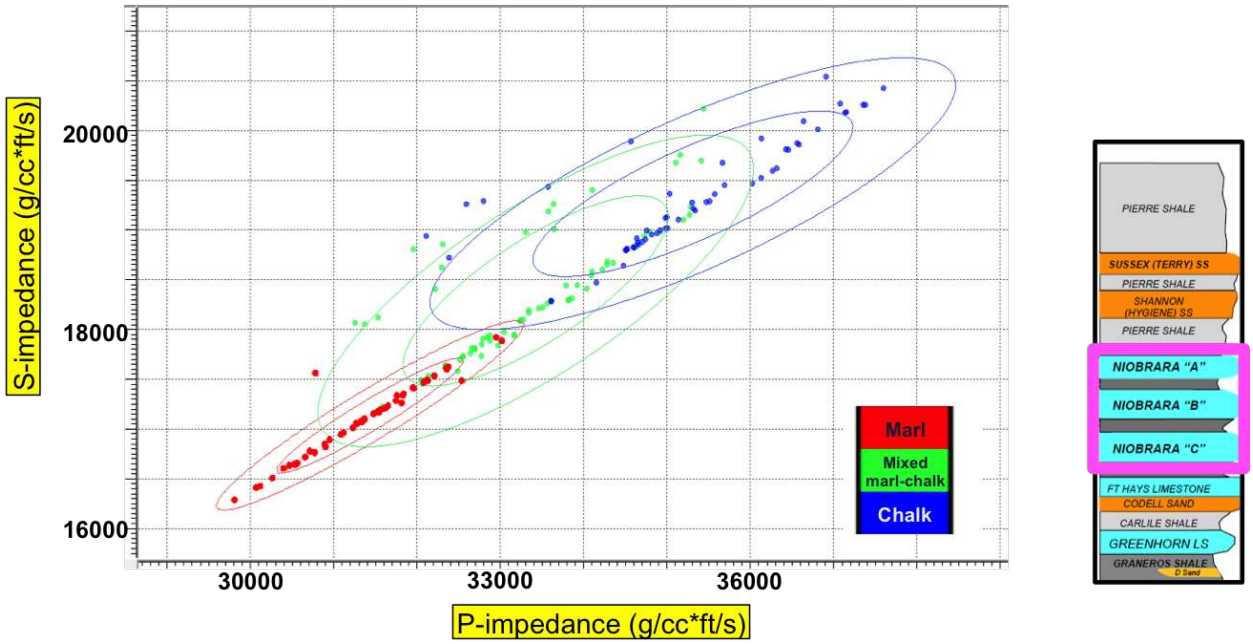

Figure 2.3: Cross-plot of P- vs S-impedance values from 13 vertical wells inside the 3D Anatoli seismic survey, color coded by the facies from clustering analysis. The ellipses represent fitted PDF for every facies, with the maximum (bigger ellipses) and minimum (smaller ellipses) PDF ranges. The input interval is highlighted (pink) in the stratigraphic section view.

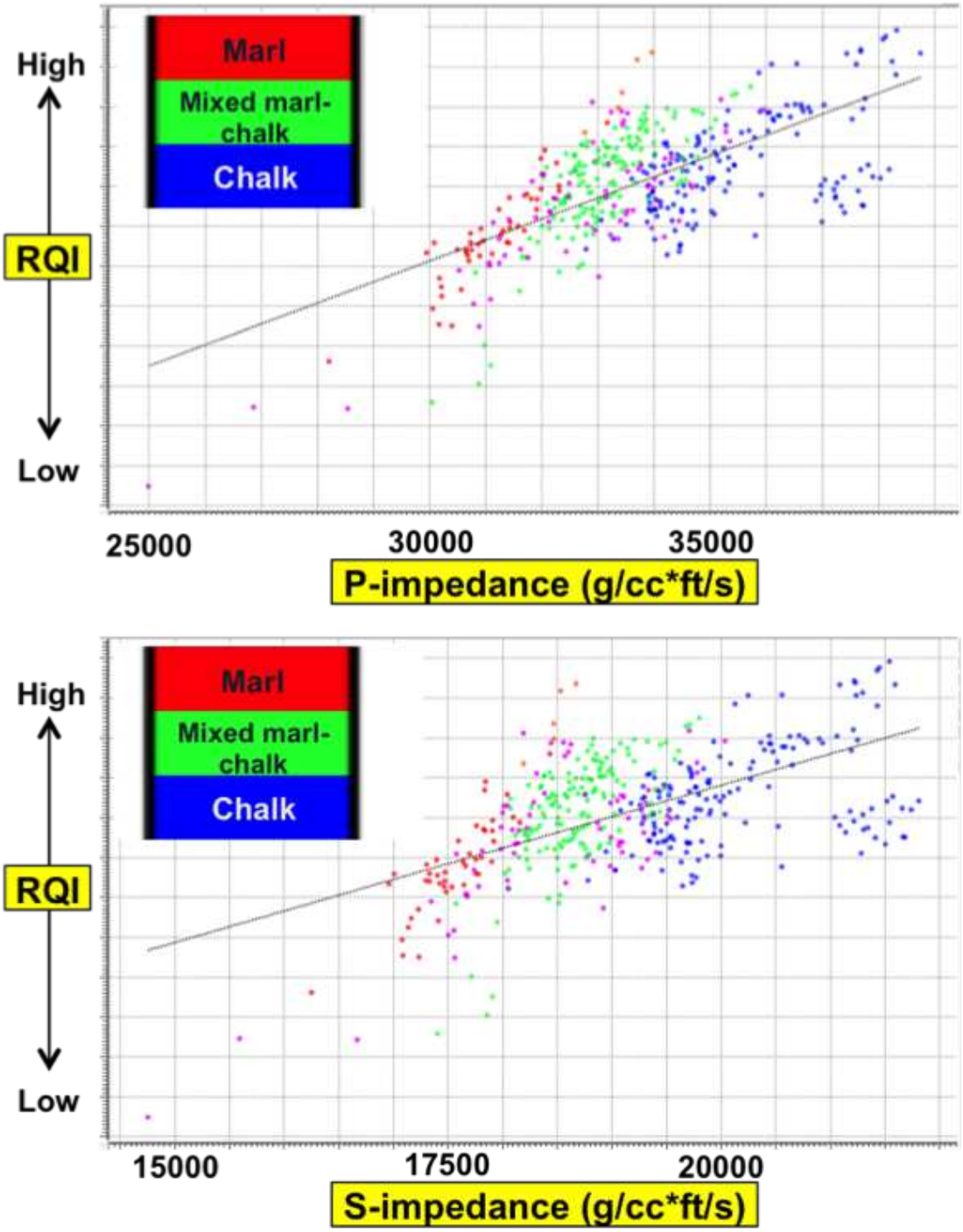

Figure 2.4: Cross-plot of P- and S-impedance vs RQI, color coded by the facies from clustering analysis. Linear relationship between higher RQI to higher impedance values is observed.

CHAPTER 3

SIMULTANEOUS SEISMIC INVERSION

Simultaneous seismic inversion is a type of inversion process that inverts for elastic properties simultaneously using pre-stack seismic data, angle gathers or partial angle stacks. With sufficient angle ranges ($\approx$>45°), it is possible to invert seismic data for P-, S-impedance, and density. However, the density property is the most difficult parameter to invert from the seismic data, as its contribution to the the overall seismic amplitude is small and only discernible on large angles. It is more common and applicable to invert the seismic data into two elastic properties, the P- and S-impedance. In general, more than one elastic property is required for discriminating between different facies. I have shown that the facies within the Wattenberg Project can be better distinguished by using the combination between P- and S-impedance. This is the reason for performing simultaneous seismic inversion in this thesis.

The seismic data used for this research have been discussed in Section 1.3.1, along with several other seismic datasets available for the Wattenberg project. On the Wattenberg project timeline (Figure 3.1), the Anatoli 3D/3C acquisition took place after the horizontal well drilling in the Wishbone Section, but before the hydraulic fracturing and well completion. Hence, the facies modeling of the 3D Anatoli represents the in-situ condition of the reservoir.

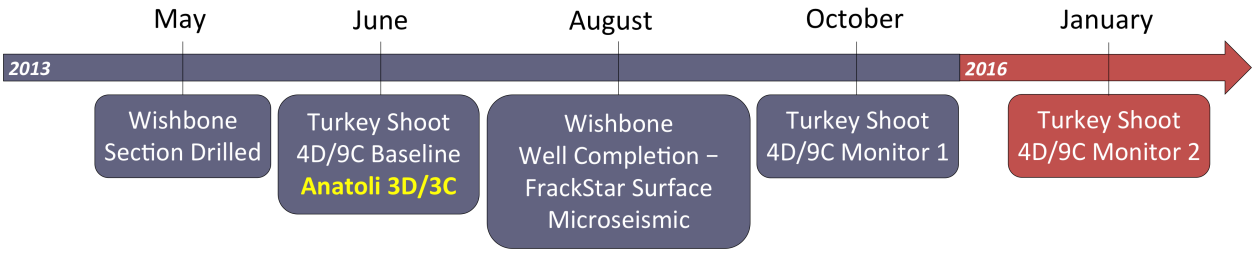

Figure 3.1: Wattenberg project timeline, highlighting the Anatoli 3D/3C seismic acquisition which took place at the same time as the acquisition of 4D Turkey Shoot baseline.

Before describing the seismic inversion work, I explain the data processing and conditioning parameters that have been applied to prepare the seismic dataset.

3.1 Seismic Data Processing

Anadarko Petroleum Corporation (APC) and Reservoir Characterization Project (RCP) jointly acquired the Anatoli 3D survey in mid-June to July 2013. It is a 3D/3C seismic survey covering a 10 square mile area, that encompasses the Turkey Shoot time-lapse seismic survey area. Sensor Geophysical Ltd. processed the seismic data in September 2014. The acquisition parameters and processing steps were adequately retrieved from the seismic file headers and theses of former RCP students: White (2015), Motamedi (2015), and Butler (2016). The Anatoli 3D seismic survey was acquired similarly to the Turkey Shoot Baseline and the geometries of shot and receiver pairings were cropped to match the Turkey Shoot Monitor 1 survey (White, 2015). Acquisition parameters for the Anatoli Survey were adapted from those of the Turkey Shoot dataset (see Table 3.1).

Table 3.1: Acquisition Parameters for Anatoli Survey (modified from Motamedi (2015))

Acquisition Parameters	**Details**
Sample Interval	2ms
Source Type and Sweep	Vibroseis, 4 sweeps of 18 seconds
Receiver Type and Azimuth	Vectorseis Geophones, single 3 component, true north azimuth
Source Line Spacing	880 ft
Receiver Line Spacing	660 ft
Source Point Interval	110 ft
Receiver Point Interval	110 ft

The seismic processing steps are summarized in Table 3.2. The processing was identical to that applied to the Turkey Shoot seismic dataset, except for the cross-equalization step that is important for time-lapse seismic dataset. The significant parts to highlight from the processing are the statics correction, Common Offset Vector (COV) Regularization, Normal Move Out (NMO) and Pre-Stack Time Migration (PSTM). The static corrections

were calculated and corrected to compensate for the near-surface velocity variation. There were two statics applied to the seismic data, refraction statics and residual statics. The refraction statics used long-wavelength statics with the intention to remove false structures (for example: sagging or structural distortion due to shallow buried channel). The residual statics used short wavelength statics and was intended to remove trace-to-trace time shifts. Common Offset Vector (COV) binning was done to the dataset to preserve both offset and azimuth information from the seismic data set, which is particularly useful for an azimuthal attribute analysis. This azimuthal variance on the dataset could be caused by the anisotropy of the reservoir section and/or the overlying sections. For this research, I analyze the dataset using an isotropic approach; hence, the azimuthal variance is not taken into consideration. NMO correction is a part of processing sequences that manages the seismic travel time variance with offsets.

The last significant part of the seismic processing is the migration, which is essentially an attempt to reconstruct the location of the event occurring in the subsurface. For the Anatoli seismic dataset, an azimuthal compliant Kirchhoff PSTM has been performed with layer anisotropic and surface consistent factors being considered.

3.2 Seismic Data Conditioning

In order to prepare the seismic data for inversion, we need to apply several additional processes to enhance the signal-to-noise ratio (S/N) of the data. The signal-to-noise ratio (S/N) enhancement or noise attenuation is commonly already applied in the seismic processing workflow; however, some of the noise attenuation are not applied too aggressively, in order to preserve the amplitude. Seismic data conditioning is an additional process for the purpose of utilizing the dataset (e.g., seismic interpretation, seismic attribute analysis, seismic inversion). Iterative testing and comparing the seismic data before and after conditioning processes were completed during this research in order to define the most optimal parameters for each step.

Table 3.2: Processing Steps for Anatoli P-wave Seismic Gathers (modified from White (2015) and Butler (2016))

Processing Step	**Parameters**
Reformat	Record Length: 4.0 seconds Sample Interval: 2.0 milliseconds
3D Geometry Assignment	55 ft by 55 ft 3D CDP Binning match Turkey Shoot Monitor 1 geometry
Amplitude Recovery	Spherical divergence correction +4 dB/second Gain
Sinusoidal Noise Filter	60 Hz notch filter
Trace Edits and Mutes	Singular-Value Decomposition filter to remove surface generated noise
Surface Consistent Deconvolution (Spiking)	Operator Length: 100 ms Prewhitening: 0.1%
Vibroseis Deconvolution Compensation	
Refraction Static Corrections (Long Wavelength)	Datum: 5200 feet Replacement Velocity: 9000 feet/second 2 layer analysis
Surface Consistent Statics 1 (Short Wavelength)	Maximum Shift: 24 ms Window: 400-2200 ms
Surface Consistent Amplitude Scaling	
Velocity Update 1	
T-F Adaptive Noise Suppression	
Offset Consistent Gain Control	
Surface Consistent Statics 2	Maximum Shift: 24 ms Window: 400-2200 ms
Velocity Update 2	
3 Term Moveout	Time Variant η
Common Offset Vector (COV) Binning	COV Regularization COV F-XY Deconvolution
COV Techco Pre-stack Summig Time Migration	Azimuthal Compliant Kirchhoff Migration Anisotropic Surface Consistent
Sort and Shift to Final Datum	
Sector for Output	CDP, Angle, Azimuth

To prepare the Anatoli P-wave seismic survey for simultaneous inversion work, I applied the following data conditioning processes using the Hampson Russell software package:

1. *Parabolic Radon Transform (PRT) for noise suppression.* This step was applied to the Common-Image-Point (CIP) Gathers to enhance the S/N. The PRT essentially transforms the CIP gathers from the travel time vs. offset domain to the τ-p domain and identifies the random noise and multiples in the data. For the dataset I use, multiples are not considered as a major issue; hence, the main goal is to suppress the random noise. Some parameters were set for the data optimization, while still preserving the relative amplitudes of the data. These parameters include time difference (ΔT) from low value of -120 ms to high value of 110 ms. Desired N/S was set to be 0.15. Figure 3.2 illustrates the CIP gather after parabolic radon noise suppression and the residual of the dataset before and after the conditioning process.

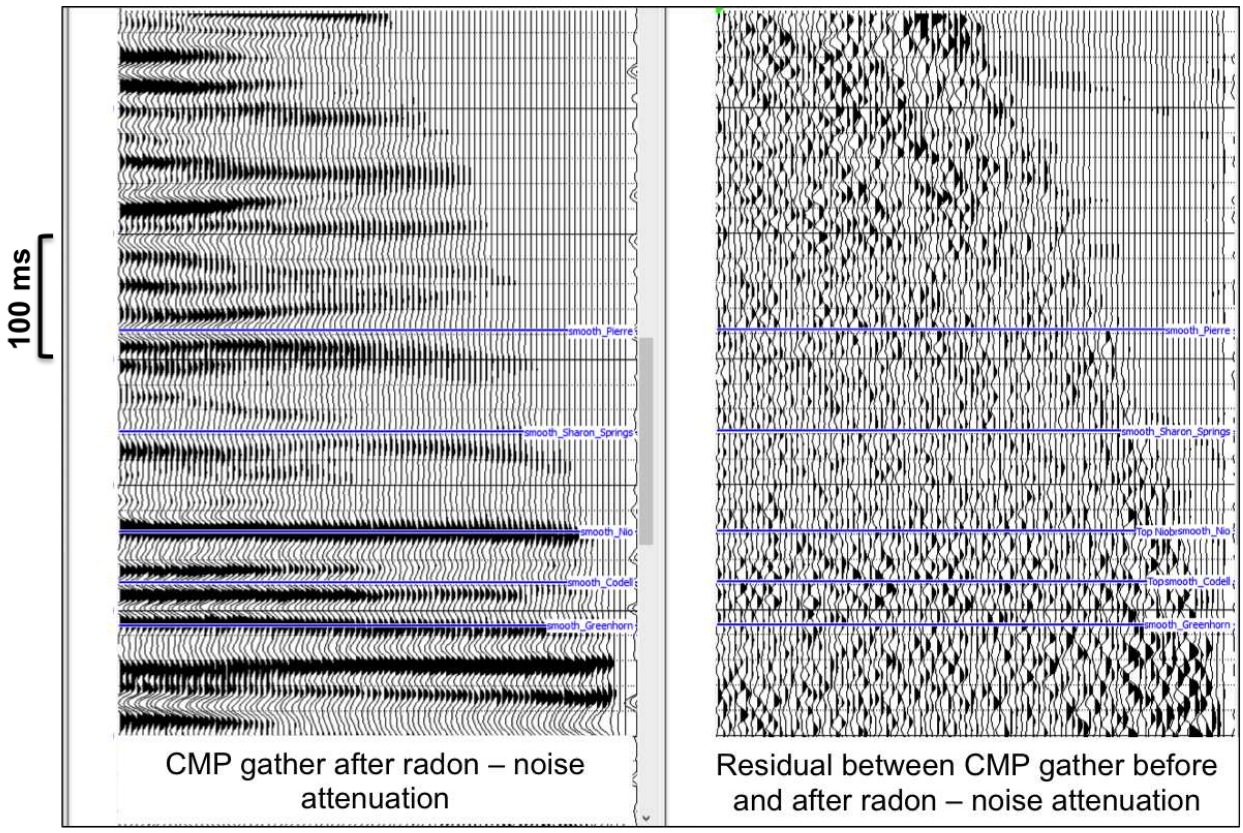

Figure 3.2: An example of the Radon noise attenuation result in one CIP gather within the seismic dataset. The image on the right is the residual between the CIP gather before and after the conditioning, showing that the attenuation was focusing on random noise while preserving the seismic signals.

2. *Trim statics.* With a proportional trim statics operator applied in the offset domain after migration, the CIP gathers are aligned to correct residual errors in the migration velocity model. An 800 ms window that encompasses the reservoir interval was set for the trim statics process. Figure 3.3 shows the difference between the CIP gathers before and after trim statics process.

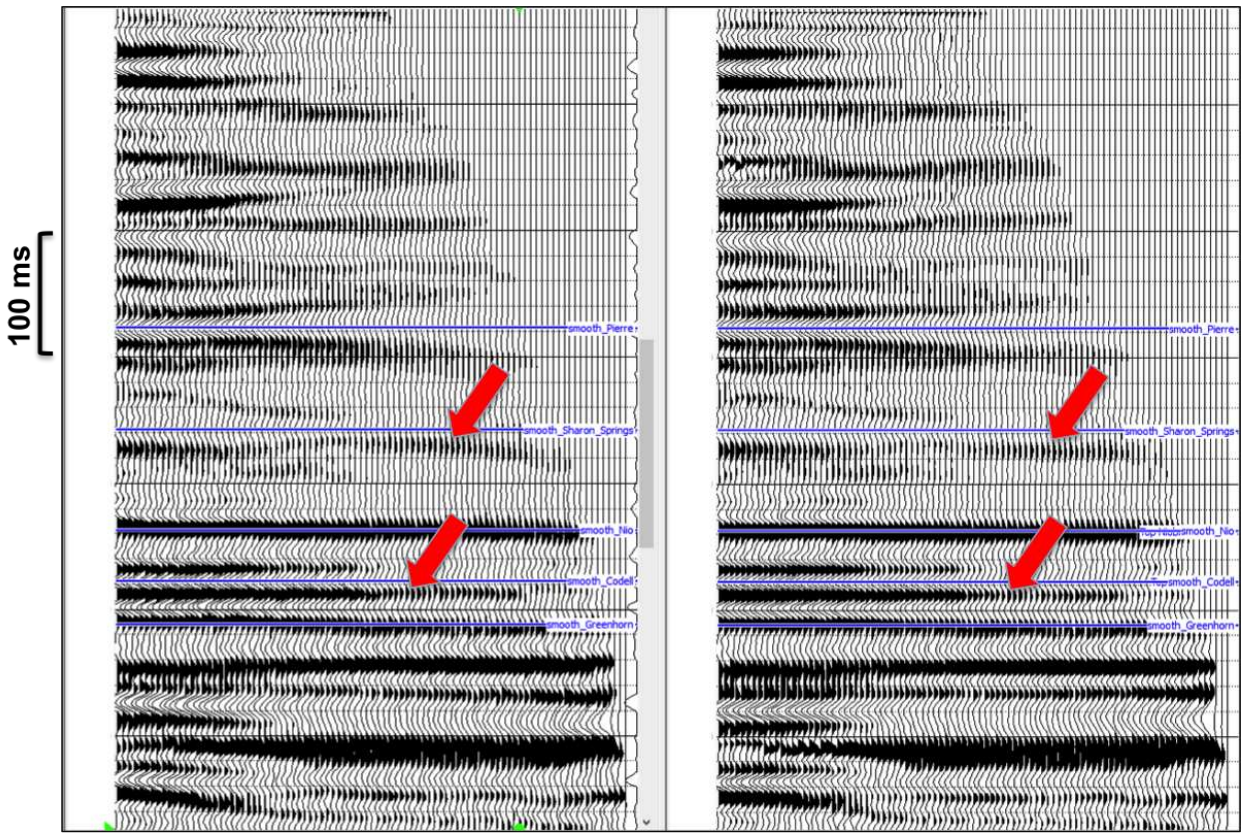

Figure 3.3: Representative CIP gather before (left) and after (right), applying trim statics conditioning process. Note the slightly more flat reflectors on the right image, highlighted by the red arrows.

3. *Offset-to-angle gather conversion.* The conversion from offset to angle is not a conditioning process; rather, it is required to prepare the dataset for inversion. Figure 3.4 shows the fold map of the 3D Anatoli P-wave seismic survey. Some wells within the seismic survey area are located close to the edge that has a significantly low acquisition fold, in which the far-angles are non-existent for performing the well-to-seismic

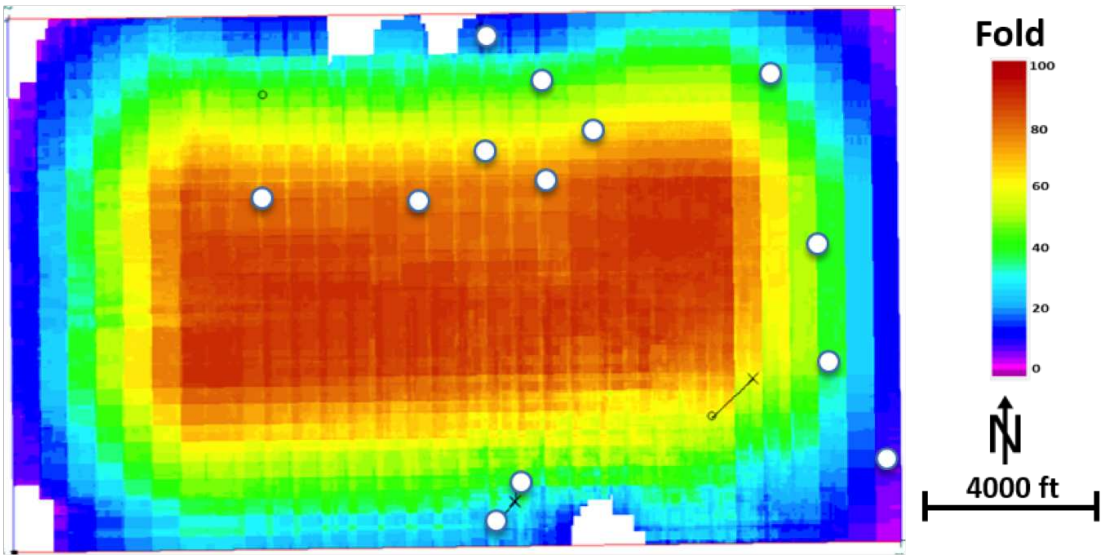

Figure 3.4: Fold Map of the 3D Anatoli P-Wave CIP gathers, overlain by all vertical wells within the survey. Some wells are located on the edge of the seismic survey, where the seismic acquisition fold is very low.

tie. Conversion from the offset to angle domain uses the velocity information, which is the interval velocity from the migration process. From Figure 3.5, it is observed that the maximum reflection angle at the reservoir interval is approximately 45°.

4. *Partially stacking seismic angle gathers.* The final step is to stack the seismic angle gathers into four different angle ranges: 5-14° (near stack), 15-24° (mid-near stack), 25-34° (mid-far stack), and 35-44° (far stack). This step prepares the seismic dataset for seismic inversion. Figure 3.6 shows the alignment of each angle stacks, which is an important QC before using the data for inversion.

After seismic conditioning of the data, I describe the main workflow of the seismic inversion and the theories behind it in the next section.

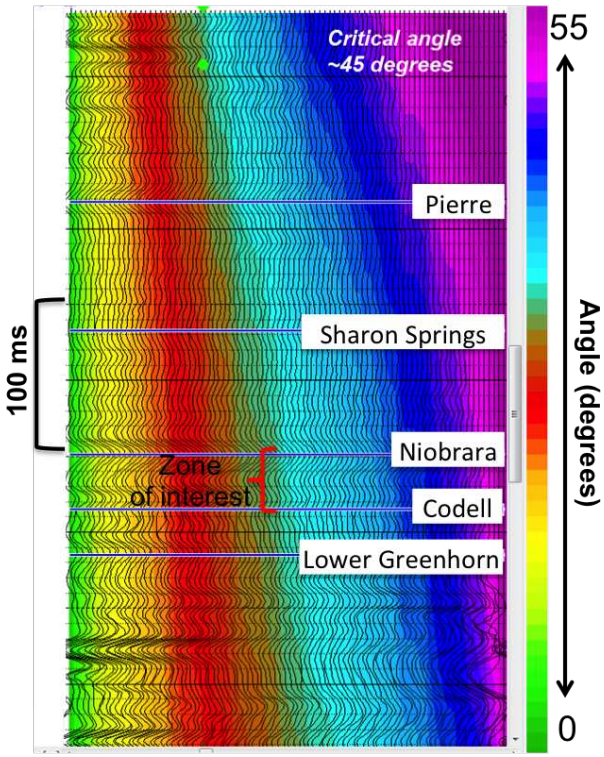

Figure 3.5: An example of one CIP gather, color coded by the reflection angle of the dataset. This image shows that the zone of interest has the critical angle of approximately 45°.

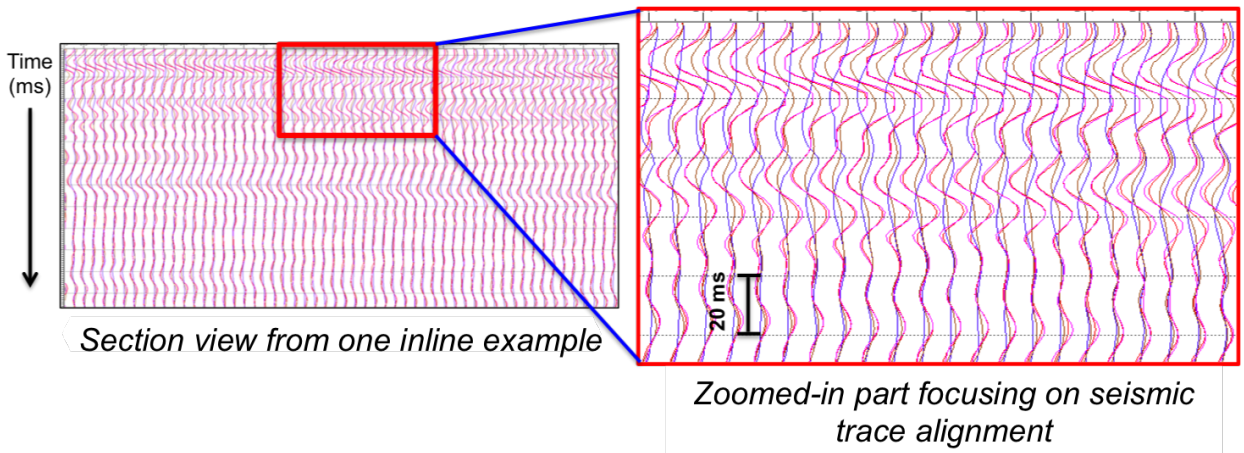

Figure 3.6: The alignment of each angle stack; near, mid-near, mid-far, far stacks, shown in one section view in different seismic trace colors. Frequency difference is observed due to wavelet stretch, but good time alignment is observed.

3.3 Simultaneous Seismic Inversion

The opening part of this chapter outlines the steps prior to performing the simultaneous seismic inversion. This section details the basic theory behind pre-stack seismic inversion and the workflow. From the petrophysical analysis in Chapter 2, observations of the lithology and its sensitivity to the elastic properties are obtained. The next step is to estimate the elastic properties that relate to the facies prediction from the seismic data. Seismic data are the only dataset covering the whole study area and regionally with a high lateral resolution compared to the well data. By performing simultaneous inversion of the pre-stack data, the elastic properties allow us to predict the lithology distribution.

3.3.1 Basic Theory

The pre-stack seismic inversion for the 3D Anatoli P-wave seismic survey was performed using the CGG-Jason software, with a constrained sparse spike algorithm. At each CIP gather, the seismic data are modeled as the convolution of a set of reflection coefficients with one or more wavelets (CGG-Jason, 2015a). The reflection coefficients are derived from the elastic parameters using the Aki-Richards approximation. Figure 3.7 illustrates the relationship between impedance, reflectivity, and seismic trace, which gives a better understanding of the concept of forward modeling (from geological model to seismic trace). In contrast, the inverse process is seismic inversion (from seismic trace to estimated geological model). In addition to the wavelet removal process from the seismic data to estimate the geological model, a priori information from the known geology (from the well logs) is used in the process. The priori information is used to generate the Low Frequency Model (LFM). In the seismic inversion process, we need to build an LFM because the wavelet we use is a band-limited wavelet which does not contain low frequencies. There are infinite geological solutions that would match the seismic traces, hence a priori information is essential for the inversion process.

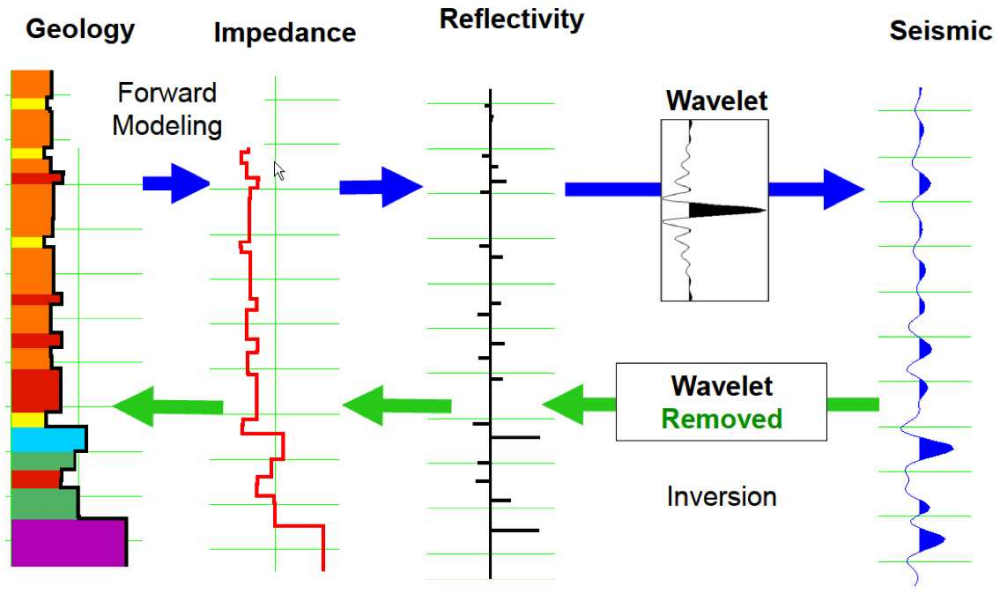

Figure 3.7: Illustration of the relationship between the geology model and the seismic trace showing forward modeling and inversion. For forward modeling, the reflectivity is convolved with a wavelet to create a seismic synthetic, while for seismic inversion, the wavelet is removed from the seismic trace to estimate the possible geological model in the subsurface (Russell, 2014).

The goal of performing pre-stack seismic inversion is to obtain a reliable estimation of P-wave velocity (V_p), S-wave velocity (V_s), and density (ρ), to predict the fluid and lithology properties. Simmons and Backus (1996) invert for linearized P-reflectivity (R_p), S-reflectivity (R_s), and density reflectivity (R_D), defined as:

$$R_P = \frac{1}{2}\left[\frac{\Delta V_p}{V_p} + \frac{\Delta \rho}{\rho}\right] \tag{3.1}$$

$$R_S = \frac{1}{2}\left[\frac{\Delta V_s}{V_s} + \frac{\Delta \rho}{\rho}\right] \tag{3.2}$$

$$R_D = \frac{1}{2}\left[\frac{\Delta \rho}{\rho}\right] \tag{3.3}$$

Additionally, the P-impedance (Z_p) and S-impedance (Z_s) are defined as:

$$Z_p = \rho V_p \tag{3.4}$$

$$Z_s = \rho V_s \tag{3.5}$$

Combining all of the equations above, the P-wave reflectivity (R_p) can be approximated by

$$R_{pi} \approx \frac{1}{2}\Delta lnZ_{pi} = \frac{1}{2}[lnZ_{pi+1} - lnZ_{pi}] \tag{3.6}$$

where i represents the interface between layers i and *i+1*.

If there are N numbers of sample reflectivity, the matrix format of the above equation can be written as

$$\begin{bmatrix} R_{p1} \\ R_{p2} \\ \vdots \\ R_{pN} \end{bmatrix} = \frac{1}{2}\begin{bmatrix} -1 & 1 & 0 & \cdots \\ 0 & -1 & 1 & \ddots \\ 0 & 0 & -1 & \ddots \\ \vdots & \ddots & \ddots & \ddots \end{bmatrix}\begin{bmatrix} L_{p1} \\ L_{p2} \\ \vdots \\ L_{pN} \end{bmatrix} \tag{3.7}$$

where $L_{pi} = \ln(Z_{pi})$.

Furthermore, the seismic trace is a convolution of the seismic wavelet with the reflectivity, written as

$$\begin{bmatrix} T_1 \\ T_2 \\ \vdots \\ T_N \end{bmatrix} = \begin{bmatrix} w_1 & 0 & 0 & \cdots \\ w_2 & w_1 & 0 & \ddots \\ w_3 & w_2 & w_1 & \ddots \\ \vdots & \ddots & \ddots & \ddots \end{bmatrix}\begin{bmatrix} R_{p1} \\ R_{p2} \\ \vdots \\ R_{pN} \end{bmatrix} \tag{3.8}$$

where T_i represents the *i-th* sample of the pre-stack seismic trace and w_j represents the *j-th* term of an extracted seismic wavelet. Using the seismic inversion method, we invert the L_p from a knowledge of T (a vector with components T1 to TN) and w (the wavelet matrix). However, matrix inversion will not recover the low frequency part of the impedance because the wavelet is band-limited. Therefore, the seismic inversion process needs an initial impedance model (low frequency) and iterate towards a solution using the conjugate gradient method (Hampson et al., 2005).

For pre-stack seismic inversion, the reflection coefficients are derived from the elastic parameters using the Aki-Richards approximation (Fatti, 1994):

$$R_{PP}(\theta) = c_1 R_P + c_2 R_S + c_3 R_D \tag{3.9}$$

where $R_{PP}(\theta)$ is an angle-dependent reflectivity, $c_1 = 1 + \tan^2\theta, c_2 = -8\gamma^2\tan^2\theta, c_3 = -0.5\tan^2\theta + 2\gamma^2\sin^2\theta$, and $\gamma = V_s/V_p$.

However, reliable V_p, V_s, and ρ are difficult to estimate due to the limitation of seismic angles. For the Anatoli seismic dataset, the critical angle at reservoir interval is around 45 degrees, which leads to poorly resolved density estimates. Understanding this limitation, the pre-stack seismic inversion of Anatoli data is focused on the estimation of P-impedance (Z_p) and S-impedance (Z_s).

The inversion process within CGG-Jason (2015a) was performed in three main steps:

- Estimate elastic parameter contrasts by creating synthetics that simultaneously honor all of the input seismic stacks;
- Integrate the elastic parameter contrasts to create elastic parameter volumes; and
- Optimize the elastic parameters by modifying the low frequency trends and enforcing compliance with any additional constraints.

The overall workflow of the seismic inversion is illustrated in Figure 3.8.

3.3.2 Wavelet Estimation and Well-to-Seismic Tie

As mentioned earlier, part of the seismic inversion process is removing the wavelet effect of the seismic traces. Therefore, the wavelet estimation is an important step within the whole workflow. Wavelets also vary with depth and offset (e.g., due to attenuation); hence for this research, the approach is to estimate the wavelets within each partial angle stacks. The Anatoli P-wave seismic survey was divided into four main angle stacks: 5-14°, 15-24°, 25-34°, and 34-44°. CGG-Jason (2015b) did an experiment to observe the optimal number of partial angle stacks used for simultaneous seismic inversion by inverting a synthetic dataset. From

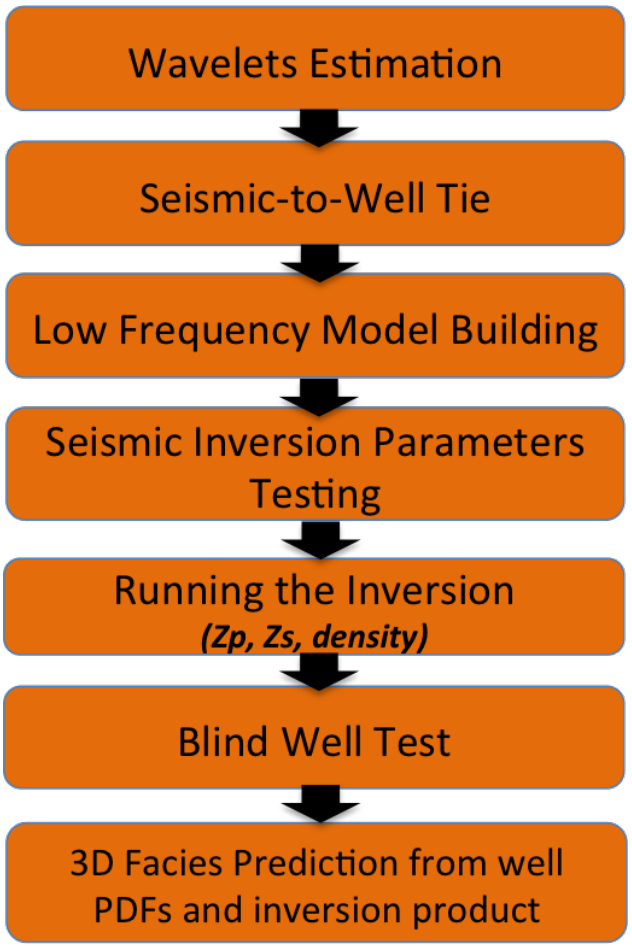

Figure 3.8: General workflow of the Seismic Inversion work

the experiment, it was observed that the greater the number of angle stacks improved density inversion results. However, the higher the number of partial angle stacks also increases the instability of the seismic inversion result (i.e., noisy results). Based on this study, four partial stacks are used for this inversion. Wavelets were estimated for each partial angle stacks using the 13 wells. Estimated wavelets were averaged for each partial angle stacks resulting in four main wavelets for seismic inversion inputs. The variable wavelets enable the inversion to effectively compensate for offset-dependent phase, bandwidth, tuning, and NMO stretch effects (Ardakani, 2003). The average wavelets estimated for each partial angle stacks are shown in Figure 3.9.

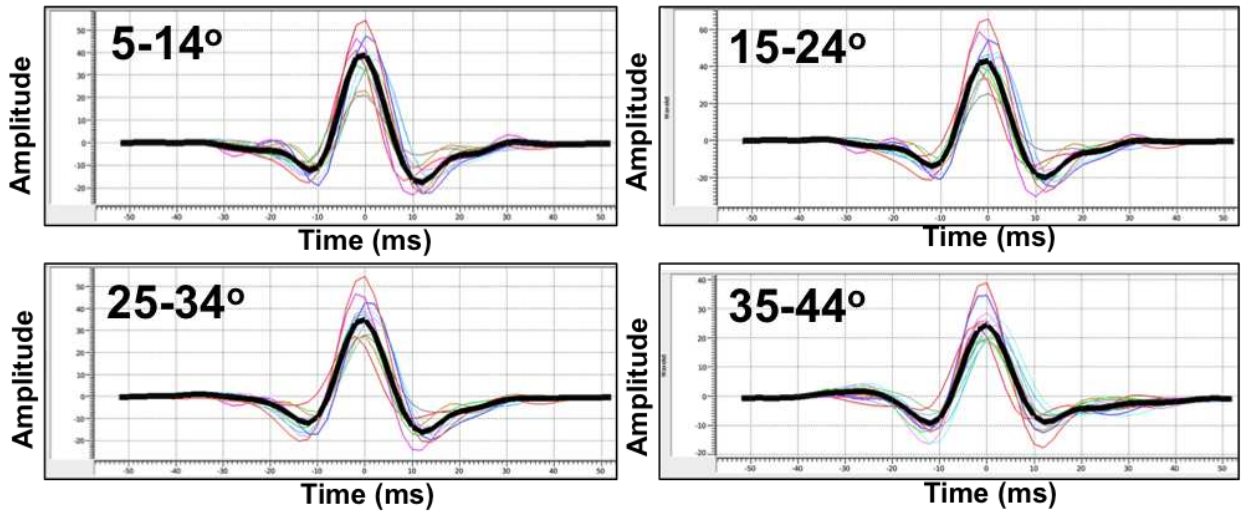

Figure 3.9: Average wavelets for each partial angle stack are highlighted in black. The background for each average wavelet is a set of estimated wavelets from all 13 wells.

After estimating a wavelet for each partial angle stack, the next step is to perform the well-to-seismic tie. Performing a well-to-seismic tie is a very important step in aligning the well data to seismic data and predicting the most accurate time-depth relationships for each well within the survey. Sonic and density logs are the main inputs to create the impedance log and reflectivity series. These reflectivity series are then convolved with the estimated wavelets (for each angle stack) to create synthetic traces through the forward modeling process. Figure 3.7 illustrates the forward modeling from impedance logs to synthetic seismic trace. Mismatches between the well and the seismic data using the initial time-depth relationship from the velocity curve is inevitable due to well logging quality, seismic quality, or anisotropy. Thus, the time-depth relationship needs further minor adjustments to achieve the highest possible correlation between the synthetic and seismic trace. These minor adjustments include time-shift, stretch and squeeze by aligning the particular peak or trough of the synthetic trace to the peak or trough of the seismic trace. With a credibly estimated wavelet and high quality well log data (e.g., good borehole condition, no missing log curves), the time-depth relationship between the well and seismic data should not have to be adjusted too significantly in order to get the best correlation. Typically, the acceptable velocity mismatch may be on

the order of 5%, allowing for anisotropy effects, dispersion, modeling errors, and others (Gunning and Glinsky, 2006). Figure 3.10 shows an example of well-to-seismic tie at Well 11.

Due to low seismic acquisition fold on the edge of the seismic survey area (Figure 3.4), two out of 13 wells are not successfully tied in the far stack, and therefore are dropped from our analysis. The correlation coefficients for the remaining 11 wells are shown in Figure 3.11.

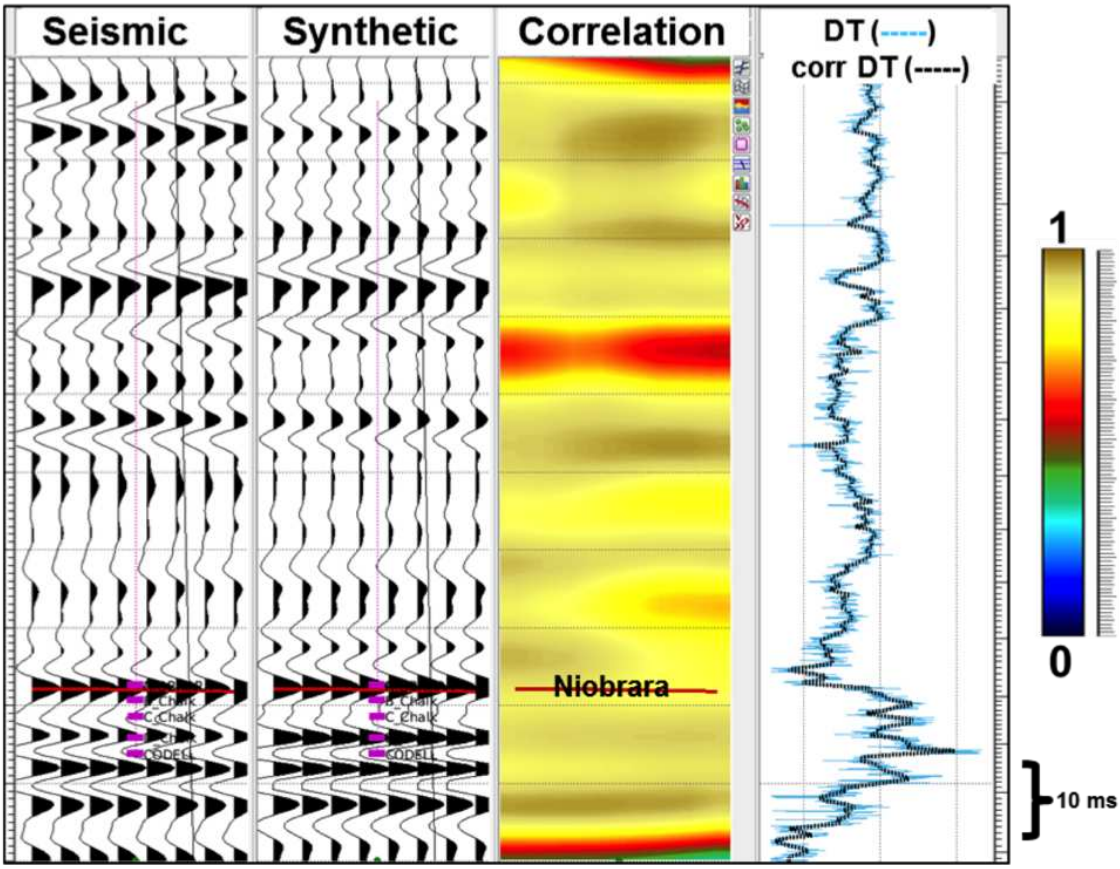

Figure 3.10: Seismic-to-well tie example from Well 11 showing a good match between the seismic and synthetic traces. High correlation is indicated by hot colors. On the right column, the comparison between time-depth relationship before and after adjustment is shown, indicating very minimum modification.

Well	Correlation Window (ms)	Near	Mid-near	Mid-far	Far
1	490	0.79	0.82	0.81	0.46
2	530	0.82	0.82	0.84	0.54
3	535	0.83	0.83	0.83	0.68
4	555	0.76	0.75	0.64	0.36
7	535	0.83	0.84	0.8	0.5
8	455	0.8	0.8	0.81	0.57
9	465	0.69	0.72	0.71	0.47
10	510	0.81	0.79	0.73	0.56
11	500	0.86	0.88	0.83	0.63
14	500	0.76	0.76	0.74	0.49
15	500	0.83	0.84	0.81	0.6

Figure 3.11: Correlation coefficient of each well-to-seismic tie from 11 wells. Overall correlations are high (in a scale of 0 to 1), except the far stack that generally has the least acquisition folds and lowest seismic frequency. Time window of the well-to-seismic process (±500 ms) was set for a stable correlation, as it is approximately four times the wavelet length.

3.3.3 Low Frequency Model Building

The seismic data have band-limited frequency content, which means they are missing both the higher frequencies (≈>75Hz) and lower frequencies (≈<6Hz). Building a Low Frequency Model (LFM) is important not only to fill the missing-low-frequency part of the full band-width dataset, but also to put the seismic inversion result into a geologic context by providing initial models (Z_p, Z_s, ρ) from the well logs. To build a LFM in this project, several parameters were required: interpreted horizons, wells, chosen parameters for the interpolation/extrapolation algorithm, and stratigraphic assumption. Given the dataset and regional geology information, I used four main horizons around the target zone (Pierre, Sharon Springs, Niobrara, and Lower Greenhorn) and four wells (well 1, 3, 11, 14). These wells were selected as they are located sparsely throughout the seismic survey area and give more spatial variability to the priori information. I chose four out of 13 wells as the input to the LFM, to leave some of the wells for blind-well test. All the relevant algorithms on the Jason software were tested and two interpolation/extrapolation parameters were set for

the model: the well curve and the horizon interpolation/extrapolation. For the well curve, Global Kriging with a variogram range of 50,000 ft provides the most reasonable geological estimation of the model (i.e., no bull-eyes or triangle features, smooth value changes). For the horizons, the Natural Neighbor interpolation type was chosen. Conformable stratigraphy was assumed for the LFM based on the geological understanding of the area. It is understood that there are existing faults within the area, but overall the stratigraphy is not identified as a complex stratigraphy. Figures 3.12 and 3.13 show the final LFM for the inversion work, in map view and section view.

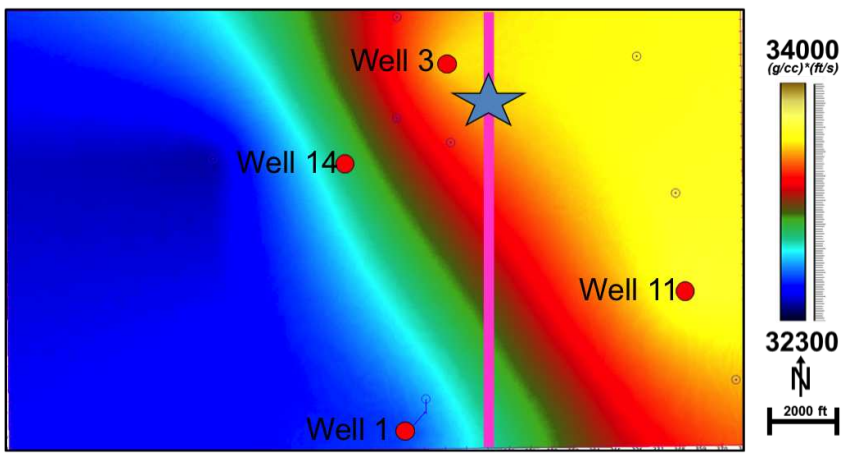

Figure 3.12: Extracted P-impedance (RMS values) from the Low Frequency Model (LFM), with the extraction window from top of Niobrara to the top of Codell. The map shows general trend of the P-impedance is higher to the east. Red dots show the input wells for the LFM. Pink line and star symbol represent the section view line on Figure 3.13 and the well location plotted on it.

3.3.4 Inversion Parameters Testing and Results

The P- and S-impedance are estimated by minimizing an objective function (F) containing multiple terms called misfit functions. Those main misfit functions are the seismic, contrast, and trend misfits:

$$F = \Sigma(Fseismic + Fcontrast + Ftrend) \tag{3.10}$$

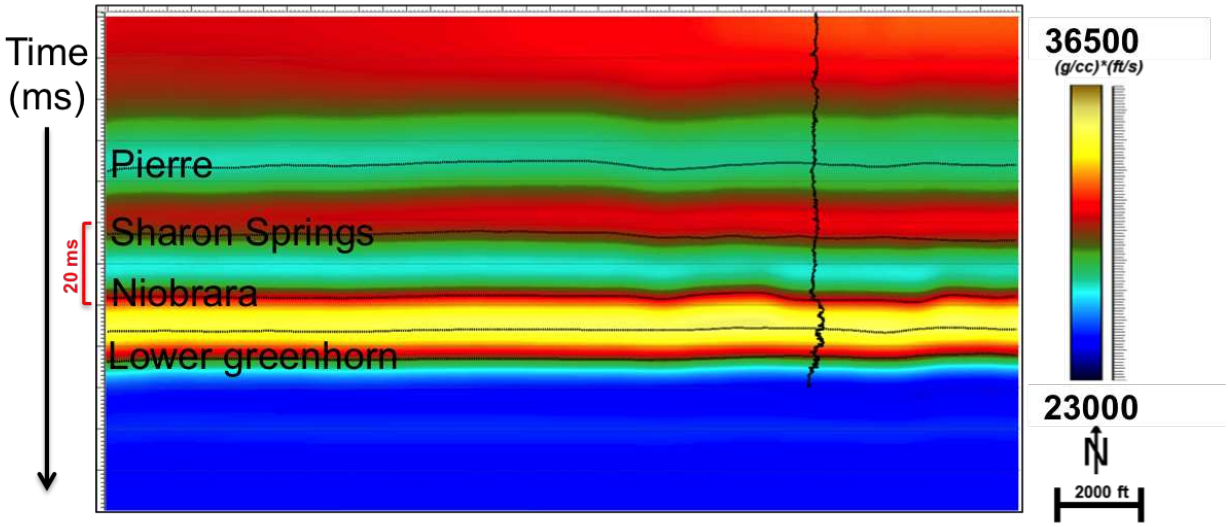

Figure 3.13: Low Frequency Model (LFM) in section view, showing four main input horizons and the higher impedance trend in the Niobrara interval. P-impedance log is plotted from Well 7 (shown as star symbol in the Figure 3.12).

The misfits are related to each other and when one terms becomes smaller, other terms tend to become larger. The objective function is evaluated after every P-impedance, S-impedance, and density update, until either the inversion process converged, or the maximum number of iterations was reached. The seismic misfit (*Fseismic*) function controls the seismic residuals, whereas the contrast misfit (*Fcontrast*) function controls the P- and S-impedance variance. These two misfits are the main parameters being tested for the inversion iteration, until the most optimal correlation is achieved. For this particular seismic inversion project, the *Fseismic* parameters were set as: *Fseismic* S/N Near [dB] = 6; *Fseismic* S/N Midnear [dB] = 7.8; *Fseismic* S/N Midfar [dB] = 18; and *Fseismic* S/N Far [dB] = 18. Additionally, for the *Fcontrast*, the parameters were optimized for the *Fcontrast* P-impedance uncertainty = 0.0388 and *Fcontrast* S-impedance uncertainty = 0.0289. After these parameters were set, the next essential misfit parameter is the trend misfit (*Ftrend*). The *Ftrend* is used to stabilize the low frequencies relative to the trend, and it is defined by setting the merge-cutoff frequency between the LFM and the seismic data. The merge-cutoff frequency needs to be set at the optimal value, so the inversion result is not biased by the LFM but still effectively

constrains the possible geological model fitting the seismic data. After several trials of inversion parameters, 11 Hz was found to be the most optimal merge-cutoff frequency between the well and seismic data (see Figure 3.14). This frequency value was chosen considering the high correlation of the seismic inversion result at the well locations and it is still reasonably low to not overshadow or bias the inversion result.

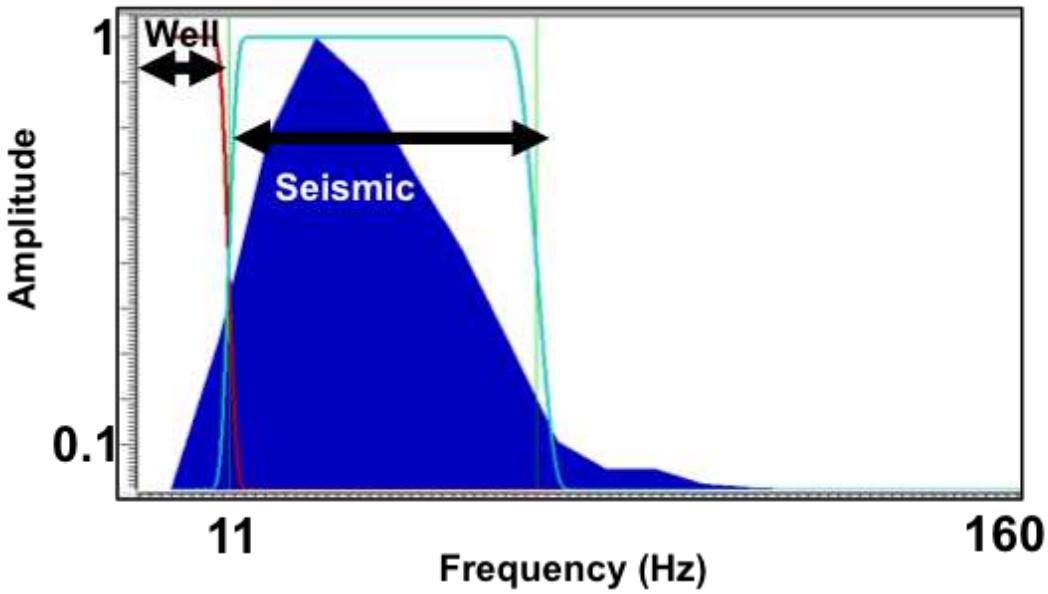

Figure 3.14: The frequency ranges of well data and seismic data, showing the overlap (merge-cutoff frequency) at 11Hz between the seismic and the well. Merge-cutoff frequency was chosen after numerous inversion parameters tests which give the most optimal final result.

Numerous inversion parameters have been tested simultaneously to obtain the most optimal P- and S-impedance results. We need to perform tests to confirm the optimal inversion result. This type of Quality Control (QC) is called the blind-well test. An acceptable inversion yields a good match between the elastic properties recovered from the wells and the seismic inversion at the blind wells, even though the particular wells are not used as input for the LFM. Figure 3.15 shows the inversion result; P- and S-impedance, in map views. The impedances were extracted from the Root-Mean-Square (RMS) values of the impedance volumes, at the window of 10-15 ms below the Top of the Niobrara horizon. The blind-well test is shown more clearly in Figures 3.16 and 3.17.

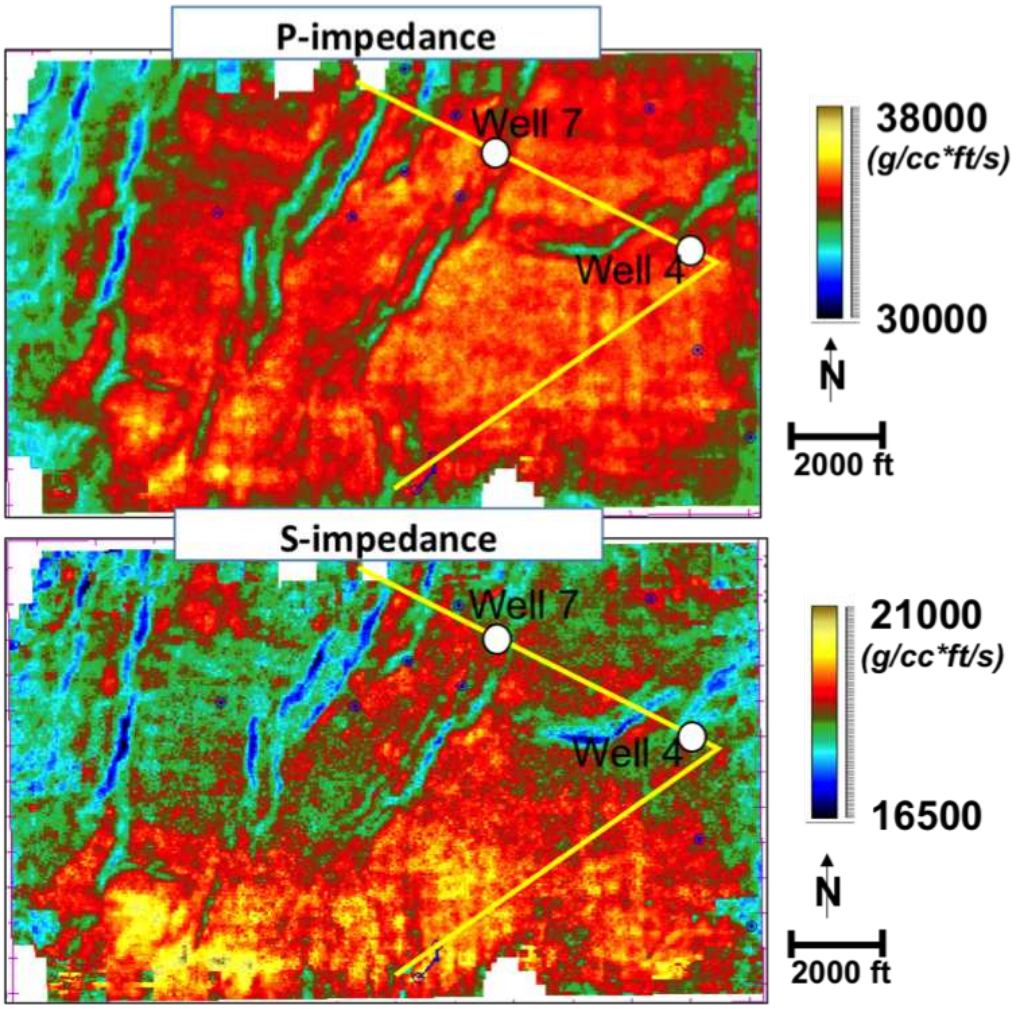

Figure 3.15: Inversion result (P- and S-impedance) on map view, extracted from the Root-Mean-Square (RMS) values at the interval of 10 ms-15 ms below the Top of the Niobrara horizon. Higher impedance areas are indicated in hotter colors. The yellow line crossing Well 7 and Well 4 as the blind wells also shows the impedances in section view (Figure 3.16).

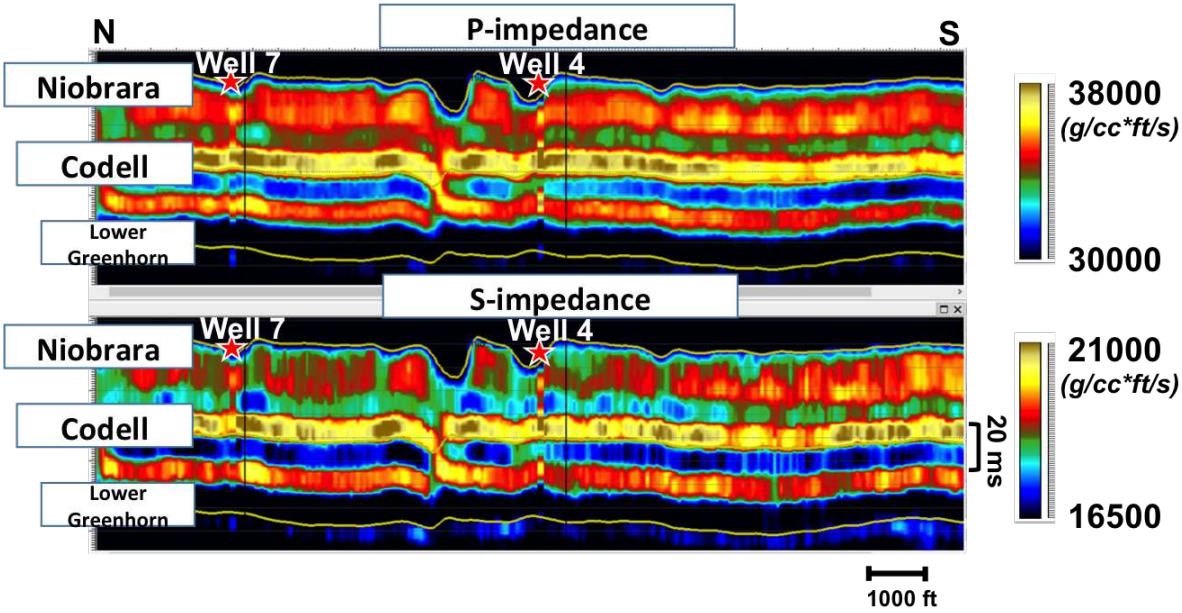

Figure 3.16: Elastic Properties: P-impedance (upper) and S-impedance (lower) volumes from seismic inversion in section view. The line crosses the Well 7 and Well 4, which are the blind wells. Note the good matches between P-impedance and S-impedance from the well and seismic inversion at the blind-well locations.

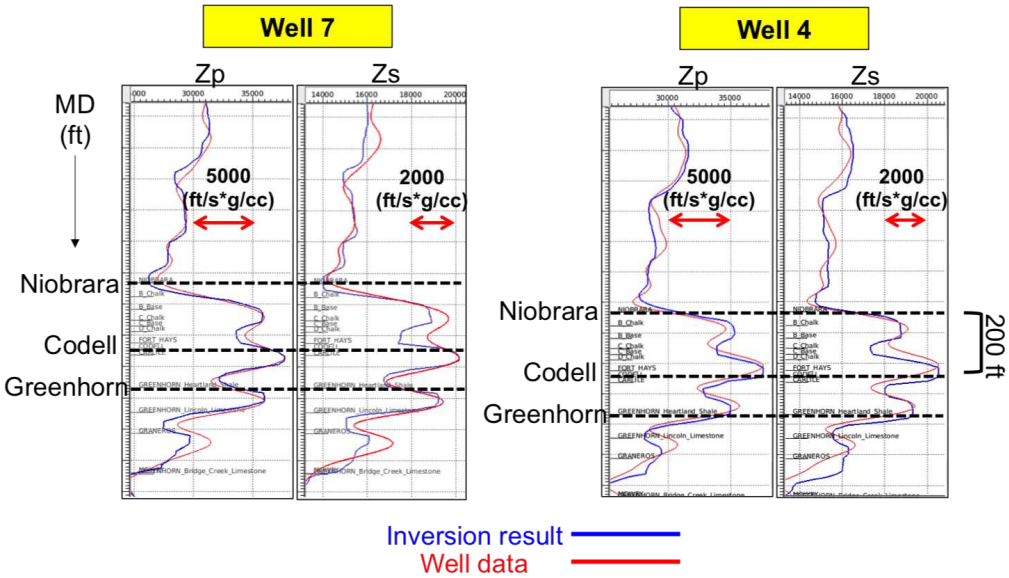

Figure 3.17: A closer look at Well 7 and Well 4 (blind wells), comparing the P-impedance (Z_p) and S-impedance (Z_s) from the well logs and seismic inversion. A good match is indicated from these curve plots (errors <5%).

In addition to the blind-well test, a second QC of the inversion result is made by plotting the elastic properties from the seismic inversion. Figure 3.18 shows the cross-plot of P- vs. S-impedance from the seismic inversion, constrained to the Smoky Hill Member interval. A more scattered distribution is observed from the inversion result, compared to the P- vs. S-impedance plot from the well logs (Figure 2.3). However, the overall distribution of the elastic properties are aligned with the petrophysical model from the well logs, as shown by the Pure-Chalk PDF overlying the highest P- and S-impedance values from the inversion. This is a good indication that the seismic inversion results are reliable for further lithology prediction, which is described in the next chapter.

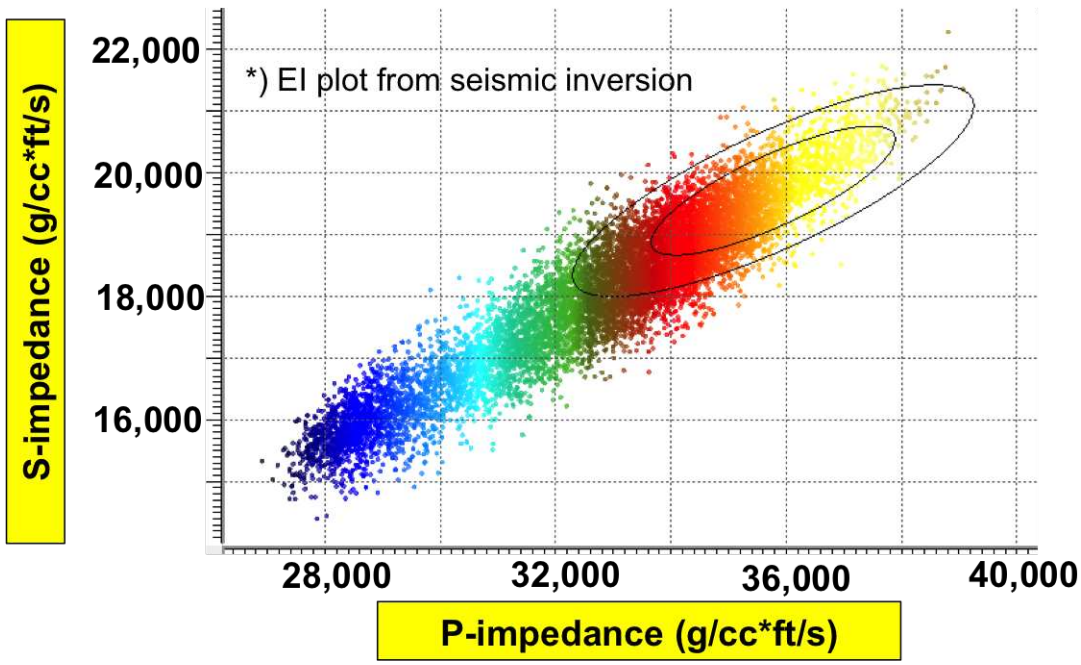

Figure 3.18: Cross-plot of estimated P-impedance and S-impedance from seismic inversion. The higher impedance values are shown in hotter color. Plotted on the top-right corner of the figure, is the Probability Distribution Function (PDF) of the Pure-Chalk from well log clustering.

CHAPTER 4

MULTI-ATTRIBUTE TRANSFORM FOR PREDICTING LOG PROPERTIES FROM SEISMIC

Obtaining reliable density information from the seismic inversion process is not feasible for the Wattenberg project, as discussed in prior sections. Therefore, another approach in estimating density is tested by utilizing the concept of Multi-Attribute Transform in the Hampson Russell software, under the EMERGE module. This work is performed to both evaluate the usefulness of additional density information in later facies modeling work and to test the reliability of this method in estimating elastic properties that cannot be obtained by conventional pre-stack seismic inversion.

4.1 Utilizing Density Information in Facies Modeling

Previous chapters of this thesis have focused on characterizing the Smoky Hill Member of the Niobrara Fm, which mainly consists of three facies: chalk, marl, and mixed marl and chalk. These facies are defined by performing a clustering analysis (Section 2.3). In addition to the Smoky Hill Member, the zones below it are also included in the clustering analysis. This analysis results in a total of six facies from the Top of Niobrara to the Base of Codell Sandstone. Table 4.1 shows Table 2.5 with three additional facies.

Table 4.1: Well log values of six facies from clustering

Facies	Vp(ft/s)	Vs(ft/s)	RES(ohm-m)	NPHI(%)	RHOB(g/cc)	GR(API)
Pure Marl	11100 -12500	6100 - 7400	0 - 40	15 - 28	2.46 - 2.62	100 - 250
Mixed Marl-Chalk	12200 - 14300	6900 - 8300	0 - 40	10 - 23	2.44 - 2.6	80 - 200
Pure Chalk	13300 - 15400	7700 - 8700	20 - 110	8 - 20	2.38 - 2.58	50 - 170
Basal Chalk	12200 - 15400	6200 - 8300	0 - 20	7 - 22	2.58 - 2.68	40 -140
Limestone	14300 - 18200	7700 - 9500	10 - 180	2 - 15	2.58 - 2.66	10 - 50
Sandstone	11100 - 13300	6100 - 7400	0 - 20	10 - 31	2.42 - 2.6	80 - 150

The characterization of the Smoky Hill Member can be achieved by using the P- and S-Impedance (Elastic Impedance). However, another property is required if we intend to include the zones below the Smoky Hill Member such as basal chalk (the D-facies), limestone (the Fort Hays), and sandstone (the Codell). The reason for adding an additional property, is that the Elastic Impedance (EI) of the D-facies and Fort Hays Limestone are similar to the chalks of Smoky Hill Member. Likewise, the EI of the Codell Sandstone is similar to the marls of Smoky Hill Member. The overlapping EI values of the Smoky Hill Member facies and the interval below it (D facies, Fort Hays Limestone, Codell Sandstone) is shown in Figures 4.1 and 4.2. It is acknowledged from the seismic dataset that the zone of interest in this research is generally conformable and no significant structural features present; therefore, similarity of the EI values of those facies is not a significant issue in the facies modeling. The facies modeling of the whole section can still be approached by dividing the zone of interest into two main intervals: the Smoky Hill Member interval and the D facies - Fort Hays Limestone - Codell Sandstone interval. If the modeling for the whole section (six facies) needs to be done in one attempt, another property (e.g.,density) is required. Figure 4.3 suggests that the combination of P-impedance and density information from the wells enables the characterization of the whole Niobrara - Codell section. For the sandstone facies (Codell Fm), the P-impedance and density are trending to the lower values, although some of the data points also show ambiguity or overlapping values between the sandstone and the pure marl facies. Considering this overlapping issue, the pure marl and sandstone facies are color coded as a same facies in the 3D modeling based on its elastic properties, as long as it is understood that the sandstone (Codell) interval is located specifically below the basal chalk (D-facies) and the limestone (Fort Hays).

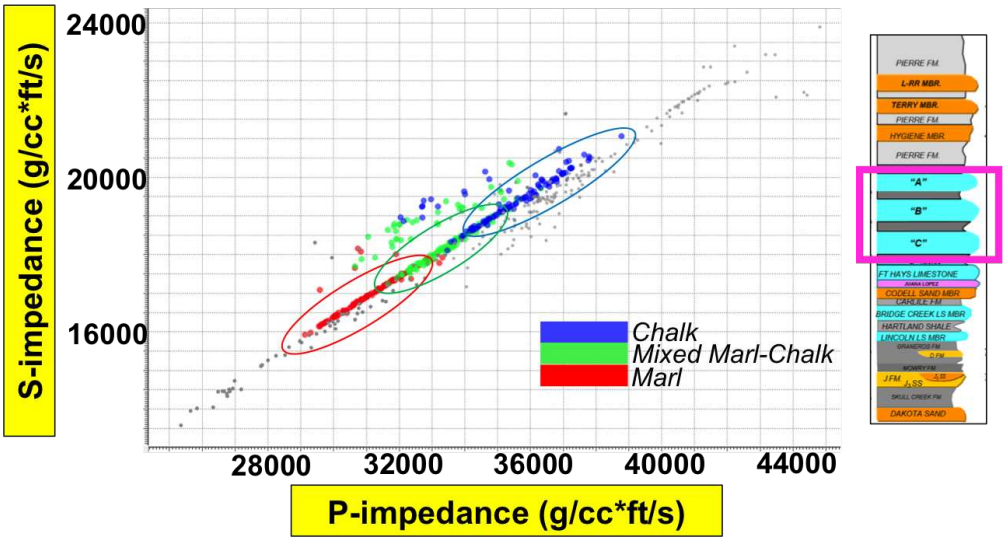

Figure 4.1: Cross-plot of P-impedance and S-impedance values from the wells inside the 3D Anatoli survey, color coded by the facies within the Smoky Hill Member. The grey dots on the background shows the overlapping facies distribution of the zones below the Smoky Hill Member.

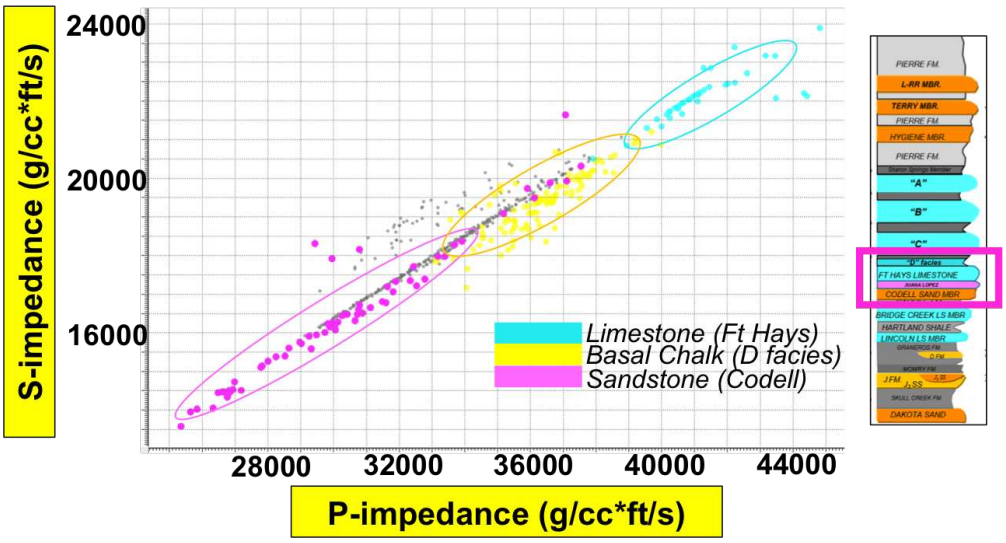

Figure 4.2: Cross-plot of P-impedance and S-impedance values from the wells inside the 3D Anatoli survey, color coded by the facies below the Smoky Hill Member. The grey dots on the background shows the overlapping facies distribution of the Smoky Hill Member zone.

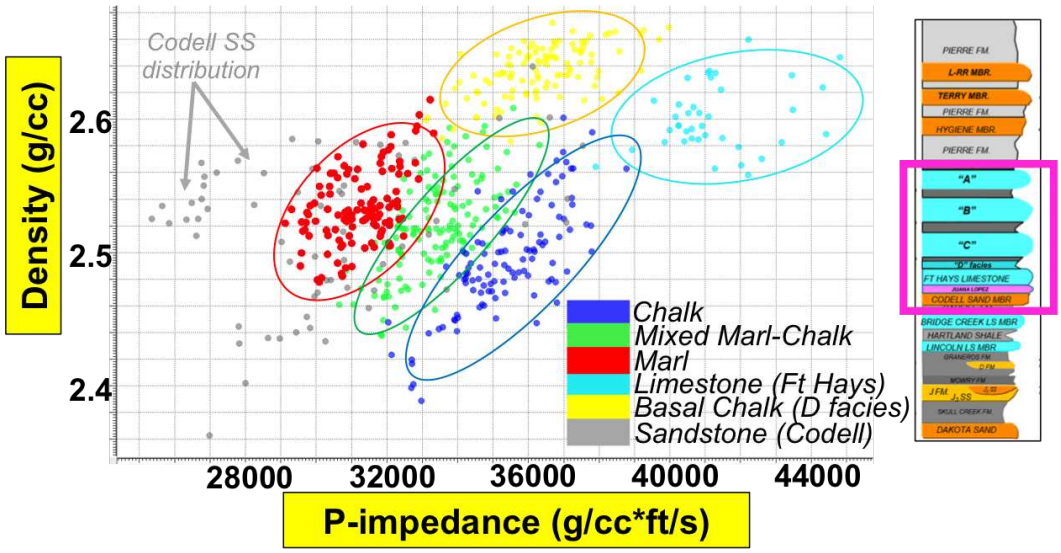

Figure 4.3: Cross-plot of P-impedance and density values from wells inside the 3D Anatoli survey, color coded by the facies from the Top of Niobrara to the Base of Codell Sandstone. By using the relationship between P-impedance and density, all of the facies between this interval can be modeled, with the exception of the Codell Sandstone which still has overlapping values to the other facies (showed in grey dots).

4.2 Multi-attribute Transform

The Multi-Attribute Transform (MAT) is essentially a method for estimating well log properties from seismic data. The method can be performed by utilizing a post-stack seismic data or pre-stack seismic data, though for this research, I used the latter. Similar to the seismic inversion method, the well-to-seismic tie step needs to be performed accurately in the initial process of the MAT. Once the well logs and seismic dataset are tied, a series of attributes can be generated from the seismic dataset. The EMERGE module within the Hampson Russell software then derives a multi-attribute transform, which is a linear or non-linear transform between the seismic attributes and the target logs. In the linear mode, the transform consists of a series of weights derived by least-squares minimization; while in the non-linear mode, a neural network is trained (Hampson et al., 2001).

During the process, I tested several parameters, such as:

1. the input wells; some wells with the highest cross-validation errors may be removed if they are affecting the results negatively (resulting large total errors for all wells);

2. type and number of seismic attributes to use; I chose the combination of attributes that optimally predict the target logs and still conform with geological features; and

3. algorithm to use for the transform.

After a trial and error process in defining the parameters, the final result is chosen based on the lowest error calculated from the cross-validation result. Cross-validation is achieved by removing each well from the training set and recalculating the transform from the remaining input wells. The prediction error is then calculated for every hidden well that was removed in the training set. The final number of the validation error is the average error for all the hidden wells. Once the most optimal transform has been finalized, the transform is applied to the whole survey area to produce the 3D volume of predicted reservoir properties. For this research, the final parameters and result of the multi-attribute transform are:

- 13 vertical wells inside the Anatoli, particularly utilizing the density logs;

- Angle gathers of 3D Anatoli seismic data;

- EI volumes from simultaneous seismic inversion (P-impedance and S-impedance)

- Probability Neural Network (non-linear mode) algorithm;

- List of attributes: Seismic Amplitude Envelope, Raw Seismic, Seismic Quadrature Trace, $P - impedance^2$, Seismic Second Derivative, $1/[S - impedance]$, and Seismic Derivative. These seven attributes are the best combination which are used simultaneously to get the final optimal transform;

- Operator Length: 3. This length determines the length of the convolutional operator centered on the target sample. This parameter is used because a single log (target log)

sample is related to a group of neighboring samples around the target point, instead of just one seismic value (Russell, 2013);

- Training zone: Top of Niobrara to the Top of Graneros (approximately 100 ms window);
- Result: cross-validation correlation of 0.75, with an average error of 0.02-0.03 g/cc (0.7-0.9%).

Figure 4.4 shows The cross-validation plots of density logs from 13 input wells, while Figure 4.5 shows the cross-plot of predicted density values versus actual density values at the well locations.

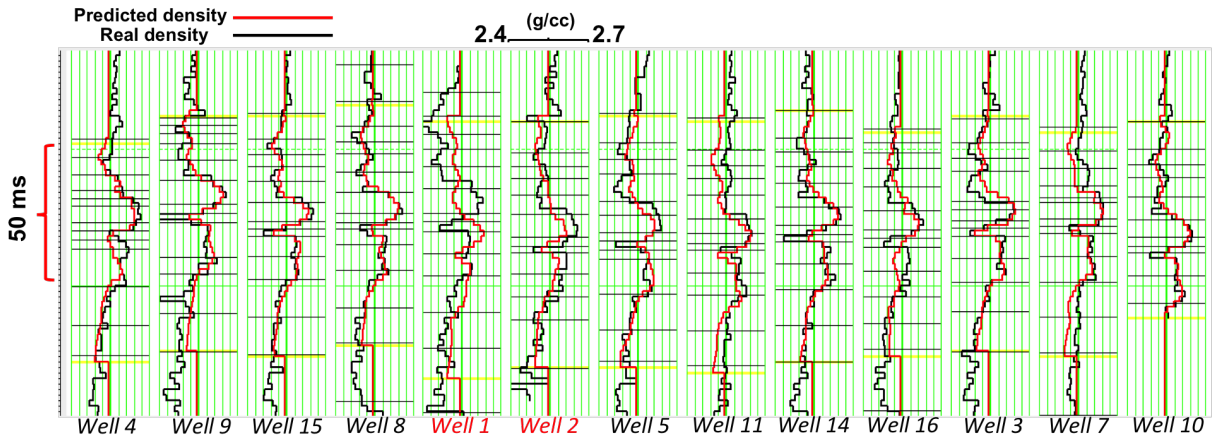

Figure 4.4: Comparison plot between predicted density from Probability Neural Network (Multi-Attribute Transform) and measured density from the well logs. The target interval is shown by the highlighted markers; approximately 100 ms between Top Niobrara to Top Graneros. Note that the biggest mismatch is found at the Well 1, which is the well with measured V_p and V_s logs.

Several methods in estimating the density have been tested in the EMERGE module of Hampson Russell, including the single-attribute regression, linear multi-attribute, and the neural network prediction. In conclusion, the Probability Neural Network (PNN) has indicated results that have the best correlation between actual and predicted density values. From Figure 4.4, a good match between measured and predicted density at the well locations are observed. At Well 1, the match is not as good as the other matches, which may be caused

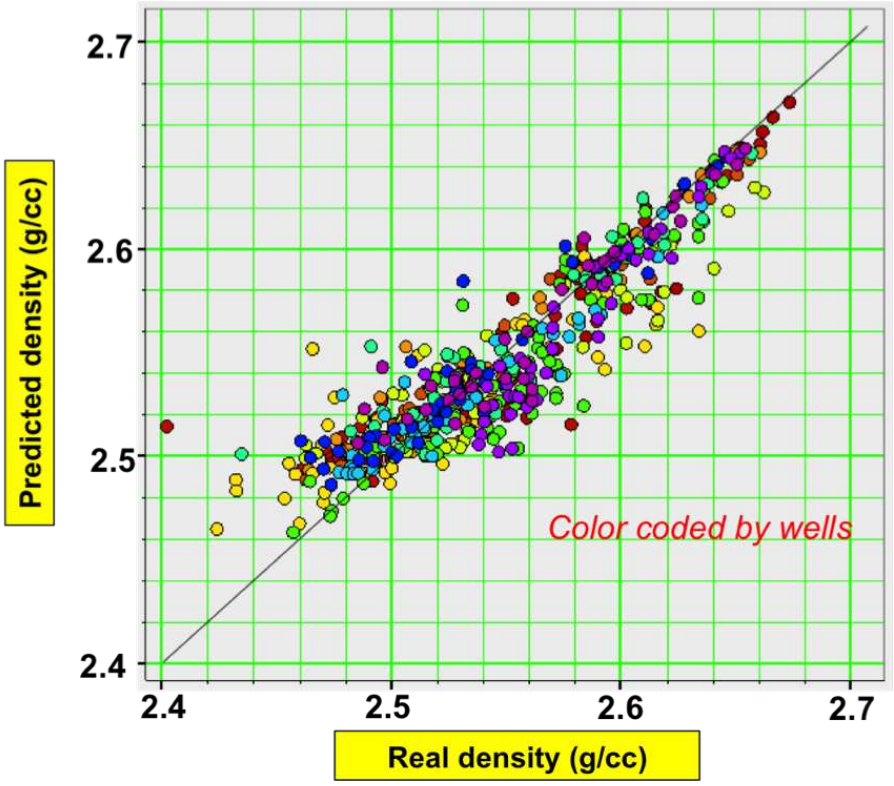

Figure 4.5: Cross-plot of actual density vs. predicted density at well locations, color coded by each of 13 input wells. This plot displays the 0.9 correlation coefficient between the two properties, with all wells used in the training set. For blind well cross-validation, the average of the correlation coefficients is 0.75.

by its location at the fault zone and the deviated well geometry. Despite this observation, Well 1 is still required in the analysis, as it is the only well in the survey area that has measured V_p and V_s logs.

Figure 4.6 shows the comparison between the density from simultaneous inversion and the density from multi-attribute PNN transform. The inverted density is highly unstable (e.g.,low frequency content, noisy), which is caused by the limited reflection angles of the seismic data. Acknowledging this limitation, the inversion parameterization has then focused on optimizing the EI results, increasing the instability of the density volume from seismic simultaneous inversion. The density result from multi-attribute PNN, though, has shown a more stable and geologically plausible density property compared to the density from simultaneous seismic inversion. This method is a good alternative for predicting the rock

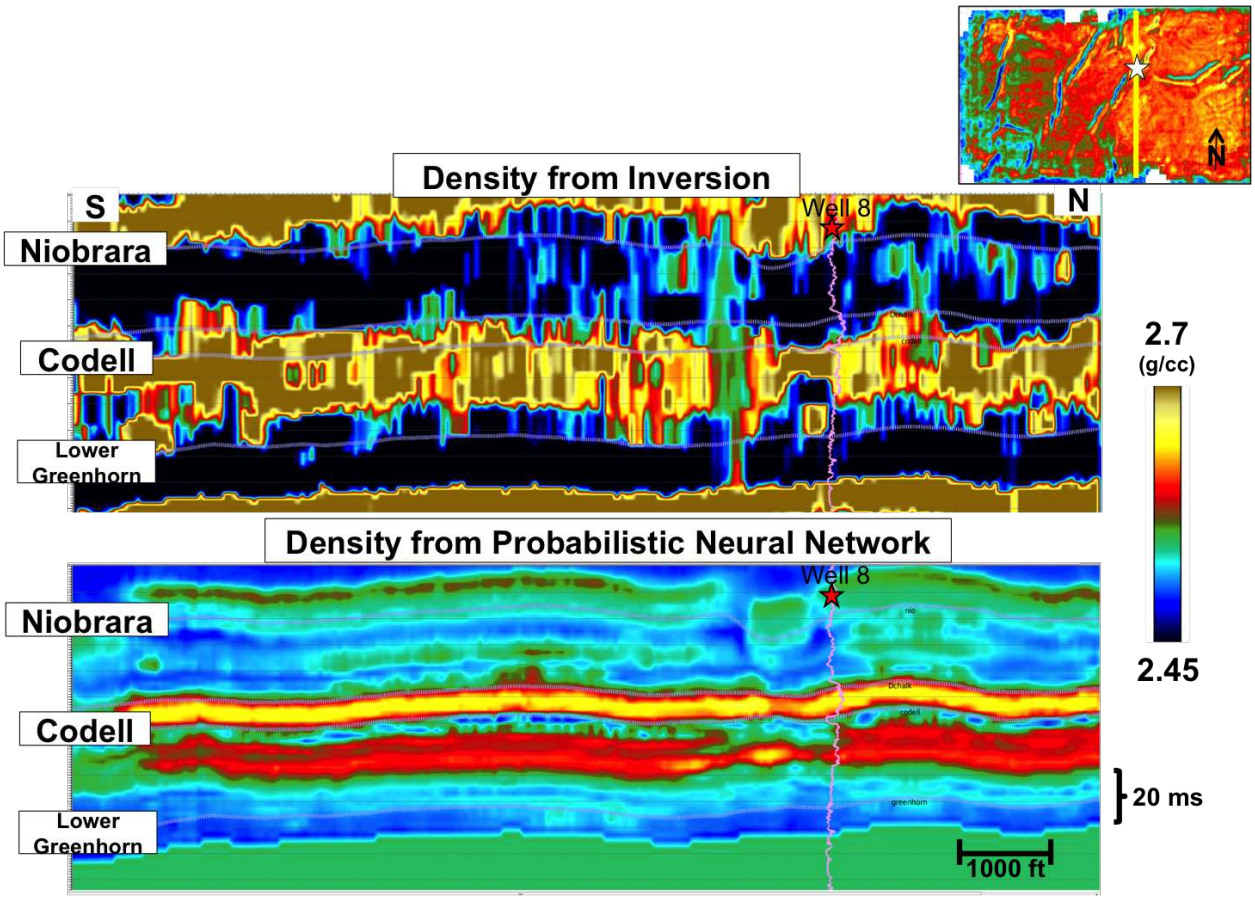

Figure 4.6: Two inline sections crossing Well 8 show the comparison between density property from seismic inversion (top) and density property from multi-attribute probability neural network transform (bottom). The extraction of density from multi-attribute PNN for Niobrara interval is shown on the top right corner map, with the location of displayed inline (yellow). For this map, the hot colors indicate higher density values, ranging between 2.52-2.58 g/cc.

density for the Wattenberg project.

In addition to the validation plots, a cross-plot of P-impedance from seismic inversion and density from multi-attribute transform is shown in Figure 4.7. This cross-plot is an additional validation to the values of predicted density, as the cross-plot aligns with the PDF from P-impedance and density from the well logs (see Figure 4.3). Note that the limestone facies is not apparent in the cross-plot, as the thickness is too thin to be resolved by the seismic data. The mixed marl-chalk facies (green) shows scattered distribution which may be caused by the priori information from the well logs. The facies color coded in red

shows two different trends for sandstone and pure marl.

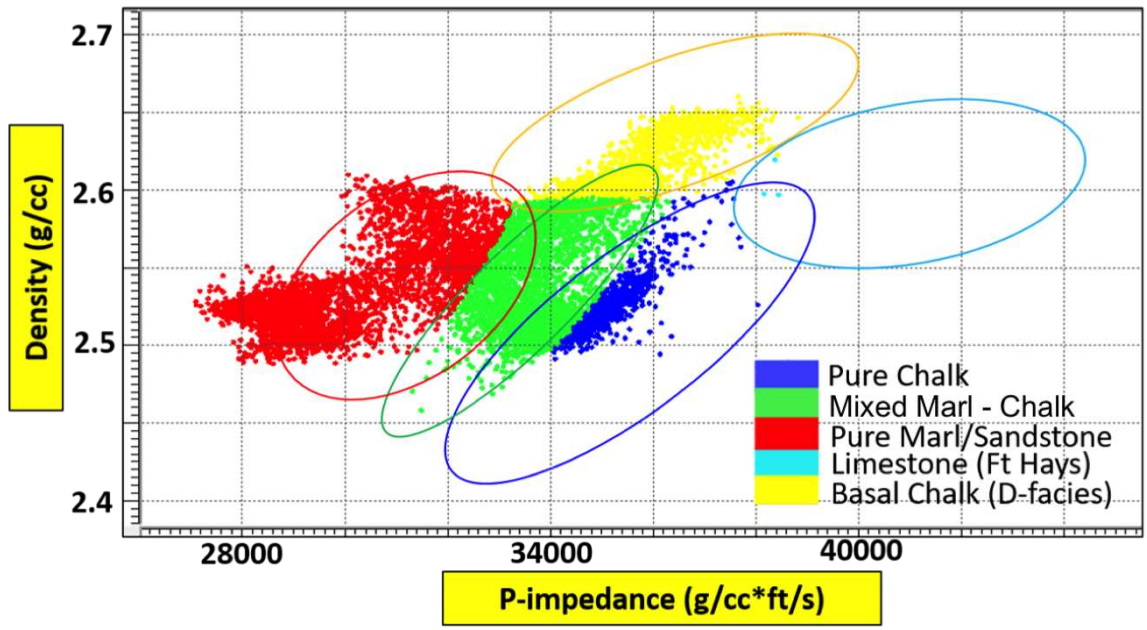

Figure 4.7: Cross-plot of P-impedance from the seismic inversion vs. density from multi-attribute transform, showing the alignment of each facies distribution to the PDF from well log cross-plot (see Figure 4.3). It is observed that there are parts of pure-chalk facies distribution identified as the mixed marl-chalk facies, and the limestone facies cannot be modeled from the seismic, which is due to the small thickness.

CHAPTER 5

FACIES MODELING AND ANALYSIS

The research presented in previous chapters has focused on developing a firm foundation for facies modeling. Using available geological information, the main investigation has largely been aimed at the most chalky parts of the Niobrara and the Codell sandstone, as these can sustain hydraulic fracturing to increase permeability. These units have been targeted by horizontal drilling and multi-stage hydraulic stimulation within the Wishbone section. The RQI study conducted by Mabrey (2016) supports targeting the most chalky part of the Smoky Hill Member - Niobrara. Tying all the information back to the rock samples from well cores is also very important (see Chapter 2). By clustering the facies from the well logs and correlating it to the RQI study and well core analysis, the final facies from the wells were defined. The petrophysical analysis in Chapter 2 suggests that we are able to use the elastic properties (P-impedance, S-impedance and density) to model the facies from the wells. After performing the workflow of seismic inversion and multi-attribute transform to estimate the elastic properties, the next step is to combine these two types of information into a single 3D facies modeling. The integration of these two data types is performed by using the principal of Bayesian probability theory, included in the Facies and Fluid Probabilities (FFP) module of the CGG-Jason tool. In Bayes Theorem, the probability of a hypothesis (the *posterior* probability) is a function of new evidence (likelihood) and previous knowledge (the *prior* probability). This relationship is described in Bayes Theorem:

$$p(A|B) = \frac{p(A)p(B|A)}{p(B)} \tag{5.1}$$

In my application, A is the facies cluster (e.g., chalk), B is the seismic attribute information (e.g., cross-plot of Z_p vs. Z_s attributes), $p(A)$ is the *a priori* probability for each facies from the well data, $p(B|A)$ is the conditional probability of the seismic attribute for a

particular facies (e.g., distribution of Z_p and Z_s for chalk facies), and $p(B)$ is the probability of the seismic attribute.

The workflow of this facies modeling includes:

1. Creating a well curve with the facies category information (as described in Chapter 2, using several well log properties as the input in clustering analysis);

2. Correlating the facies information to the elastic properties (in this case, Z_p and Z_s and Z_p and ρ);

3. Creating Probability Distribution Function (PDF) for each identified facies in the target zone;

4. Defining the priori information of each facies in the target zone based on other independent geological information of the area; and

5. Applying the PDFs for each facies to the seismic elastic property volumes (Z_p and Z_s, Z_p and ρ).

After performing the listed workflow, a facies model is generated as two output volumes:

- A probability volume for each facies (in a scale of 0 to 1, with 1 being the highest certainty); and

- A most probable facies volume, constructed by assigning the facies type as the most probable facies for a particular data point (CGG-Jason, 2016).

The facies modeling in the area mainly utilizes the P- and S-impedance, and P-impedance and density relationships. As described in Chapter 4, by using the P- and S-impedance relationship, we will be able to model the Smoky Hill Member, which mainly consists of chalk, marl, and mixed marl and chalk facies. Furthermore, the use of well log density information is required in identifying basal chalk (D-chalk) and the limestone facies (Fort Hays). For the sandstone facies (Codell), the elastic property values are very similar to the

pure marls. However, the sandstone interval (Codell) within the focus area is located below the basal chalk (D-facies) and the limestone (Fort Hays), in which the deposition is entirely separated from the pure marl facies of the Smoky Hill Member. For this reason, the pure marl facies and the sandstone are color coded as a same facies (red). It is also observed from the 3D facies model that generally the marls within the Smoky Hill Member (i.e., A, B, C marl; see Figure 1.2) are modeled as the mixed marl-chalk facies (green). Referring to the comparison between the facies log and facies at the cores (see Figure 2.2), the interval identified as marls within the Smoky Hill Member (i.e., A,B,C marl) largely comprised of mixed marl-chalk facies with thinly bedded pure marl facies within it. This low thickness of the pure marl ($\approx$<20 ft) are not resolved by the seismic inversion. For the interval with the richest content of chalk, it is generally identified as the pure chalk facies, hence the recommendation will be to target this modeled facies within the Smoky Hill Member (blue).

5.1 Facies Modeling Results

As described in Chapters 2 and 4, the combination of the elastic properties that are used to model the facies in this study are the elastic impedances (Z_p vs. Z_s) and P-impedance (Z_p) vs. density (ρ). For the first relationship, the PDFs for the Bayesian modeling are shown in Figure 2.3. The facies modeling using the P-impedance and S-impedance focuses in modeling the three main facies within the Smoky Hill Member. For this reason, the basal chalk (D-facies) and limestone (Fort Hays) are both characterized as the pure chalk facies. In the second relationship, P-impedance vs. density is shown by the PDFs in Figure 4.1. These PDFs were then applied to the P-impedance volume from the simultaneous seismic inversion and the density volume from the multi-attribute transform in Chapter 4. Figures 5.1 and 5.2 show the comparison between these two facies modeling.

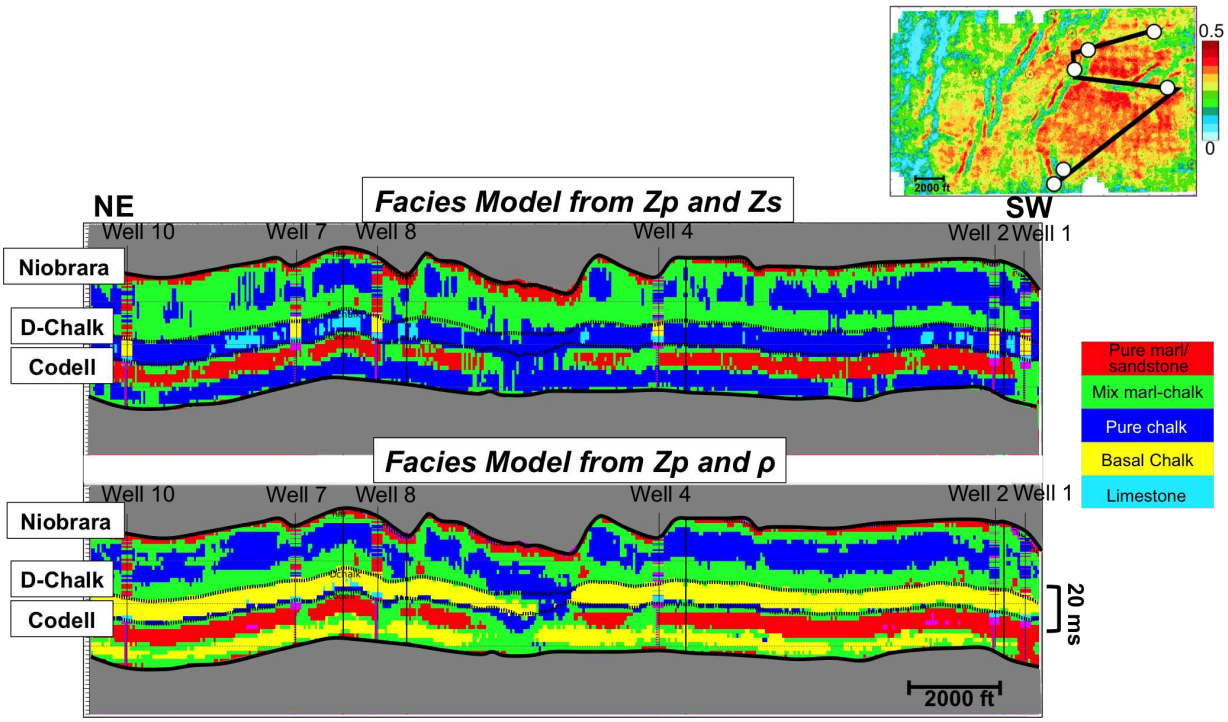

Figure 5.1: Arbitrary line crossing six wells across the Anatoli seismic survey, showing the Bayesian most probable facies from the PDFs generated by Z_p and Z_s (above) and Z_p and ρ (below) relationships. The top-right corner map is extracted from the chalk probability of the Smoky Hill Member interval, using the facies modeling from Z_p and ρ, with the black lines indicating the map view of the arbitrary section.

Figure 5.1 illustrates the facies model derived from Z_p and ρ information, which characterizes the basal chalk (yellow) in addition to the three main facies of Smoky Hill Member: pure chalk, pure marl, and mixed marl-chalk. It was previously noted that the marly part of the Smoky Hill Member is modeled as the mixed marl and chalk (green). Other than the ability to model an additional facies within the whole target interval, the facies model from Z_p and ρ is also observed to be more stable compared to the facies model from Z_p and Z_s. In particular, each modeled interval exhibits a leaking feature towards over- and underlying intervals for the Z_p and Z_s modeling. The regional geological understanding of the area is that the depositional system is typically continuous and conformable for each lithological units, which makes it more reasonable to use the model from Z_p and ρ relationship.

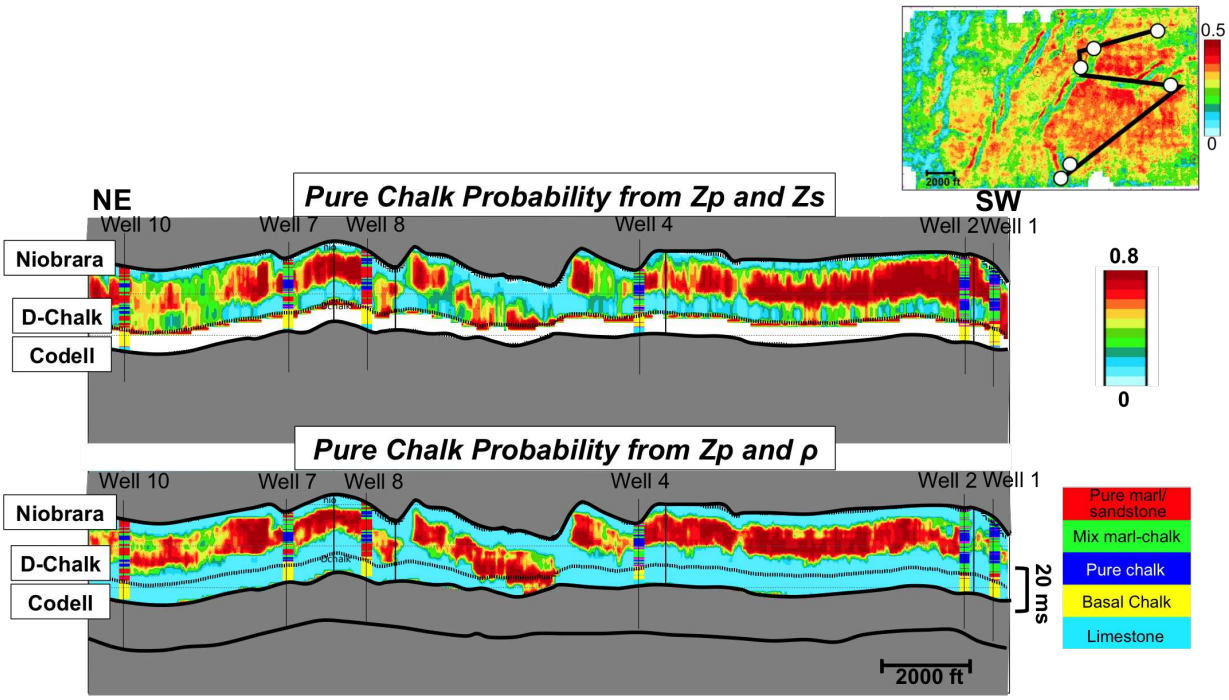

Figure 5.2: Arbitrary line crossing six wells across the Anatoli seismic survey, showing the pure chalk probability from the PDFs generated by Z_p and Z_s (above) and Z_p and ρ (below) relationships. The top-right corner map is extracted from the chalk probability of the Niobrara interval using the facies modeling from Z_p and ρ.

As argued earlier in this thesis, the most chalky part of the Smoky Hill Member is the highly targeted interval. Figure 5.2 shows the pure chalk probability volume. By using the Bayesian modeling, we derive an estimate for this facies probability or any other facies included in the modeling. Comparing the pure chalk probability from Z_p vs. Z_s and Z_p vs. ρ, we observe that the pure chalk facies from wells have a better match to the lateral distribution of highest probability chalk in the Z_p vs. ρ model. Note that Well 4 and Well 7 are blind wells and the facies at the wells and the 3D facies model are well matched (the pure chalk (blue) facies log is plotted on top of the high probability value).

As described in the Chapters 2 and 3, the input data are the vertical wells inside the 3D Anatoli seismic survey and two additional wells outside the seismic survey area having core data. The next step is to validate the 3D facies modeling by plotting the existing horizontal wells excluded from the modeling workflow. The lithology drilled along the horizontal wells

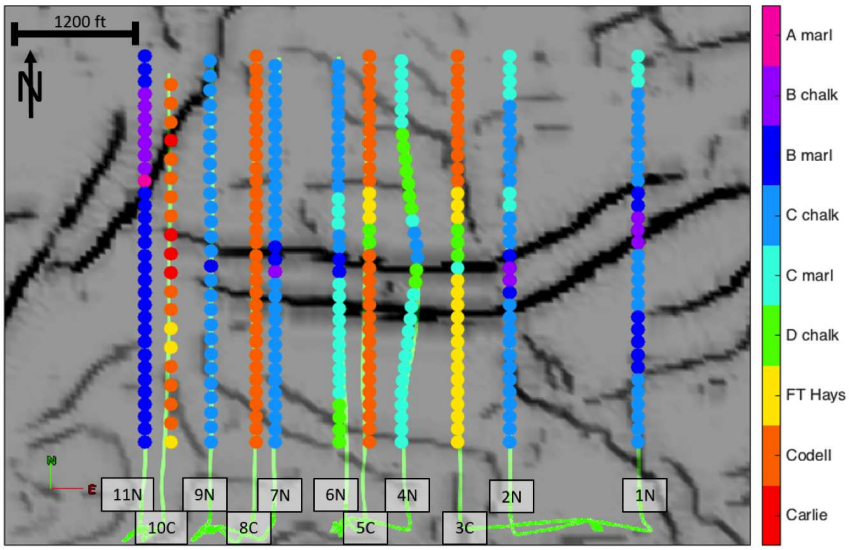

Figure 5.3: Base map of the Wishbone section within the Wattenberg field, with 11 horizontal wells. The horizontal wells are plotted with the hydraulic stimulation stages and lithology information for each stages determined by the geosteering paths (Butler, 2016). Note that the 5C and 1N wells are used in the next figures for the facies modeling evaluation.

in Wishbone section is shown in Figure 5.3.

Figures 5.4 and 5.5 show the section views of the 3D model crossing two of the horizontal wells. Note that the B Chalk and C Chalk are considered as one facies (pure chalk), the A Marl, B Marl, and C Marl are considered as the mixed marl and chalk zones. These cross-sections show good matches to the lithology encountered by the horizontal wells. The third row of the figure is the most probable facies modeled from the P-impedance (first row) and density (second row), with priori information from wells modeled in Figure 4.3. Figure 5.4 represents one of the horizontal wells that were targeting the Codell sandstone, while Figure 5.5 represents the horizontal well that targeted the most chalky part of the Smoky Hill Member. By evaluating the facies modeling result, this type of modeling is the recommended approach for predicting facies from the well locations and extending the prediction laterally between wells. By mapping out facies based on the probability cut-off (for example: 30% as the lowest probability of each facies to map) and combining it with the average facies thickness at well locations, one can estimate the volumes of each facies

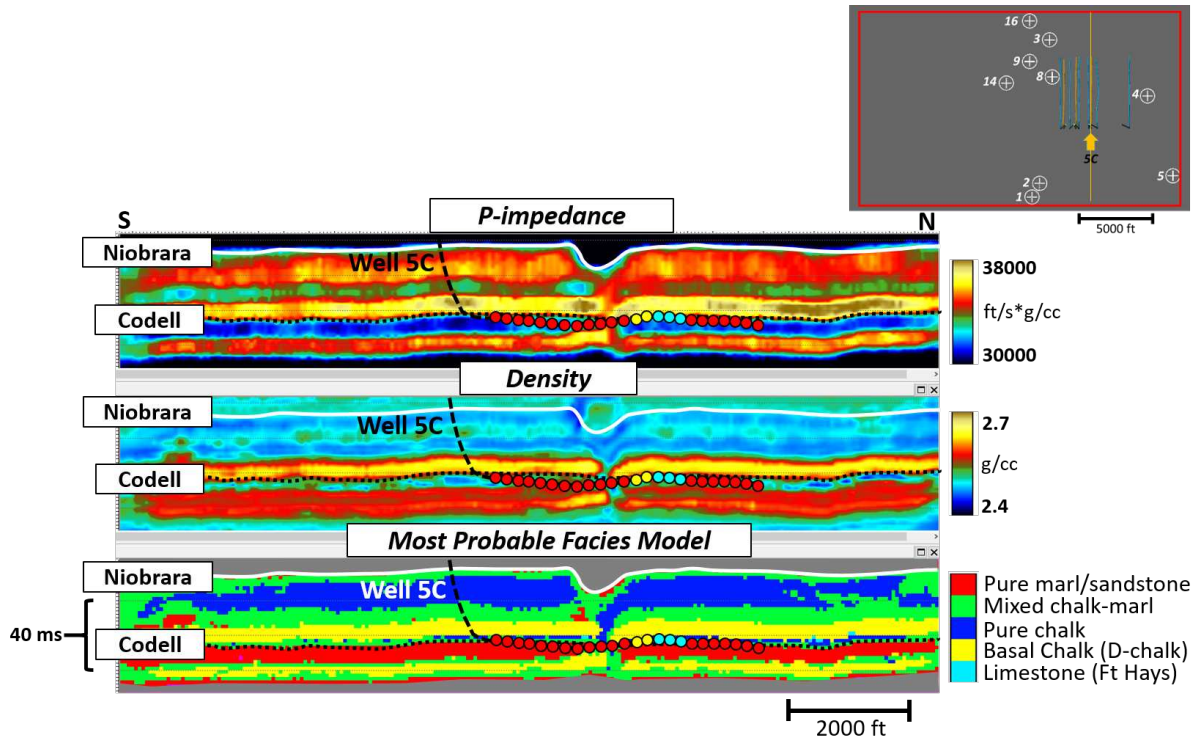

Figure 5.4: Cross-section views of three different attributes: the P-impedance from seismic inversion, density from the multi-attribute transform, and the most probable facies model generated from the two attributes. The section crosses the 5C horizontal well targeting the Codell sandstone interval. The top-right corner map shows the relative locations of the horizontal wells and the vertical wells within the 3D Anatoli seismic survey area.

component.

This type of facies modeling will support locating future drilling target location based on targeting the high quality chalk proportion laterally throughout the survey area, as shown in Figure 5.6. This probability map is extracted as the RMS values of pure chalk probability within the Smoky Hill Member, which consists of both B Chalk and C Chalk. The extraction window is from the Top of Niobrara horizon to 20 ms below it. The higher value of the probability indicates that more chalk proportion contributes to the data point. The color scales on the map show both probability value and estimated thickness of the pure-chalk facies. This probability to thickness domain transform was derived from the cross-plot shown in Figure 5.8. The cross-plot is generated by plotting the pure-chalk probability value at

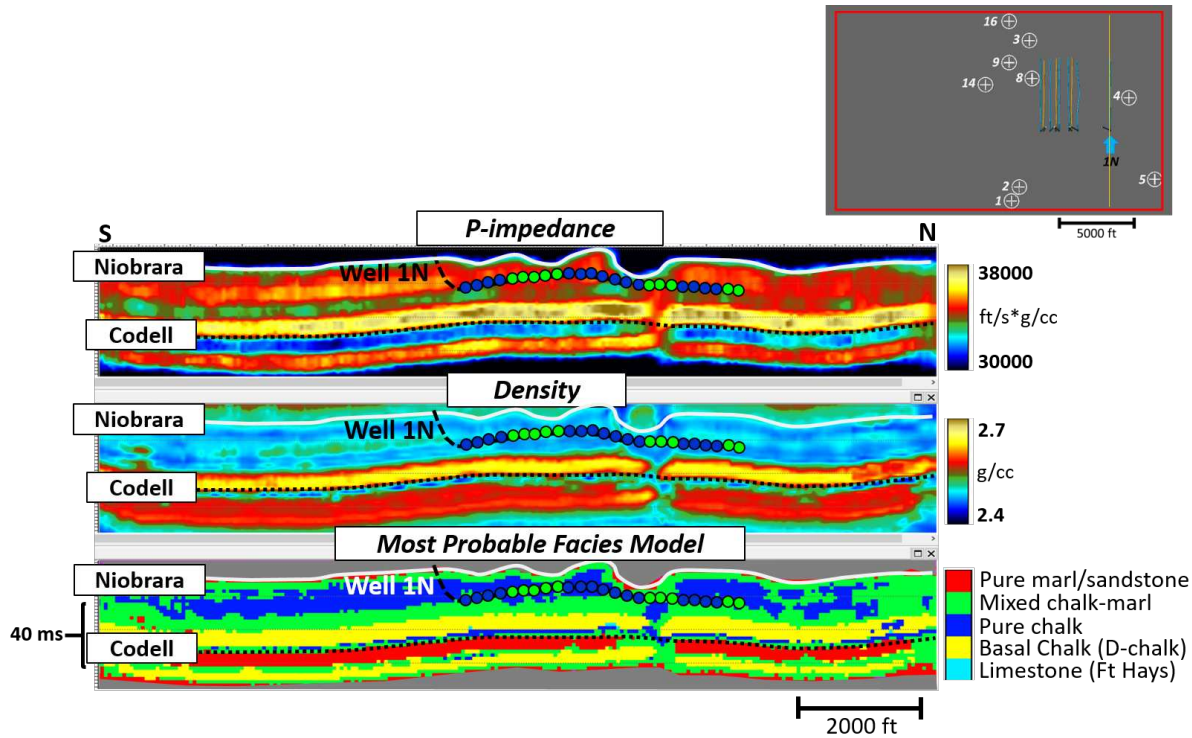

Figure 5.5: Cross-section views of three different attributes: the P-impedance from seismic inversion, density from the multi-attribute transform, and the most probable facies model generated from the two attributes. The section crosses the 1N horizontal well targeting the chalks of Smoky Hill Member. The top-right corner map shows the relative locations of the horizontal wells and the vertical wells within the 3D Anatoli seismic survey area

well locations (from the extraction map) and the sum of pure-chalk facies thickness at wells.

Similarly, Figure 5.7 shows the map of sandstone (Codell) probability extracted as the RMS values of sandstone probability, with the extraction window from the Top of Codell to 15 ms below it. The Codell Sandstone is also a highly targeted interval for horizontal wells and hydraulic stimulation within the area. The sandstone lateral distribution is relatively continuous throughout the survey and facies discontinuities often appear at fault zones. The color scales of the map show both the sandstone probability value and the estimated thickness derived from the cross-plot in Figure 5.9.

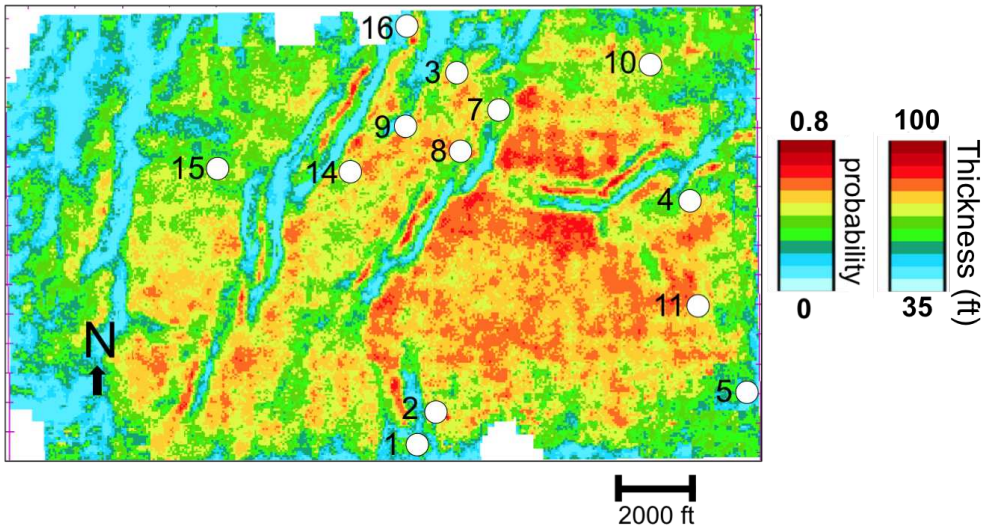

Figure 5.6: Extraction map of the pure chalk facies probability within the Smoky Hill Member interval and the plotted vertical wells inside the survey area (RMS amplitude of the pure chalk facies probability, at the window of the Top of Niobrara horizon to 20ms below it).

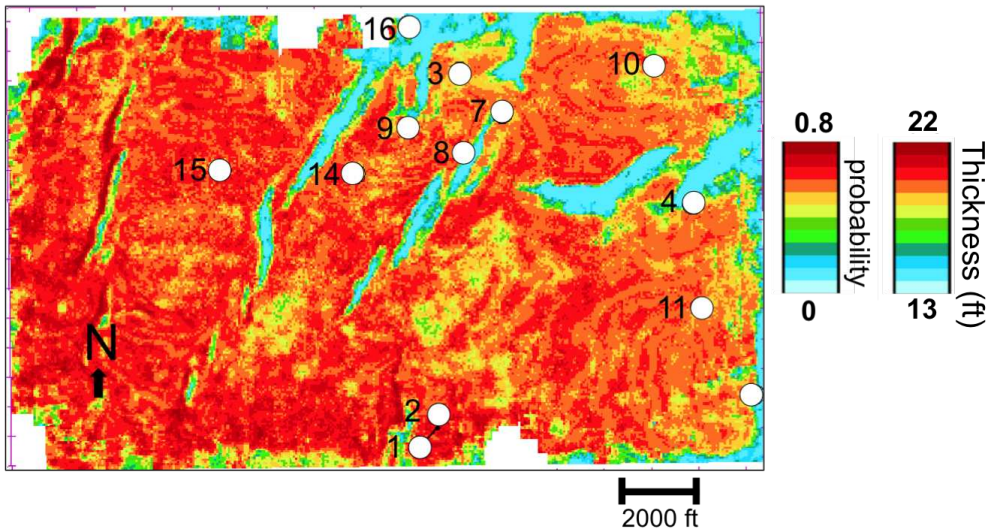

Figure 5.7: Extraction map of the sandstone facies (Codell) probability and the plotted vertical wells inside the survey area (RMS amplitude of the sandstone facies probability, at the window of the Top of Codell horizon to 15ms below it).

A cross-plot of pure-chalk probability value from the extraction map at well locations (Figure 5.6) versus the sum of pure-chalk thickness at each well is shown in Figure 5.8. From this cross-plot, it is observed that there is a linear trend between the facies probability to

the sum of facies thickness at the well locations. This observation indicates that for the area with low probability (<0.2), there is a pure-chalk facies presence, although the sum of the facies thickness will be approximately <40 feet. A similar cross-plot was generated for the sandstone facies (Codell) as shown in Figure 5.9. From the cross-plot, it is observed that the sandstone thickness which ranges from 15 - 25 feet, is relatively consistent from all wells within the survey.

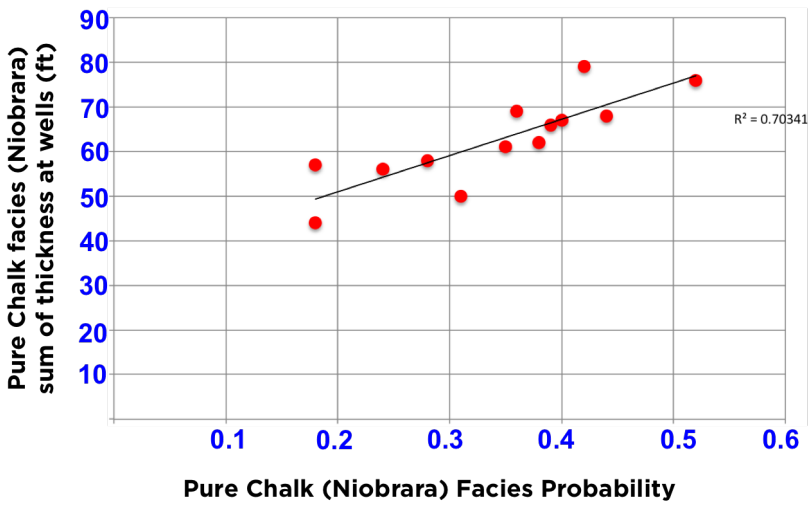

Figure 5.8: Cross-plot of pure chalk facies probability from the map in Figure 5.6 at well locations (13 wells inside the seismic survey) versus the sum of the pure chalk facies thickness at each well.

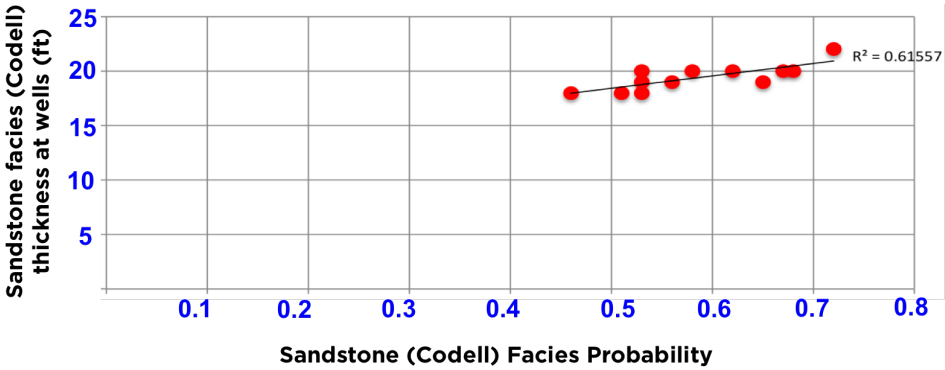

Figure 5.9: Cross-plot of sandstone facies (Codell) probability from the map in Figure 5.7 at well locations (12 wells inside the seismic survey) versus the sandstone facies thickness at each well.

5.2 Application for Preliminary Evaluation of Greenhorn Exploration

Chapters 1 and 2 described in detail the information of the Greenhorn interval that was deposited earlier than the Niobrara interval. The reason behind researching the Greenhorn is that this unit is identified as an analogous area to the highly prolific Niobrara zone of interest, and age equivalent to the Eagle Ford Formation of the Gulf Coast region (Sonnenberg et al., 2016). In addition, there have been vertical wells drilled into the Greenhorn interval around the Denver Basin which suggest that the zone is productive. In terms of its mineralogy, the Bridge Creek and Lincoln members of the Greenhorn are identified as limestone facies containing a high carbonate content and high TOC, similar to the chalk beds of the Smoky Hill Member. Using the facies modeling approach outlined in this chapter, one can also evaluate the Greenhorn interval, particularly the Greenhorn - Bridge Creek Limestone (see Figure 1.2). Sonnenberg et al. (2016) discusses the mechanical stratigraphy of the Greenhorn formation, where the highest values of the Young's modulus are found in the Bridge Creek member of the Greenhorn, which contributed to the high brittleness of the interval. With the relatively higher brittleness of the Bridge Creek member compared to the Hartland Shale underlying it, the Bridge Creek member is recommended as the horizontal drilling target. Based on the elastic properties, Greenhorn - Bridge Creek interval is identified as more similar to the basal chalk (D-facies) than when compared to the chalks of the Smoky Hill Member. The basal chalk (D-facies) is known to be a non-productive zone within the whole interval with a small TOC percentage. However, this evaluation is based on the elastic properties, P-impedance and density, which are significantly affected by the depositional compaction. The Greenhorn is located deeper than the rest of the evaluated facies, hence, the significantly high density values may be related more to the high compaction rather than the low organic content. In addition, the significantly high P-impedance and density values of the Greenhorn unit may be related to the high brittleness of the facies, as reflected in the well evaluation of Poisson's Ratio and Young's Modulus of the Greenhorn interval by Sonnenberg et al. (2016). A more comprehensive evaluation of this hypothesis is needed for

further validation.

Based on the hypothesis that the Greenhorn - Bridge Creek interval is a relatively brittle reservoir with an adequate organic content, it is valuable to map the distribution of the interval throughout the survey area. Figure 5.10 shows the extracted Greenhorn-Bridge Creek Limestone interval, which is modeled as a similar facies to the basal chalk (D-facies) based on the elastic properties. From the facies probability extraction map, lateral deposition of the limestone is primarily distributed on the western part of the Anatoli 3D survey area. A preliminary volumetric calculation of the prospective area can be obtained by mapping the outline of the high probability facies combined with the average thickness of the facies at the wells. The probability extraction map is used to generate the cross-plot shown in Figure 5.11, by examining the correlation between probability value at the well locations and the thickness of the limestone (Greenhorn-Bridge Creek) from each well. From this domain transform, we can estimate the distribution of the limestone interval varies from 0 to 91 feet throughout the survey. This map indicates the locations of the sweet spots for exploration drilling targets in the interval.

Despite the usefulness of this facies modeling work, there are some uncertainties in the modeling result that are discussed below.

5.3 Uncertainties

As optimal as the facies modeling results validated by the well data, there are uncertainties that need to be acknowledged, including the following:

- Seismic inversion results are non-unique, meaning that there are infinite numbers of models that can fit the same seismic data. To address this, it is understood that there is no single facies model that is considered the most accurate; hence the probability volume will be the closest proximity in identifying the targeted facies. The probability values are also relative values to the surrounding area, which means that different input parameters for the facies modeling results in different minimum and maximum

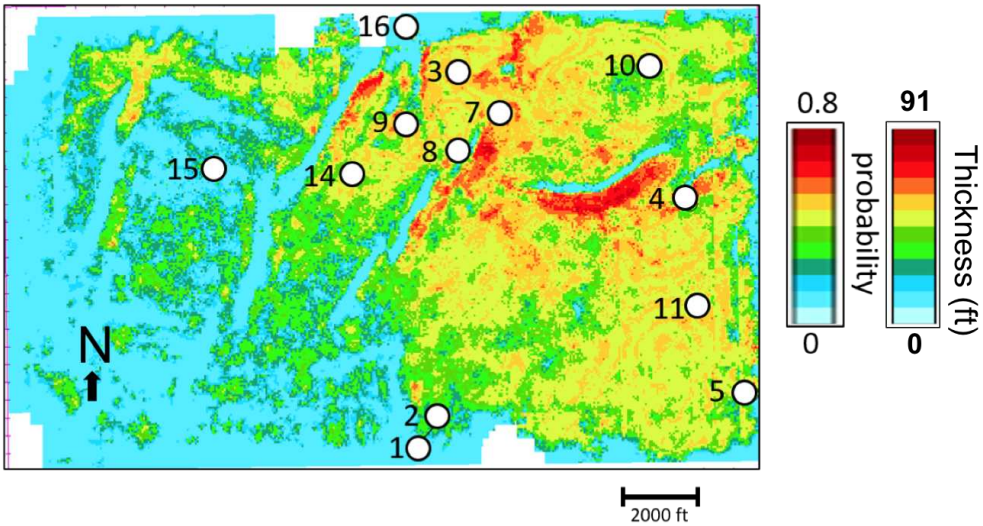

Figure 5.10: Extraction map of the limestone facies (Greenhorn-Bridge Creek) probability and the plotted vertical wells inside the survey area (RMS value of the basal chalk facies probability, at the window of 10 to 25 ms below the Top of Codell horizon). The limestone is modeled similarly to the basal chalk facies (D-facies), in terms of the high density and P-impedance values. These high values of elastic properties may be caused by the high compaction of the limestone interval as it is deposited deeper than the other facies. The hotter color shows the higher facies probability.

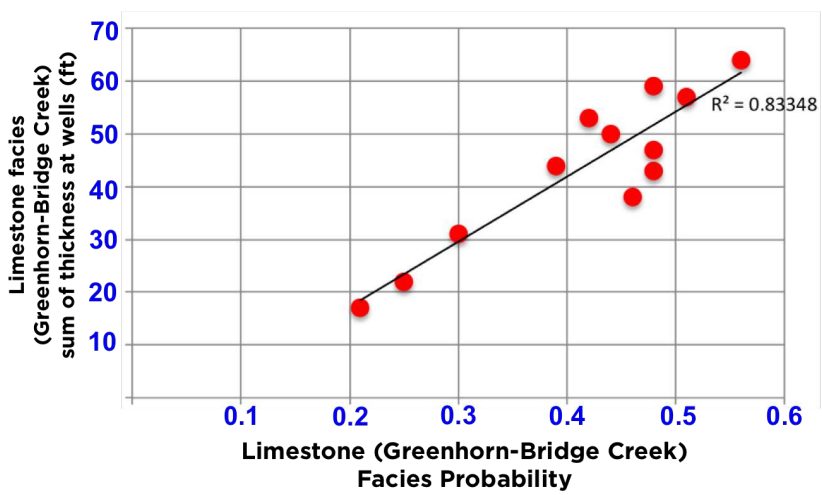

Figure 5.11: Cross-plot of limestone facies (Greenhorn - Bridge Creek) probability from the map in Figure 5.10 at well locations (12 wells inside the seismic survey) vs. the sum of the limestone facies thickness at each well.

probability cut-offs.

- Layer thickness. Depending on seismic frequency and interval velocity, there is a minimum thickness of the facies beds that can be resolved by seismic data. Theoretically, the seismic inversion process includes the wavelet compensation which increases the vertical resolution. However, there are limitations in the attempts to reach the well vertical resolution. Upscaling the facies definition from the well scale to the seismic scale is important to understand the methodology limitation. For this research, this issue is most prominent for limestone facies (Fort Hays) that is deposited between the basal chalk (D-facies) and sandstone (Codell), and the pure marl facies of the Smoky Hill interval.

- The use of synthetic V_p and V_s logs for the main processes. As mentioned in the Chapter 1, Section 1.3.2, most of the vertical wells used for this research do not have measured compressional and shear sonic logs. For most of these wells (11 of 15), the compressional and shear sonic logs were created using the neural network calculation. This is the reason we observe a relatively linear relationship of P-impedance and S-impedance cross-plot from well data, which is unlikely seen in the real data. To compensate for this limitation, the low frequency part of the model was set sufficiently low to not highly affect the seismic inversion result. The P-impedance and density properties were used to perform the facies modeling, acknowledging that the density logs are one of the measured well log datasets.

Analysis of the uncertainties of a scientific project is an important consideration, as the results will be used later for more advanced and quantitative modeling within the project area. Overall, the seismic dataset used for this research is of good quality and can deliver a reliable result that can be validated by lithology information at wells, and is useful for future reservoir modeling work.

CHAPTER 6
CONCLUSIONS AND RECOMMENDATIONS

6.1 Conclusions

Pre-stack simultaneous seismic inversion and multi-attribute transform processes have been applied to the Wattenberg dataset, in particular the 10 square mile 3D Anatoli survey area. The outputs of the inversion are the elastic properties (P-, S-impedance, and density) that are used to characterize the facies within the Niobrara, Codell, and Greenhorn formations. Inverting for density from pre-stack seismic inversion in the project dataset is challenging due to the angle limitation from the limited seismic acquisition aperture. However, the multi-attribute transform using the non-linear relationship (Probability Neural Network) has been beneficial in estimating a density volume that is well correlate with the borehole measurements. The combination of the P-impedance from seismic inversion and the density from multi-attribute transform enables facies modeling within the target interval. The two outputs, the probability and the most probable facies volumes are mainly useful for:

- Field development: Information of facies lateral distribution (background trend) for more advanced reservoir modeling work (higher resolution model with the information of faults, fractures, porosity, and permeability), especially for the pure chalk facies within the Niobrara - Smoky Hill Member interval. This facies is the main reservoir that has the highest Rock Quality Index (RQI) for hydraulic fracturing targets (Mabrey, 2016). Additionally, the Codell Sandstone is also a highly targeted interval for horizontal well drilling and hydraulic fracturing within the Wattenberg Field and the information on the regional facies lateral distribution within the Anatoli survey can help support the field development plans in the future.

- Exploration: Preliminary evaluation of the potential Greenhorn interval has resulted in a facies probability map that can be useful for further rock volume calculation. There are still many potential areas that have not been drilled in this interval. Beyond the facies modeling work, information on the fracture networks needs to be evaluated and incorporated into the facies model, in order to help mitigate the exploration/development drilling risk.

As demonstrated in the facies modeling section, the facies probability volume correlates to the general thickness of each facies between the zone of interest. This information can support the sweet spot identification for next drilling target, which have relatively higher reservoir thickness.

In terms of the methodology, the available technology and tools for estimating rock properties from seismic data at the Wattenberg Field has been advanced significantly to support delivering a reliable facies model and validated by the well information. As demonstrated, it is important to test available technology depending on the dataset limitations and recognize the values and limitations of performing the methodology.

6.2 Recommendations

There are many types of inversion methods available in the geophysical software market, that could potentially improve the facies modeling result. For this type of geological environment, it would be valuable to test geostatistical inversion to improve the vertical resolution of the facies model. Another type of seismic inversion that can be tested is the Joint Impedance and Facies Inversion (JIFI). This methodology in particular provides more detailed parameters in the Low Frequency Model, by establishing information on the elastic properties vs. depth trends for each modeled facies. This method could potentially deliver more reliable S-impedance and density properties in addition to the general P-impedance output from seismic inversion.

For the field development point of view, it is recommended to use the 3D estimated density, P- and S-impedance produced from this research for future advanced reservoir modeling work. The facies model obtained from this research can also be used for the future development plan by keeping the horizontal well drilling path within the formation during the drilling process.

In terms of the data availability, it is highly recommended to acquire additional sonic logs (compressional and shear) for the wells inside the seismic survey area. Current facies modeling work only utilizes one out of 13 vertical wells with real sonic logs, inside the seismic survey. These synthetic sonic logs create consistent V_p/V_s values for all modeled facies from the well data. Additional sonic logs can be used to build a more constrained geology model as a priori information to the inversion process.

Additionally, the facies modeling in the ten square mile Anatoli area gives more regional information of the basin compared to the four square mile hydraulic stimulation area. This evaluation allows for suggestions for future exploration in the Greenhorn interval. For future work, it is suggested that similar type of facies modeling be performed on seismic dataset covering more regional area than the 3D Anatoli survey. This evaluation will be useful for identifying other potential targets around the project area that can be explored and developed in the future, by extending the current findings from the research on the 3D Anatoli survey.

REFERENCES CITED

Ardakani, E. P. (2003). Lithology Discrimination Using Elastic Rock Properties and Simultaneous Seismic Inversion in the Leduc Reservoir, NE Alberta. pages 42–46.

Brugioni, D. N. (2017). Fault, Fracture, And Geomechanical Analysis Of The Niobrara Formation, Wattenberg Field, Colorado.

Butler, E. (2016). P-Wave Seismic Time-Lapse Analysis of Horizontal Well Completions Causing Pressure Compartmentalization. page 68.

CGG-Jason (2015a). Jason InverTrace-Plus Module - Technical Background.

CGG-Jason (2015b). Jason RockTrace Module.

CGG-Jason (2016). Facies and Fluids Probabilities Tutorial.

Cipolla, C., Lewis, R., Maxwell, S., and Mack, M. (2012). Appraising unconventional resource plays: Separating reservoir quality from completion effectiveness. *International Petroleum Technology Conference*, pages 1524–1550.

Davey, H. (2012). Geomechanical characterization of the Montney Shale northwest Alberta and northeast British Columbia, Canada. *Masters Abstracts International*, pages 33–27.

Duda, R. O. (2001). *Pattern Classification 2nd Edition*.

Durkee, H. (2016). Reservoir Characterization and Geomechanical Evaluation of the Greenhorn Formation in the Northern Denver Basin, Colorado. Master's thesis, Colorado School of Mines.

Fatti, J. L. (1994). Detection of gas in sandstone reservoirs using AVO analysis: A 3-D seismic case history using the Geostack technique. *Geophysics*, 59(9):1362.

Gunning, J. and Glinsky, M. E. (2006). WaveletExtractor : A Bayesian well-tie and wavelet extraction program. 32.

Hampson, D. P., Russell, B. H., and Bankhead, B. (2005). Simultaneous inversion of prestack seismic data. *SEG Technical Program Expanded Abstracts 2005*, (7):1633–1638.

Hampson, D. P., Schuelke, J. S., and Quirein, J. A. (2001). Use of multiattribute transforms to predict log properties from seismic data. 66(1):220–236.

Higley, D. K. and Cox, D. O. (2007). Oil and Gas Exploration and Development along the Front Range in the Denver Basin of Colorado , Nebraska , and Wyoming. *US Geological Survey Digital Data Series*, pages 1–40.

Higley, D. K., Cox, D. O., and Weimer, R. J. (2003). Petroleum system and production characteristics of the Muddy (J) Sandstone (Lower Cretaceous) Wattenberg continuous gas field, Denver basin, Colorado. *AAPG Bulletin*, 87(1):15–37.

Kamruzzaman, A. (2015). Petrophysical Rock Typing of Unconventional Shale Plays: A Case Study for the Niobrara Formation of The Denver-Julesburg (DJ) Basin. Master's thesis, Colorado School of Mines.

Kohonen, T. (1990). The self-organizing map. *Proceedings of the IEEE*, 78(9):1464–1480.

Mabrey, A. N. (2016). Rock Quality Index for Niobrara Horizontal Well Drilling and Completion Optimization, Wattenberg Field, Colorado. Master's thesis, Colorado School of Mines.

Matthies, N. (2014). Understanding and mapping variability of the Niobrara Formation across Wattenberg Field, Denver Basin. Master's thesis, Colorado School of Mines.

Motamedi, T. (2015). Time-Lapse Characterization of The Niobrara Reservoir From Multicomponent Seismic Data, Wattenberg Field, Colorado. pages 1–96.

Pitcher, T. M. (2015). Joint Geophysical and Geomechanical Analysis of In-Situ Stress, Wattenberg Field, Colorado, USA. Master's thesis, Colorado School of Mines.

Russell, B. (2014). Seismic Reservoir Characterization and Pre-stack Inversion in Resource Shale Plays. *AAPG database*, 41467.

Russell, H. (2013). Guide to Emerge. pages 1–124.

Simmons, J. L. and Backus, M. (1996). Waveform-based AVO inversion and AVO prediction-error. *Geophysics*, 61(6):1575.

Sonnenberg, S. a. (2012). The Niobrara Petroleum System, Rocky Mountain Region. *Search and Discovery*, 80206:107–112.

Sonnenberg, S. a. (2013). New reserves in an old field, the Niobrara resource play in the Wattenberg Field, Denver Basin, Colorado. *URTeC*, 1562913(December):1–13.

Sonnenberg, S. a. (2015). Geologic Factors Controlling Production in the Codell Sandstone, Wattenberg Field, Colorado. 20346.

Sonnenberg, S. a., Durkee, H., and Kaiser, C. (2016). The Graneros-Greenhorn Petroleum System, a possible new resource play, Rocky Mountain Region, USA. *Search and Discovery*, 10898(10898):39pp.

White, M. D. (2015). Time-Lapse Interpretation of P-Wave Data for a Hydraulically Fractured Reservoir, Wattenberg Field, Colorado. page 91.